IS-T 1898

Structure and High-Temperature Properties of Ti5Si3 with Interstitial Additions

by

Williams, Jason

PHD Thesis submitted to Iowa State University

Ames Laboratory, U.S. DOE

Iowa State University

Ames, Iowa 50011

Date Transmitted: 1999

PREPARED FOR THE U.S. DEPARTMENT OF ENERGY

UNDER CONTRACT NO. W-7405-Eng-82.

DISCLAIMER

TABLE OF CONTENTS

CHAPTER 1: GENERAL INTRODUCTION

Dissertation Organization

The following sections of this chapter include a detailed literature survey on germane properties of Ti_5Si_3, as well as a summary that gives reasons for the need for additional research and describes the significance of this dissertation. Chapters 2 through 5 consist of manuscripts submitted to various journals. Chapters 2 through 4 attempt to determine the structure and bonding of Ti_5Si_3-based materials and make a correlation to known properties. The secondary authors acquired some data used in these manuscripts. Chapters 2 and 4 contain neutron diffraction data taken by S.K Malik at Missouri University's Research Reactor. Chapter 4 contains theoretical electronic structure calculations made by Y.Y Ye at Wuhan University, China. Chapters 2 and 5 examine two properties of Ti_5Si_3-based materials that are critically important for engineering applications: thermal expansion anisotropy and oxidation behavior. Finally, Chapter 6 summarizes the most important results of these studies and includes suggestions for future research.

All but Chapter 4 include my major professor, Dr. Mufit Akinc, as co-author since he was an integral part in shaping this dissertation. His insightful comments and patience is greatly appreciated. Dr. Matthew Kramer is also included as co-author on several papers for his help on Rietveld analysis, neutron diffraction and giving me the opportunity to perform research at the synchrotron sources. I must also mention the unsung work of Dr. Andrew Thom, whose technical discussions and critical assessments are also greatly appreciated.

The Current Interest in Silicides

The large interest in silicides, currently present in the research community, has been driven by essentially two industrial applications. The first, which occurred in the early 1980's and has unequivocally altered the world's economy and development, is the large scale production of silicon based computers. Silicides are used primarily as ohmic contacts due to their low electrical resistivity and thermal compatibility with silicon.[1] Compatibility is achieved by using phases that are in thermodynamic equilibrium with silicon, namely the disilicides. Of the many that exist, $TiSi_2$, $CoSi_2$ and WSi_2 exhibit the most useful properties; thus, much of the research has focused on these compounds. This research on disilicides includes: oxidation behavior[2-6], which is important in photolithographic and thermal processing of circuits; atomic diffusivities[7], which are important in predicting chemical reactivity of circuits; and the nature of chemical bonding in silicides[8-12], which is important in understanding, predicting, and tailoring a material's electrical response in circuits.

The second area of research was spawned by the seemingly insurmountable limitation of metallic alloys to exceed structural applications in excess of 1100°C. Specifically, superalloys, which are the primary materials used in these applications, rapidly lose their resistance to creep and oxidation above 1100°C. Yet, a structural material that could withstand temperatures from 1300 to 1600°C would conceivably have as large an impact on the economy as the microelectronics industry. Not only would such a material improve the efficiency of current applications, but it would also enable new and more demanding applications. This desire to increase application temperatures in combination with many promising properties seen in a certain class of materials, the intermetallics, led to an

extensive research effort beginning in the late 1980's and continuing today. The properties of intermetallics that were initially responsible for this interest included very high melting points, many in excess of 2000°C, densities typically lower than 7 g/cm^3, and a large alloying potential. In fact, the number of intermetallic compounds is so substantial that much of the research from 1987 to 1993 focused on characterizing many compounds based on a few properties in an attempt to efficiently find the most promising materials.

The necessary criteria for high temperature applications and the materials that met these criteria were primarily developed through research by Anton, Shaw *et al.*[13-18] and by Fleischer *et al.*[19-24]. The criteria included: good creep and oxidation resistance above 1000° C, low density, retention of strength at elevated temperatures and alloying or compositing possibilities to improve the ambient temperature brittleness inherent to most intermetallics. Based on these criteria, aluminides and silicides proved most promising; although, an intermetallic alloy that possesses all of the above characteristics has yet to be developed.

This vast body of research has not produced the perfect high-temperature structural material; but from it, two very important aspects of synthesizing intermetallics have become known. The first important aspect is that alloying additions, even in very small amounts, may dramatically affect the properties. For example, previous research by Meyer and Akinc[25] on Mo_5Si_3 based compounds has shown that the addition of only 2wt% boron can improve the high temperature oxidation resistance by three orders of magnitude. As another example, a small addition of boron, carbon or beryllium has been shown to increase the ductility of Ni_3Al and Ni_3Si by modifying grain boundary properties.[26] The second important aspect is that the processing route also plays an essential role in determining the properties. Important

factors include microstructure, porosity, microcracks, residual stress and impurity content. A classic example is of the catastrophic oxidation (pesting) of $MoSi_2$ at low temperatures. Research has shown that this pesting phenomenon is primarily due to the presence of excessive microcracks and porosity.[27]

The existence of countless permutations on alloying additions and processing conditions will insure the continuation of intermetallic research for decades. In addition, the known importance of impurity and defect content on properties requires a more critical look at earlier research. This is especially true for Ti_5Si_3, which will be discussed below.

The Promises of M_5Si_3 Based Compounds (M = transition metal)

Silicides with the M_5Si_3 stoichiometry offer many advantages over other silicides. The crystal structure is either a hexagonal Mn_5Si_3 type ($P6_3/mcm$, M= Sc, Y, Ti, Mn), body-centered tetragonal Cr_5B_3 type (I4/mcm, M= La, Nb, Ta, Cr), or body-centered tetragonal W_5Si_3 type (I4/mcm, M= V, Mo, W). In contrast to disilicides, substitutional alloying possibilities in these structures are much more numerous. In addition, all M_5Si_3 compounds, except La_5Si_3, revert to the hexagonal form in the presence of smaller atoms (i.e. B, C, O or N). This hexagonal structure can accommodate up to 11at% of these small interstitial atoms. Thus, M_5Si_3 compounds also exhibit substantial interstitial alloying possibilities, which are not seen with any other silicide stoichiometry. Other advantages include higher melting points and the potential for ductile phase toughening. Silicides richer in silicon than M_5Si_3 compounds are not in thermodynamic equilibrium with ductile phases; thus, they can not form stable composites with them.

Disadvantages of pure M_5Si_3 compounds include only marginal oxidation resistance, low fracture toughness at ambient temperature, and anisotropic properties. This last property, which is a result of anisotropic crystal structures, leads to processing obstacles such as residual stress and microcracks. Additionally, processing of pure hexagonal M_5Si_3 is difficult due to the strong tendency of carbon, oxygen and nitrogen to fill the interstitial sites. Because of these processing difficulties, research on M_5Si_3 compounds, including Ti_5Si_3, must be viewed critically.

Properties of Ti_5Si_3

Thermodynamic Data

Figure 1 shows the most recent phase diagram of the Ti-Si system, which is taken from Seifert *et al.*[28]. It was produced through a least-squares optimization of known phase equilibrium and thermodynamic data, as well as theoretical modeling of the liquid phase and non-stoichiometry of Ti_5Si_3. A previously published and frequently cited phase diagram was assessed by Murray[29] and was primarily based on data from Svechnikov *et al.*[30]. However, lattice parameters for Ti_5Si_3 given in this study suggest a significant amount of interstitial impurity. Studies on rare earth Mn_5Si_3[31,32] type silicides indicate that interstitial impurities noticeably decrease the melting point of these compounds; thus the melting point of Ti_5Si_3 given by Murray, and possibly, the homogeneity range are questionable. Unfortunately, the homogeneity range for Ti_5Si_3 given in Seifert *et al.*[28] must also be called into question. This study modeled the non-stoichiometry by substitutional defects, but work by Corbett *et al.*[33] on compounds with an identical crystal structure suggest that interstitial defects are likely.

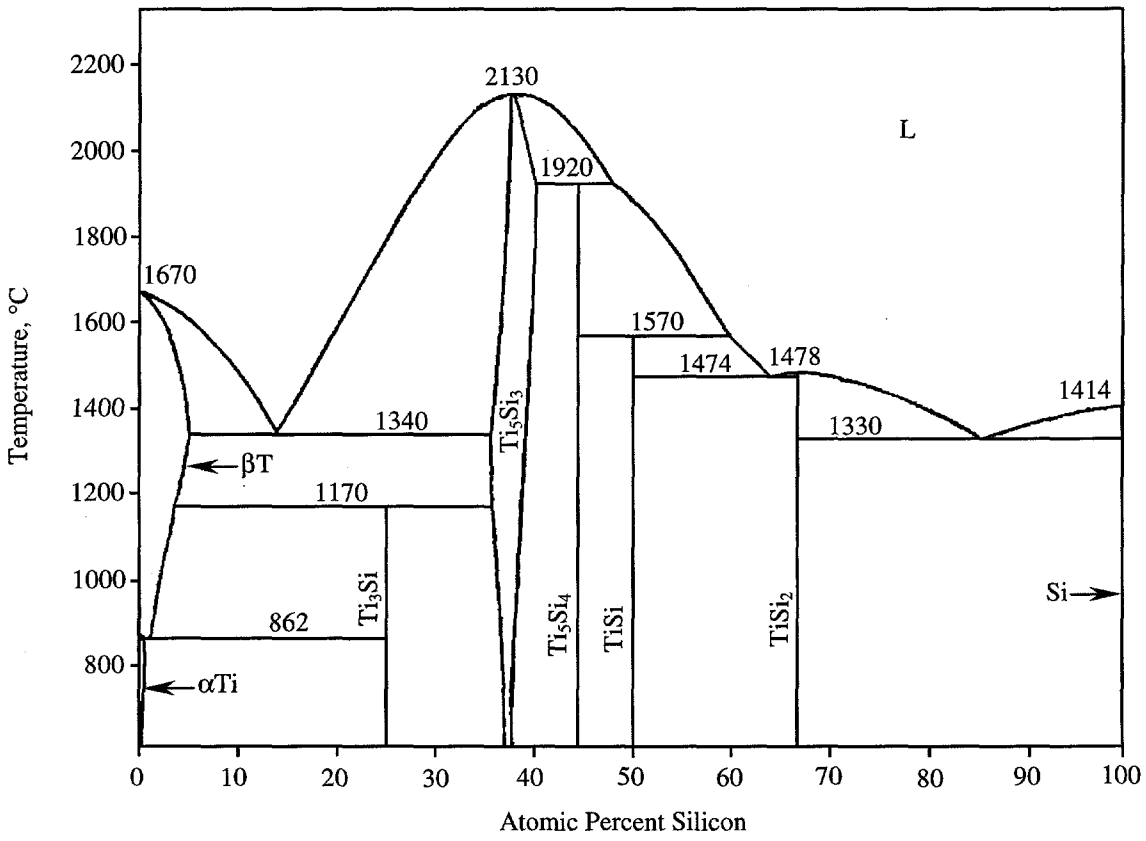

Figure 1. Ti-Si binary phase diagram produced by optimizing published data of titanium silicides.[28]

Table I and Figure 2 give known thermodynamic data of Ti_5Si_3.[34-36] A critical review by Schlesinger[34] in 1990 on the thermodynamic properties of solid transition metal silicides illustrates the lack of good data for these systems. To date, only reliable measurements of enthalpy of formation and low temperature heat capacity have been documented. Although not as reliable, the data of Figure 2 clearly show that Ti_5Si_3 is among the most stable of the silicides.

Several isothermal phase equilibrium studies also exist on Ti-Si-Z systems (Z=C, N or O).[37-39] Figure 3 gives the isothermal phase diagrams from these studies, all of which, were produced through a series of diffusion couples. These ternary phase diagrams illustrate two important and previously mentioned properties: Ti_5Si_3 exhibits a large homogeneity range for interstitial atoms, and the existence of this homogeneity range enables Ti_5Si_3 to be in thermodynamic equilibrium with all silicide phases, most TiZ_x compounds and titanium metal. Thus, properties can be tailored through the many possible phase assemblages. The combinations become even larger if another transition metal is added to produce a quaternary system, of which none have been assessed.

Structural/ Interstitial Chemistry

The crystal structure of Ti_5Si_3 is the hexagonal Mn_5Si_3 type (Space group = $P6_3/mcm$)(Fig 4). The structure consists of essentially two chains of atoms; one being a linear chain of titanium atoms, the other being a chain of face-shared octahedra formed by six titanium atoms. The center of these octahedra is where interstitial atoms would sit. According to published data[40], the diameter of this interstitial hole is approximately 1.34 Å,

Table I. Thermodynamic Data for Ti_5Si_3 at 298K

C_p, J/(K mol)	ΔH_f, kJ/mol	ΔG_f, kJ/mol	θ_D, K	Source
181.4	-510.4	-514.2		Barin[36]
	-581.4	-581.3		Seifert *et al.*[28]
180.3	-579.2	-571.5	670	Archer *et al.*[35]

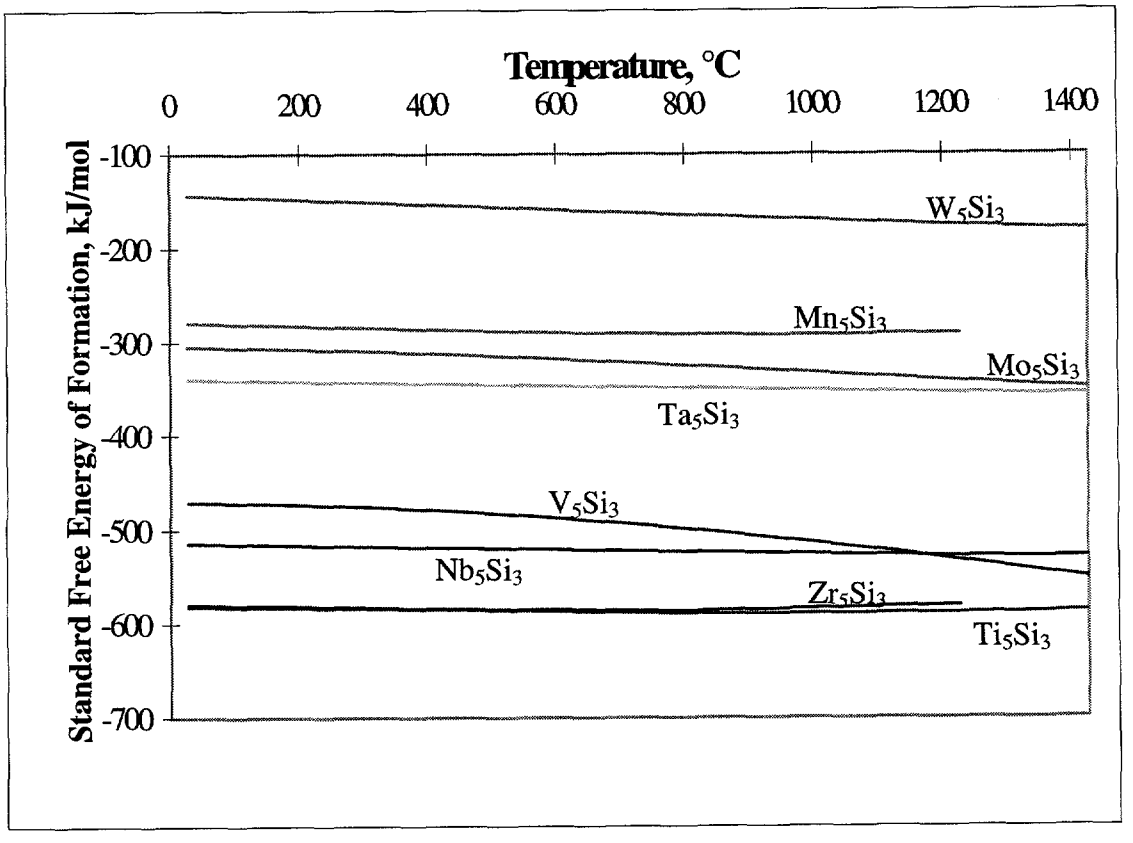

Figure 2. Standard free energy of formation of various M_5Si_3 compounds. Silicides of the second and third groups of transition metals are generally more stable than later transition metal silicides.[36]

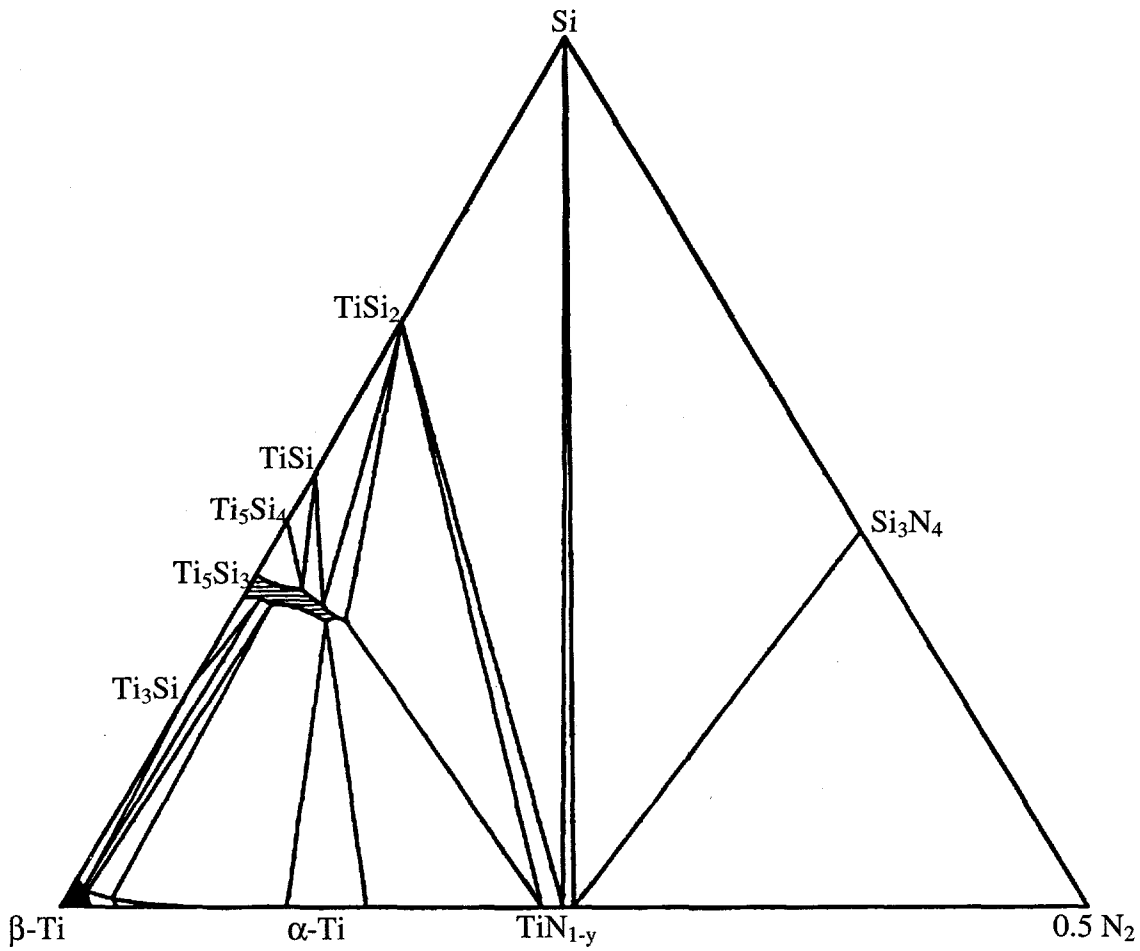

a. Ti-Si-N phase diagram. $Ti_5Si_3N_x$ is in equilibrium with every compound but nitrogen, silicon and Si_3N_4. [38]

Figure 3. Ternary Phase Diagrams

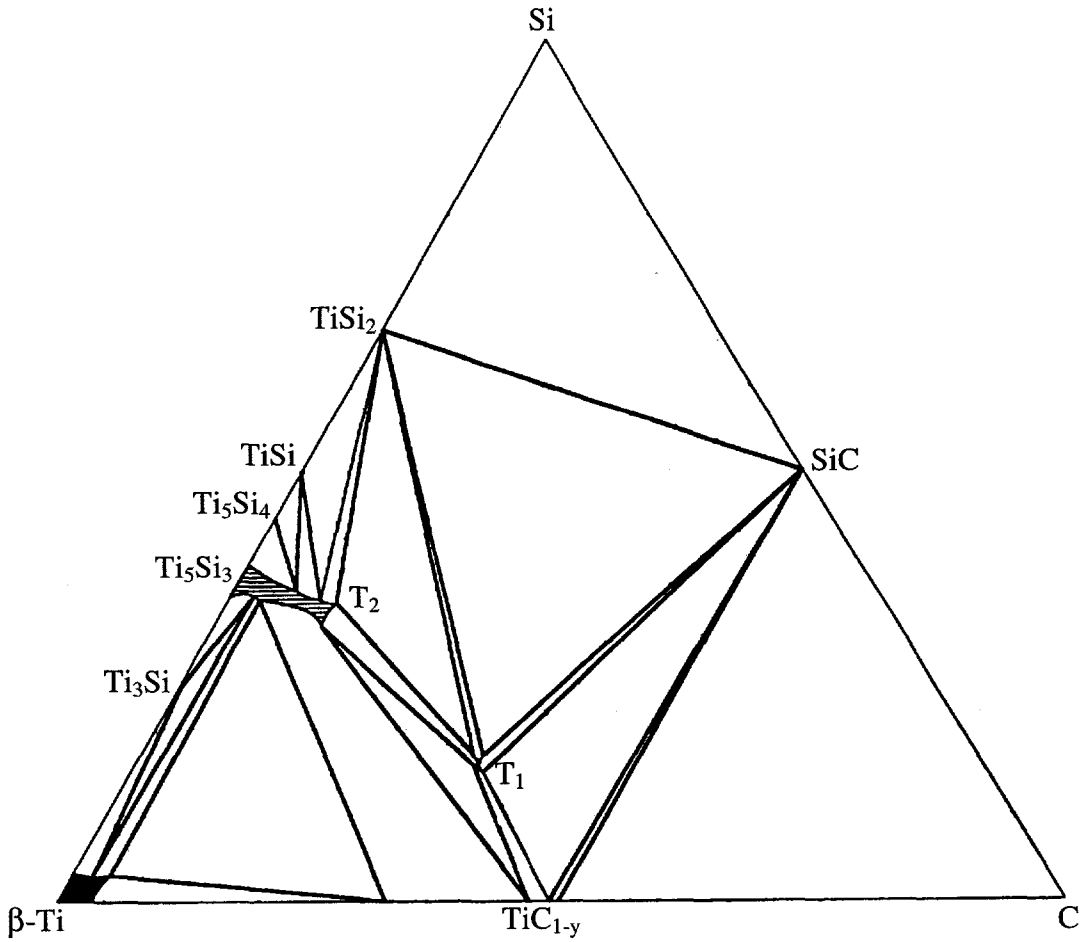

b. Ti-Si-C phase diagram. $Ti_5Si_3C_x$ (T_2) is in equilibrium with every compound but carbon, silicon and SiC. Also note that this is the only Ti-Si-Z system that has a second ternary compound, Ti_3SiC_2 (T_1).[38]

Figure 3. (continued)

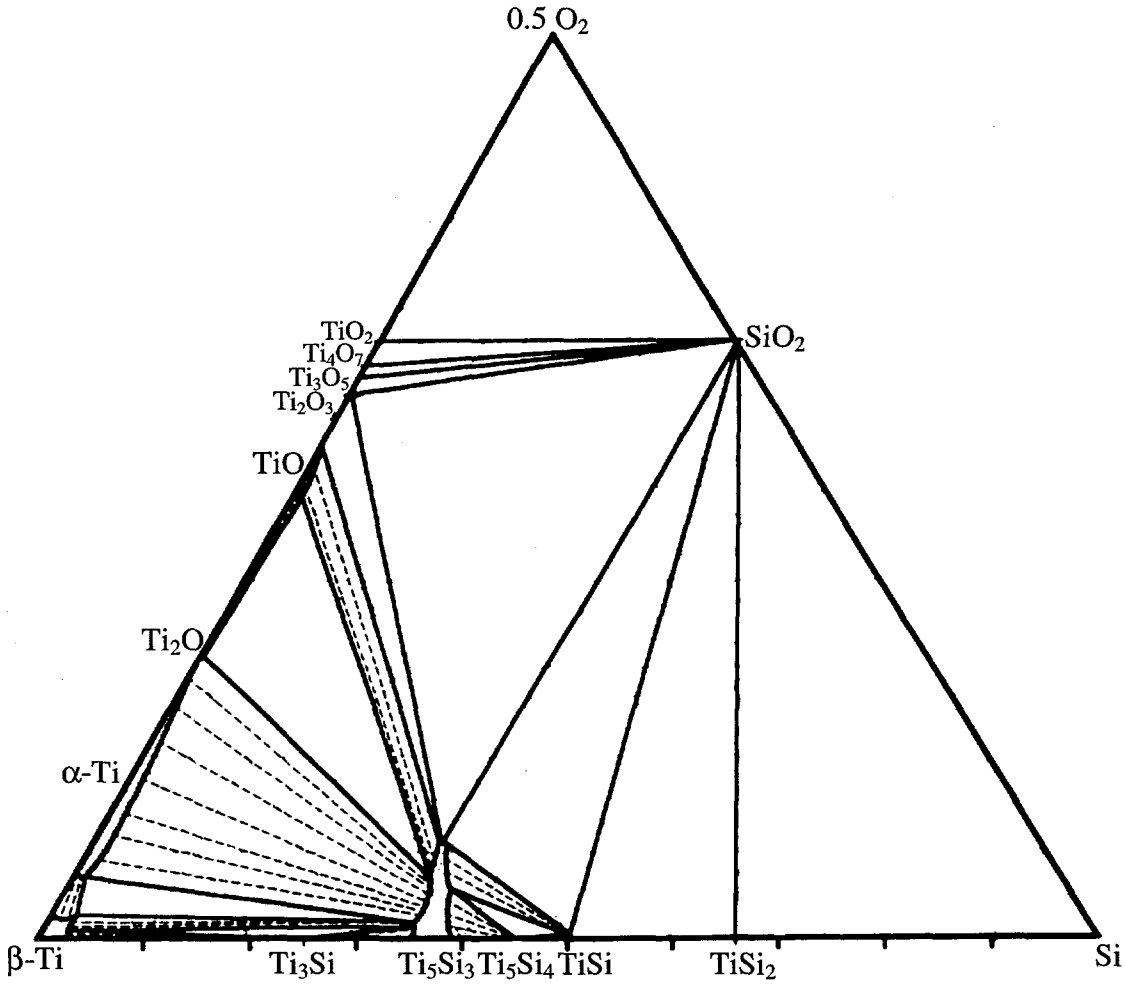

c. Ti-Si-O phase diagram. $Ti_5Si_3O_x$ is in equilibrium with every compound but oxygen, silicon, Ti_4O_7, TiO_2 and $TiSi_2$.[39]

Figure 3. (continued)

Table II. Lattice Parameters of Ti_5Si_3

a, Å	c, Å	Study
7.465(2)	5.162(2)	Pietrokowsky *et al.*[41], 1951
7.429(?)	5.1392(?)	Swanson *et al.*[43], 1959
7.4440(4)	5.1430(5)	Quakernaat *et al.*[42], 1974
7.4543(4)	5.1474(6)	Thom *et al.*[40], 1995
7.4610(3)	5.1508(1)	Kajitani *et al.*[44], 1986
7.459 ± 0.002*	5.150 ± 0.002*	This Study

* The error value represents the standard deviation of several measurements.

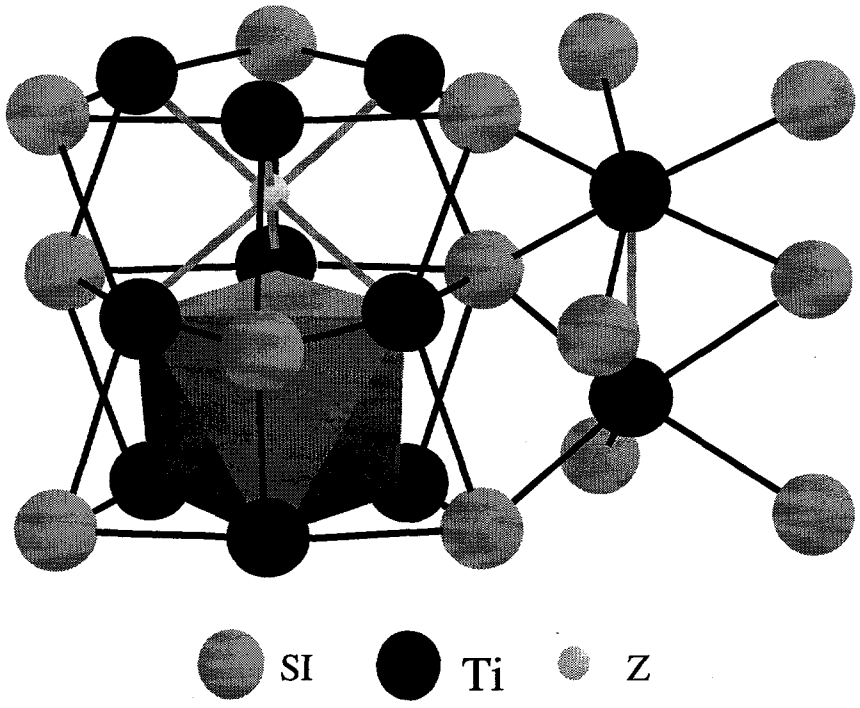

Figure 4. Partial crystal structure of $Ti_5Si_3Z_x$. Interstitial atoms (Z) sit at the center of the irregular, face-sharing octahedra of Ti atoms.

which is large enough to accommodate second period elements. In fact, work done on compounds with identical crystal structures by Corbett *et al.*[33] has shown that atoms as massive as fourth period elements can be incorporated into the interstitial position, resulting in a significant expansion of the lattice. As seen in Table II, the published lattice parameters[40-44] of Ti_5Si_3 show considerable scatter. This would indicate considerable impurity content gained from the starting materials or the fabrication technique. The lattice parameters given by Quakernaat *et al.*[42] and Swanson *et al.*[43] are suspiciously small compared to recent works, which would indicate oxygen and nitrogen impurities. Although the description of the starting materials is insufficient, Quakernaat *et al.*[42] indicate detectability limits only good to 1wt% for the light elements, and Swanson *et al.*[43] synthesized Ti_5Si_3 via solid state reaction of elemental powders. A recent study by Radhakrishnan *et al.*[45] has shown that use of elemental powder leads to a significantly larger interstitial content in Ti_5Si_3 than does use of large pieces as starting materials.

The studies by Kajitani *et al.*[44] and Thom *et al.*[40] synthesized Ti_5Si_3 via arc melting of bulk elemental pieces. This and the larger lattice parameters suggest a lower interstitial content. However, the difference in lattice parameters between the two studies is significant. Both used the Rietveld method to refine lattice parameters and atomic positions; however, Kajitani *et al.*[44] used a powdered sample with an internal standard, and Thom *et al.*[40] used a single crystal. There is a possibility that the small single crystal used in the study by Thom *et al.*[40] was not representative of the much larger arc melted ingot. A study by Margulies *et al.*[46] has shown by high-resolution powder diffraction that an arc melted ingot of Ti_5Si_3 may actually contain many distinct Ti_5Si_3 phases. Although the exact mechanism is unknown,

crystals solidified on the outer surfaces may have a different composition than those in the interior. Whether this composition gradient is due to differing interstitial content or differing titanium to silicon ratios is also unknown. Arc melting of similar intermetallic compounds by Garcia *et al.*[47] typically yielded broad diffraction lines, indicative of compositional heterogeneity and/or high concentrations of crystalline defects.

This review of the literature suggests that studies which use elemental powders in synthesis of Ti_5Si_3, should be viewed as suspect. In studies that use elemental powders, significant interstitial content in Ti_5Si_3 seems unavoidable. Also, in studies that use arc melting, a representative sample or thermal annealing may be necessary to avoid misleading results due to heterogeneity. This review also suggests that lattice parameters could be a very effective way to monitor the purity of hexagonal M_5Si_3 type compounds. In fact, Thom *et al.*[40] quantified the effect of varying boron, carbon, nitrogen or oxygen content on the lattice parameters of Ti_5Si_3. However, the accuracy of these results needs improvement since no internal standard was used during XRD and little data were taken at lower interstitial contents. In any case, the trends appear as follows: boron and to a lesser extent carbon tend to expand the lattice; oxygen and nitrogen tend to contract it.

Thermal Expansion

Considerable scatter exists in the thermal expansion coefficients of Ti_5Si_3 just as it does in published lattice parameters. As given in Table III, thermal expansion has been measured by high temperature x-ray diffraction and through dimensional changes in bulk samples for a variety of processing methods.[48-51] The only consistent result between these

Table III. Thermal Expansion Data for Ti_5Si_3

Sample	Materials / Processing	Bulk CTE[a], $x10^{-6}\ C^{-1}$	CTE, a axis $x10^{-6}\ C^{-1}$	CTE, c axis $x10^{-6}\ C^{-1}$	CTE anisotropy α_c/α_a	Measurement
Ti_5Si_3	float zone	8.7 / 9.5[b]	5.3/5.2[b]	15.6/18.1[b]	2.9/3.5[b]	Displacement[48]
Ti_5Si_3	powders/hip	7 / 9[b]				Displacement[49]
Ti_5Si_3	solids/arc melt	11.8	8.7	20.4	2.3	XRD[50]
Ti_5Si_3	powders/arc melt	13.3	11	18	1.6	XRD[51]
$Ti_5Si_3\ C_{0.85}$	Solids/arc melt	12.2	9.4	17.9	1.9	XRD[50]
$Zr_3Ti_2Si_3$	powders/arc melt	12.7	12	14	1.2	XRD[51]

[a] Bulk CTE values for XRD studies were estimated by $1/3(2\alpha_a + \alpha_c)$. The error of this approximation approaches zero as α_c/α_a approaches one.

[b] The first two studies showed a positive temperature dependence of the CTE's. The first value is at 20°C, the second at 1000°C.

studies is that the coefficient of thermal expansion (CTE) along the c-axis is measurably larger than the CTE along the a-axis. This suggests a larger anharmicity along the c-axis, which would be due to different and/or weaker bonds along that direction. Evidence for a more metallic bonding character along the c-axis is given by Nakashima *et al.*[48]. This study shows that the electrical conductivity along the c-axis is approximately twice that along the a-axis for temperatures between 4 and 300K. Also important, the studies by Thom *et al.*[50] and Ikarashi *et al.*[51] show that interstitial and substitutional additions, respectively, alter the bonding in Ti_5Si_3 so as to lower the thermal expansion anisotropy. As previously stated, this would be crucial in reducing the amount of microcracks and residual stresses during processing.

Due to the large scatter in data, the exact value of the CTE and the anisotropy is

unknown. Based on experimental procedures, the studies by Thom *et al.*[50] and Nakashima *et al.*[48] are expected to have the most chemically pure samples. However, little is known about the presence of heterogeneity and plastic strain in these samples and about the effects that these defects would have on the properties. Certainly, knowledge of the CTE is crucial for eventual application of this material in high temperature environments. The CTE will determine the material's compatibility with other materials in a composite, for example, as well as with compounds, such as oxides, that might form on the surface under different environmental conditions.

Oxidation

Several studies exist on the oxidation behavior of Ti_5Si_3 at 700 to 1000°C, and all show fairly good agreement.[52-58] Two temperature regimes have been reported, above and below approximately 900°C. The regimes, as discussed by Abba *et al.*[52], are thought to be due to changes in predominant diffusion mechanisms. Below 900°C, Ti_5Si_3 forms a mixed scale of crystalline TiO_2 (rutile) and amorphous SiO_2. The scale grows inwardly by diffusion of oxygen along grain boundaries or through oxygen vacancies in rutile. Abba *et al.*[52] reported a linear mass gain rate of 0.02 mg/cm^2/hr at 800°C and suggested the growth rate was controlled by the following interfacial reaction:

$$Ti_5Si_3 = 5Ti_{Ti} + 3Si_{Si} + 16V_o^{\bullet\bullet} + 32e'.$$

In slight contrast, Thom *et al.*[54] reported an initial rapid mass gain followed by a faster linear steady state rate of 0.05 mg/cm^2/hr. Based on experimental descriptions, Abba *et al.*[52] are expected to have purer samples. In any case, the external scales reported by both studies

were similar and were expected based on thermodynamic data. However, according to Abba *et al.*[52], an inner mixed scale of TiO or TiN and Si should also form (Fig. 5). The study by Abba *et al.*[52] detected TiN by XRD in only one sample oxidized at 750°C. No other study has detected TiO or Si in oxidized scales of Ti_5Si_3 under any time-temperature conditions; although a study by Kim *et al.*[53] noted the possible existence of TiO based on EDS of samples oxidized at 1000°C for 75 hours.

Above 900°C interstitial titanium diffusion in rutile becomes significant with respect to oxygen vacancy diffusion. This is in full agreement with observations: above 900°C, an external scale of rutile grows outwardly from the inner mixed scale of rutile and SiO_2. Thus, a combination of inwardly diffusing oxygen and outwardly diffusing titanium is responsible for scale growth. The mass gain associated with these diffusion mechanisms at 1000°C was reported by Thom *et al.*[54] to be 14 mg/cm^2 after 60 hours, which is an unacceptably rapid oxidation rate. The scale consisted of an external rutile scale 10μm thick, followed by a mixed scale of rutile and SiO_2 100μm thick, and finally an internal scale of unknown composition that penetrated an additional 100μm.

Based on this research alone, Ti_5Si_3 would not be an acceptable material for use above 900°C in oxygen-rich environments. However, an additional study by Thom *et al.*[56] has shown that the oxidation resistance of Ti_5Si_3 is improved by more than two orders of magnitude through the addition of the interstitial elements boron, carbon and oxygen. The vast improvement in oxidation resistance is due to the higher SiO_2 content in the scale. Although the scales are also composed of a rutile-SiO_2 mixture, the rutile is isolated such that no continuous diffusion path exists through the rutile and to the Ti_5Si_3 interface.

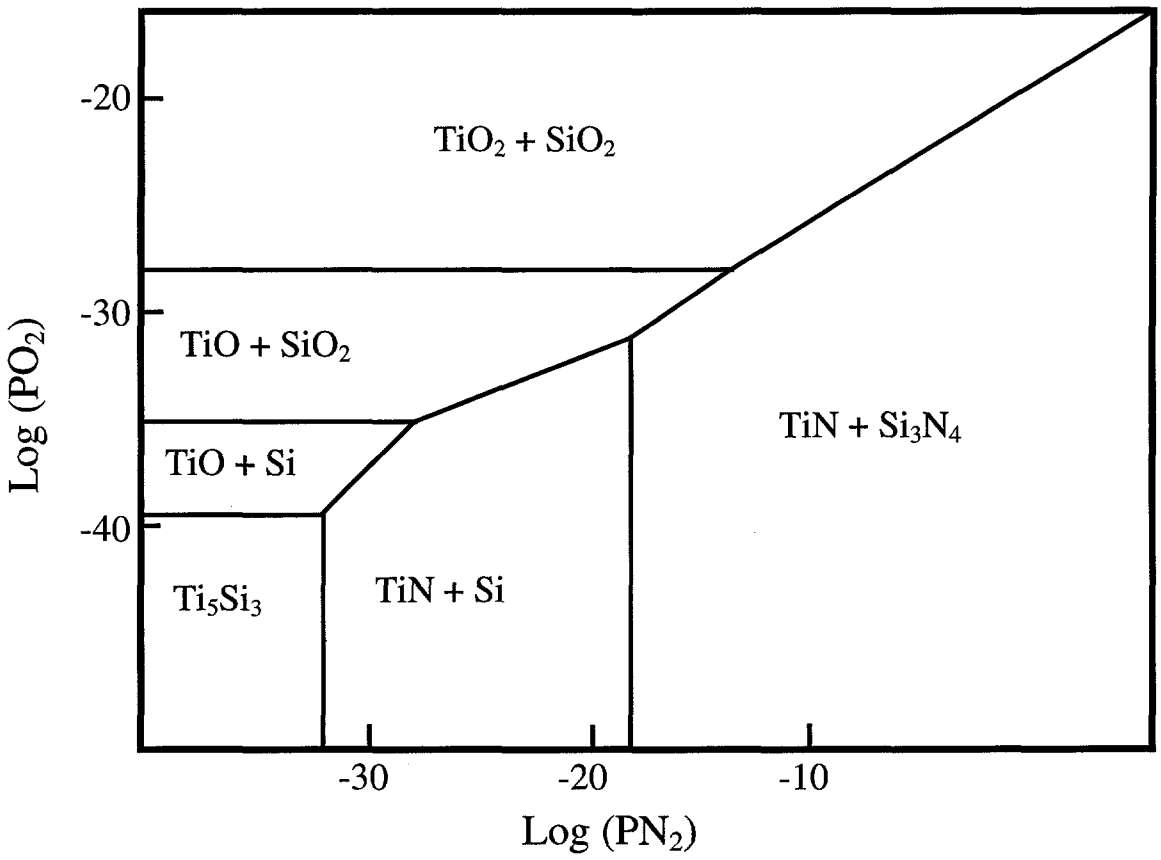

Figure 5. Stability diagram for 5 Ti + 3 Si as a function of partial pressures of nitrogen and oxygen.[52]

Thus, the growth rate now depends on diffusion through SiO_2, which is several orders of magnitude slower than through rutile.

This subtle shift in scale composition was attributed to the lowering of the titanium activity in Ti_5Si_3 due to strong bonding between the titanium atoms and the interstitial atoms; although no further evidence exists to support this hypothesis. In fact, the lack of improvement in the oxidation resistance with the addition of nitrogen seems to contradict this hypothesis. Thus, further work is needed to fully understand the effects of interstitial atoms on the oxidation behavior of Ti_5Si_3.

Summary

As explained in previous sections much of the existing research on Ti_5Si_3 is suspect due to the presence of interstitial carbon, nitrogen and oxygen impurities. This is readily seen in the large scatter of lattice parameters and thermal expansion data on supposedly pure Ti_5Si_3. New data show that the $Ti_5Si_3Z_x$ samples used in the oxidation experiments by Thom *et al.*[56] also contained significant amounts of impurities. Certainly, purer samples are needed to determine the real effect that an interstitial element has on the oxidation behavior.

Since the goal of this study is to determine the effect that a given interstitial element has on the properties of Ti_5Si_3, sample purity is of utmost concern. Thus, the primary method of synthesis is arc melting, from which high purity samples are readily obtained. The properties of interest are: ambient and high temperature structure, including atomic positions and bond distances; crystalline and bulk thermal expansion and thermal expansion anisotropy; oxidation behavior, including scale development and growth.

References

1. Gambino, J.P. and E.G. Colgan. *Material Chemistry and Physics* **52**: 99-146. 1998.
2. Thomas, O., L. Stolt, P. Buaud and J.C. Poler. *Journal of Applied Physics* **68**[12]: 6213-6223. 1990.
3. Liu, R., S. P. Murarka, J. Pelleg. *Journal of Applied Physics* **60**[9]: 3335-3342. 1986.
4. Thomas, O., L. Stolt, P. Buaud and J.C. Poler. *Journal of Applied Physics* **68**[10]: 5133-5139. 1990.
5. Lie, L.N., W.A. Tiller and K.C. Saraswat. *Journal of Applied Physics* **56**[7]: 2127-2132. 1984.
6. Sandwick, T. and K. Rajan. *Journal of Electronic Materials* **19**[11]: 1193-1199. 1990.
7. Gas, P., V. Deline, F.M. D'Heurle, A. Michel. *Journal of Applied Physics* **60**[5]: 1634-1639. 1986.
8. Yarmoshenko, Y.M., S.N. Shamin, L.V. Elokhina, V.E. Dolgih, E.Z. Kurmaev, S. Bartkowski, M. Neumann, D.L. Ederer, K. Goransson, B. Nolang and I. Engstrom. *Journal of Physics: Condensed Matter* **9**: 9403-9414. 1997.
9. Weijs, P.J.W., H.van Leuken, R.A. de Groot, J.C. Fuggle, S. Reiter, G. Wiech and K.H.J. Buschow. *Physical Review B* **44**[15]: 8195-8203. 1991.
10. Weijs, P.J.W., M.T. Czyzyk, J.C. Fuggle, W. Speier, D.D. Sarma and K.H.J. Buschow. *Zeitschrift fur Physik B - Condensed Matter* **78**: 423-430. 1990.
11. Speier, W., E. van Leuken, J.C. Fuggle, D.D. Sarma, L. Kumar, B. Dauth and K.H.J. Buschow. *Physical Review B* **39**[9]: 6008-16. 1989.

12. Speier, W., L. Kumar, D.D. Sarma, R.A. de Groot and J.C. Fuggle. *Journal of Physics* **1**: 9117-29. 1989.

13. Anton, D.L., D.M. Shah, D.N. Duhl and A.F. Giamei. *Journal of Metals* **9**: 12-17. 1989.

14. Anton, K.L. and D.M. Shah. *Materials Research Society Symposium Proceedings*, **133**: 361-371. 1989.

15. Anton, D.L. and D.M. Shah. *International Symposium on Intermetallic Compounds – Structure and Mechanical Properties*: 379-386. 1991.

16. Shah, D. M. and D. L. Anton. *Materials Research Society Symposium Proceedings*, **213**: 63-68. 1991.

17. Shah, D. M. *International Symposium on Superalloys*, **7**: 409-422. 1992.

18. Shah, D.M., D. Berczik, D.L. Anton and R. Hecht. *Materials Science and Engineering* **A155**: 45-57. 1992.

19. Fleischer, R.L. *Journal of Materials Science* **22**: 2281-2288. 1987.

20. Fleischer, R.L., R.S. Gilmore and R.J. Zabala. *Actual Metallics* **37**[10]: 2801-2803. 1989.

21. Fleischer, R.L., D.M. Dimiduk, and H.A. Lipsitt. *Revolutionizing Materials Science* **19**: 231-63. 1989.

22. Fleischer, R.L. and A.I. Taub. *Journal of Materials*: 8-11. 1989.

23. Fleischer, R.L. and R.J. Zabala. *Metallurgical Transactions* **21A**: 2709-2715. 1990.

24. Fleischer, R.L. *Journal of Materials Research* **8**[1]: 49-67. 1993.

25. Meyer, M. K. and M. Akinc *Journal of the American Ceramic Society* **79**[4]: 938-44. 1996.

26. Takasugi, T. *Materials Research Society Symposium Proceedings*, **213**: 403-416. 1991.

27. Grabke, H. J. and G. H. Meier. *Oxidation of Metals* **44**[1.2]: 147-177. 1995.

28. Seifert, H.J., H.L. Lukas and G. Petzow. *Z. Metallkd* **87**[1]: 2-13. 1996.

29. Murray, J.L. Si-Ti (Silicon-Titanium). Binary Alloy Phase Diagrams. Metals Park, Ohio Ed. T. B. Massalski, American Society for Metals: 2054-2057. 1986.

30. Svechnikov, V.N., Y.A. Kocherzhinskii and E.A. Shishkin. *Doklady Akademii Nauk SSSR* **193**[2]: 393-396. 1970.

31. Al-Shahery, G.Y.M., R. Steadman and I.J. McColm. *Journal of the Less-Common Metals* **92**: 329-338. 1983.

32. Button, T.W. and I.J. McColm. *Journal of the Less-Common Metals* **97**: 237-244. 1984.

33. Corbett, J.D., E. Garcia, A.M. Guloy, W. Hurng, Y. Kwon and E.A Leon-Escamilla. *Chemical Materials* **10**: 2824-2836. 1998.

34. Schlesinger, M.E. *Chemical Reviews* **90**: 607-628. 1990.

35. Archer, D.G., D. Filor, E. Oakley and E.J. Cotts. *Journal of Chemical and Engineering Data* **41**: 571-575. 1996.

36. Barin, I. Thermochemical Data of Pure Substances, 2nd ed. Weinhiem; New York, VCH 1993.

37. Wakelkamp, W. Eindhoven University of Technology Thesis, Eindhoven, Netherlands. 1991.

38. Sambasivan, S. and W.T. Petuskey. *Journal of Materials Research* **9**[9]: 2362-2369. 1994.

39. Goldstein, J.I., S.K. Choi, F.J.J. van Loo, F.B. Guillaume and R. Metselaar. *Journal of the American Ceramic Society* **78**[2]: 313-322. 1995.

40. Thom, A.J., V. Young and M. Akinc. Submitted to *Journal of Alloys and Compounds.*

41. Pietrokowsky, P. and P. Duwez. *Transactions of the American Institute of Mining and Metallurgical Engineers* **191**: 772-773. 1951.

42. Quakernaat, J. and J.W. Visser. *High Temperatures - High Pressures* **6**: 515-517. 1974.

43. Swanson, H.E. N. and T. Gilfich. *U.S. National Bureau of Standards Circular* **539**[8] 64-65. 1959.

44. Kajitani, T., T. Kawase, K. Yamada and M. Hirabayashi. *Transactions of The Japan Institute of Metals* **27**[9]: 639-647. 1986.

45. Radhakrishnan, R., J. Williams, M. Kramer, and M. Akinc, *Ceramic Engineering and Science Proceedings*, **19**(3): 381-88. 1998.

46. Margulies, L., M.J. Kramer, R.W. McCallum, S. Kycia, D.R. Haeffner, J.C. Lang and A.I. Goldman. Submitted to *Review of Scientific Instruments.*

47. Garcia, E. and J.D. Corbett *Inorganic Chemistry* **29**[18]: 3274-3282. 1990.

48. Nakashima, T. and Y. Umakoshi. *Philosophical Magazine Letters* **66**[6]: 317-321. 1992.

49. Rosenkranz, R. and G. Frommeyer. *Materials Science and Engineering* **A152**: 288-294. 1992.

50. Thom, A.J., M. Akinc, O.B. Cavin and C.R. Hubbard. *Journal of Materials Science Letters* **13**: 1657-1660. 1994.

51. Ikarashi, Y., K. Ishizaki, T. Nagai, Y. Hashizuka and Y. Kondo. *Intermetallics* **4**[1]: 141-145. 1996.

52. Abba, A., A. Galerie and M. Caillet. *Oxidation of Metals* **17**[1]: 43-54. 1982.

53. Kim, Y., A.J. Thom and M. Akinc. *Processing and Fabrication of Advanced Materials for High Temperature Applications*, **2**: 189-208. 1993.

54. Thom, A.J., Y. Kim and M. Akinc. *Materials Research Society Symposium Proceedings*, **288**: 1037-1042. 1992.

55. Thom, A. J., M. K. Meyer, Y. Kim and M. Akinc. *Processing and Fabrication of Advanced Materials*, **3**: 413-438. 1994.

56. Thom, A. J. and M. Akinc. *Advanced Ceramics for Structural and Tribological Applications*: 619-627. 1995.

57. Thom, A.J., M.K. Meyer, J.J. Williams and M. Akinc. *Processing and Fabrication of Advanced Materials*, **4**: 139-142. 1995.

58. Murata, Y., T. Higuchi, Y. Takeba, M. Morinaga and N. Yukawa. *International Symposium on Intermetallic Compounds – Structure and Mechanical Properties*: 627-631. 1991.

CHAPTER 2: EFFECTS OF INTERSTITIAL ADDITIONS ON THE STRUCTURE OF Ti_5Si_3

A paper submitted to the Journal of Materials Research

J.J. Williams, M.J. Kramer, M. Akinc and S.K. Malik

Abstract

Changes in the structure of Ti_5Si_3 were measured by x-ray and neutron diffraction as carbon, nitrogen or oxygen atoms were systematically incorporated into the lattice. Additionally, the lattice parameters and variable atomic positions of pure Ti_5Si_3 were determined to be a= 7.460Å, c= 5.152Å, x_{Ti}= 0.2509 and x_{Si}= 0.6072. The measured trends in lattice parameters as carbon, nitrogen or oxygen atoms are added to Ti_5Si_3 show that most of the previous studies on supposedly pure Ti_5Si_3 were actually contaminated by these pervasive light elements. Also, oxygen and carbon additions were shown to strongly draw in the surrounding titanium atoms – evidence for bonding between these atoms. The bonding changes that occur on addition of carbon, nitrogen or oxygen act to decrease the measured anisotropic properties of Ti_5Si_3 such as thermal expansion.

I. Introduction

Published values of the lattice, thermodynamic quantities and thermal properties of Ti_5Si_3 from 1985 to present show considerable scatter. For example, published lattice

parameters vary by 0.5%[1-6], thermal expansion coefficients by 90%[4-8] and enthalpy of formation by 15%[2,9,10], all of which are significant variations. Without question, a primary reason for this scatter in properties is the presence of interstitial impurities. Two recent studies by Radhakrishnan *et al.*[11] and Thom *et al.*[12] highlight the improbability of synthesizing and consolidating Ti_5Si_3 without interstitial contamination of carbon, nitrogen and oxygen. Particularly, studies that use metal powder as a starting material are highly likely to result in oxygen impurity of at least one to two weight percent. Not only titanium powder, but yttrium, zirconium and other early transition metal powders that have a high affinity for carbon, nitrogen and oxygen are expected to yield silicides with a significant impurity content after synthesis and processing. Furthermore, studies on Ti_5Si_3 with carbon, nitrogen or oxygen intentionally added show a very dramatic effect on crystal and thermal properties, an effect that does account for some of the scatter in the literature data. For example, Thom *et al.*[5] have shown a reduction in thermal expansion anisotropy by 20% when carbon is intentionally added to Ti_5Si_3.

In conjunction with contaminated starting materials, an additional reason for the difficulty in synthesizing Ti_5Si_3 without impurities is the presence of large, unoccupied interstices in the lattice. Figure 1a shows a (001) orthographic projection of the hexagonal Ti_5Si_3 lattice, which has Mn_5Si_3 as its prototype structure (Space Group = $P6_3/mcm$). The occupied atomic sites for pure Ti_5Si_3 are:

Ti at 4d sites at (1/3, 2/3, 0)

Ti at 6g sites at (x_{Ti}, 0, 1/4), where $x_{Ti} \approx 0.25$

Si at 6g sites at (x_{Si}, 0, 1/4), where $x_{Si} \approx 0.61$

Impurity atoms of carbon, nitrogen and oxygen would occupy interstices located at (0, 0, 0) 2b sites, herein described as Z sites. As seen in Figure 1b, these interstices and the surrounding Ti^{6g} atoms form trigonal antiprisms along the c-axis. This may be alternatively described as a chain of (trigonally distorted) face-shared octahedra formed by Ti^{6g} atoms along the c-axis with a Z site at the center of each octahedron. The Si atoms form a chain of distorted face-shared trigonal antiprisms also parallel to the c-axis such that one Ti^{4d} site is at the center of each antiprism. This leads to a stacking sequence along the c-axis of ABAC where A planes consist solely of Z and Ti^{4d} sites. The B and C planes contain the Ti^{6g} and Si sites such that atoms on B planes are rotated 180° with respect to atoms on C planes.

The primary goal of this study is to measure changes in lattice parameters and atomic positions by x-ray and neutron diffraction when carbon, nitrogen or oxygen is intentionally added to Ti_5Si_3. Because purity is of utmost concern, samples were synthesized via arc melting of bulk pieces, not powders. Knowledge of lattice changes as a function of interstitial content can be used to estimate the compositions of previous studies that reported the lattice parameters of supposedly pure Ti_5Si_3. This will aid in de-convoluting the inherent properties of Ti_5Si_3 from those of Ti_5Si_3 contaminated with carbon, nitrogen and oxygen. Additionally, changes in bonding may be inferred from the measured structural changes on addition of interstitial atoms to aid in explaining the effects of interstitial content on the thermal and electronic properties of Ti_5Si_3.

Three systematic studies currently exist on the effects of interstitial content on the structure of Ti_5Si_3. One by Kajitani *et al.*[1] has shown that interstitial hydrogen tends to contract the a-axis and expand the c-axis. Another study, by Thom and Akinc[12], has shown

that interstitial nitrogen and oxygen tend to contract both the a-axis and c-axis. The measured trend in lattice as a function of nitrogen enabled Thom and Akinc[12] to estimate the level of nitrogen impurity in a sample synthesized by Quakernaat *et al.*[13] based on Quakernaat's reported lattice parameters. The third study by Thom *et al.*[14] measured the lattice changes by single crystal and powder x-ray diffraction of $Ti_5Si_3Z_X$ for Z= boron, carbon, nitrogen or oxygen. Whereas the effects of nitrogen and oxygen were identical to the previous study, boron and carbon tended to expand the lattice, probably because of their larger size. All interstitial additions tended to pull in the surrounding titanium atoms, which indicates a significant change in bonding. This bonding change could aid in explaining an interstitial atom's effect on the thermal and electric properties.

Unlike previous studies, this study includes structural refinements at several levels of interstitial content for each interstitial atom so that trends may be clearly discerned. Also, a strong effort was made to improve the sampling statistics and measurement accuracy over those of previous studies.

II. Experimental Procedure

All materials in this study were synthesized via arc melting. Arc melting was performed in an ultra high purity (UHP) argon atmosphere on a water-chilled copper hearth. Samples, which weighed approximately 10g each, were melted at least three times via a non-consumable tungsten electrode. This procedure led to weight losses of less than 0.5 wt% in most samples. The likely reasons for weight loss were due to use of starting materials with high rates of disassociation (TiO_2 and TiN) at arc melting temperatures and spalling of brittle

materials (Ti_5Si_3, Si, TiO_2 and TiN) during arc melting.

The starting materials included sponge titanium (Timet, 99.7 wt%), silicon pieces (Alfa Æsar, 99.9999 wt%), spectrographic grade graphite electrodes for carbon, titanium nitride for nitrogen (Johnson Matthey, 99.8 wt%) and titanium dioxide for oxygen (Fischer Scientific, 99.8 wt%). The sponge titanium was pre-melted two times to volatilize surface contamination before being used in synthesis of $Ti_5Si_3Z_X$. Also, the titanium nitride and oxide, which were purchased as powders, were pressed into pellets and partially sintered before using. This practice reduces material loss since the force exerted by an electric arc easily blows around powders. X-ray diffraction and metallography on the starting materials have confirmed that they were single phase. Additionally, lattice parameter measurements for TiN and TiO_2 have shown them to be on stoichiometry, and lattice parameters for the titanium metal indicate a negligible interstitial content.

Changes in lattice parameters of Ti_5Si_3 on addition of carbon, nitrogen or oxygen were measured by x-ray diffraction (Scintag Model X1 with solid-state detector). Samples were of arc melted material ground to < 20μm in an agate mortar with 10 wt% silicon (NIST SRM 640b) added as an internal standard. Diffraction scans were run on 0.15g samples from a two-theta of 10° to 130° at a step size of 0.03° and counting time of 3 seconds. The x-ray source was copper Kα; the source and detector slits were 2 to 4mm and 0.5 to 0.3mm, respectively. Lattice parameters, atomic positions, thermal parameters and preferred orientations were refined using Rietveld software (GSAS, Los Alamos National Laboratory 1985). Generally, the standard error of measurement was less than 0.0001Å for lattice parameters and less than 0.001Å for atomic positions. The weighted residuals, wR_p, were

0.10 to 0.15 for samples with interstitial carbon or oxygen and 0.15 to 0.20 for samples with interstitial nitrogen. The weighted residual function is defined as a sum over the entire diffraction pattern:

$$wR_p = [\Sigma\, w(I_o-I_c)^2]/[\Sigma\, wI_o^2] \quad (1)$$

I_o is the observed intensity, I_c the calculated intensity, and the weights, w, are assumed to be uncorrelated. On average, $Ti_5Si_3N_X$ compositions yielded measurably broader diffraction lines than other samples. Specifically, samples with nitrogen were on average 20% broader than the silicon standard (lines from samples with carbon and oxygen were similar in width to those of the silicon standard). This broadening suggests a slight heterogeneity and/or a higher defect concentration.

Using the Missouri University Research Reactor (MURR), the atomic positions and site occupancies of $Ti_5Si_3C_X$, (X = 0.15, 0.25 and 0.5; nominally) and of $Ti_5Si_3O_Y$ (Y = 0, 0.15, 0.25, 0.35, 0.5; nominally) were determined from neutron diffraction. Scans were run from 10 to 110° with a source wavelength of 1.765Å for samples with interstitial carbon and of 1.486Å for samples with interstitial oxygen. Wavelength was selected by a curved monochromator, and a position sensitive detector recorded intensities. Diffraction spectra were analyzed using the same Rietveld software as mentioned above. The wR_p was less than 0.06 for all refined neutron spectra, and the standard error for atomic position measurements was less than 0.0003Å. The titanium positions, x_{Ti}, and silicon positions, x_{Si}, refined from neutron diffraction spectra were within 0.5% of those refined from x-ray spectra. However, unlike the x_{Ti} positions, the correlation between the x_{Si} positions obtained from neutron and x-ray diffraction spectra was poor. This difference may be attributed to a smaller x-ray cross-

section for silicon atoms relative to titanium atoms. For this reason, the x_{Si} positions obtained from x-ray diffraction spectra were not used in atomic separation calculations.

Oxygen and nitrogen content were measured on a Leco TC-436 analyzer; carbon content was measured on a Horiba EMIA-520 analyzer. The accuracy of these instruments, based on calibration standards, are reported to be ±2% relative for carbon, ±4% for oxygen and ±10% for nitrogen. Samples were sub-millimeter size granules weighing 0.2 to 0.5g, total. The total carbon, nitrogen and oxygen impurities for all samples, as measured by these techniques, were less than 0.02 formula units. However, samples with oxygen or nitrogen intentionally added showed less nitrogen and oxygen than the nominal starting composition (up to 20 wt% less for samples with a nominal interstitial content greater than 0.5 formula units). This validates the statement that some of the measured weight loss during arc melting was due to the volatilization of oxygen or nitrogen. In contrast, the measured carbon content of samples with carbon intentionally added was within 6 wt% of the nominal composition.

The carbon and oxygen content, as measured by chemical analysis, were within 5 wt% of the site occupancy refinements obtained from the neutron diffraction spectra, a difference that is similar to the expected accuracy of both measurement techniques. The fact that chemical analysis and neutron diffraction yielded identical results (within measurement accuracy) provides direct evidence that the vast majority of the carbon and oxygen (and nitrogen) in the arc melted ingots are located in the interstices at (0, 0, 0) in $Ti_5Si_3Z_X$ as was anticipated.

III. Results and Discussion

A. X-ray Spectra

Figure 2 gives the experimental and calculated x-ray spectra of $Ti_5Si_3O_{0.019}$ and $Ti_5Si_3C_{0.47}$. Most X-ray spectra confirmed that samples were single phase and well crystallized. Samples that were not single phase included $Ti_5Si_{3.12}$, $Ti_5Si_3C_{1.0}$ and $Ti_5Si_3O_{1.0}$, which were intentionally synthesized in two-phase regions. Note the difference in (100) peak intensity relative to the (110) peak intensity for the two spectra as illustrated in Figure 2. The ratio of the (100) to (110) integrated peak intensity as a function of interstitial content is plotted in Figure 3. Integrated intensities were determined by fitting both diffraction lines to a Pearson VII profile. As a first approximation, the interstitial content of Ti_5Si_3 can be estimated by using the integrated intensity ratio of the (100) and (110) peaks and comparing to Figure 3. However, longer counting times are required to accurately estimate interstitial content below approximately 0.1 and above 0.5 formula units. At these levels of interstitial content, one of the two peaks was generally too small to accurately estimate the intensity.

Plotted in Figure 3 are also the calculated integrated intensity trends for Ti_5Si_3 with carbon or oxygen incorporations. These trends were calculated by:

$$I^{100}/ I^{110} = [S \cdot Lp^{100} \cdot M^{100} \cdot |F^{100}|^2] / [Lp^{110} \cdot M^{110} \cdot |F^{110}|^2] \qquad (2)$$

Lp is the Lorentz-polarization term, M is the line multiplicity (equal to 6 for both lines), $|F|^2$ is the square of the structure factor and S is a scaling factor equal to approximately 0.5. The need for a scaling factor is most likely due to neglecting an absorption coefficient or less likely, due to preferred orientation. Thus, this scaling factor will be different for different types of diffractometers. As such, one would need one sample of known

composition to adjust the trend in Figure 3 for a different diffractometer. Although the explicit expressions for the calculated trends are quite unwieldy, by ignoring the anomalous dispersion correction to the scattering factors, a good approximation is obtained:

$$\frac{I^{100}}{I^{110}} = \frac{S\,[A_Z^{100}X + 2A_{Ti}^{100}\cos(2\pi x_{Ti}) + A_{Si}^{100}(2\cos(2\pi x_{Si}) + 1)]^2}{[A_Z^{110}X + A_{Ti}^{110}(\cos(2\pi x_{Ti}) + \cos(4\pi x_{Ti}) + 2) + A_{Si}^{110}(\cos(2\pi x_{Si}) + \cos(4\pi x_{Si}))]^2} \quad (3)$$

$$A_{atom}^{hkl} = 2f_{atom}^{hkl} \cdot T_{atom}^{hkl} \cdot (Lp^{hkl})^{1/2} \quad (4)$$

Regarding Equations (3) and (4), X is the interstitial content, f_{atom}^{hkl} is the atomic scattering factor and T_{atom}^{hkl} is the thermal parameter for a particular atom and for a given diffraction line. The scattering factors, thermal parameters and Lorentz- polarization term are actually functions of X because incorporation of interstitial atoms changes the lattice and hence, slightly shifts a given diffraction line. Although, when performing the calculations, this X dependence is quite negligible. However, the atomic positions x_{Ti} and x_{Si}, which are also (linear) functions of X (see Fig. 5), must be treated as such to obtain accurate calculated intensities.

B. Lattice Parameters and Atomic Positions

Figure 4 gives the changes in lattice parameters of Ti_5Si_3 as a function of interstitial content. The horizontal error bars represent the accuracy of measuring the carbon, nitrogen and oxygen content (see Section II). The vertical error bars represent 3σ, where σ is the average standard deviation of three replicate measurements of five different compositions. Along each ordinate is a bar that marks the range of lattice values reported in the literature for supposedly pure Ti_5Si_3. Based on this figure, the scatter in reported lattice parameters can be

explained by combinations of interstitial carbon, nitrogen and oxygen, as well as excess silicon. The large expansion of the lattice due to the addition of excess silicon suggests that excess silicon also occupies the interstitial position. Also, note that the trends in lattice parameters as a function of carbon, oxygen and nitrogen all converge to a similar value when extrapolated to zero interstitial content. The lattice parameters for pure Ti_5Si_3, as listed in Table I, were determined by extrapolating the oxygen trends to the zero interstitial level. Similarly, x_{Ti} and x_{Si} for pure Ti_5Si_3 were calculated by extrapolating the atomic position data shown in Figure 5. These values are in good agreement with those found by Kajitani *et al.*[1] Additionally, most trends show a relative extremum near the 0.5 interstitial level, which corresponds to the point at which the interstices become more than half-filled. The reason for the extrema may be due to close Z-Z separations, which will be discussed in the next section.

Although not shown, excess titanium actually causes a relatively negligible contraction of the lattice. This would indicate that, unlike excess silicon, excess titanium is not incorporated into the Z site at (0, 0, 0). However, this result should be regarded with caution because samples with excess silicon and titanium almost certainly require thermal annealing after arc melting to achieve an equilibrium state. The reason is that unlike the other samples which solidified congruently, samples with excess silicon and titanium were in a two-phase region during solidification; and as such, these samples most likely had a significant chemical heterogeneity. Evidence for this was manifested as broader diffraction lines than the single-phase compositions.

Also plotted in Figure 4 are the powder x-ray diffraction data of Thom *et al.*[14] The much larger vertical error bars from Thom *et al.*[14] are due to samples that are more

heterogeneous and/or a lack of an internal standard during x-ray diffraction. Regardless of these inaccuracies, the trends in lattice parameters between studies are similar.

C. Atomic Separations

Nearest-neighbor separations in Ti_5Si_3 calculated from the extrapolated structural parameters are listed in Table II and are illustrated in Figure 1. Based on first-principle calculations, bonding in Ti_5Si_3 primarily consists of d(Ti)-p(Si) covalent bonding below the Fermi level and d(Ti)-d(Ti) interaction at and around the Fermi level.[15] The crystal structure and atomic separations suggest that most of the d(Ti)-p(Si) bonding falls in the B and C planes and most of the d(Ti)-d(Ti) interaction parallel to the c-axis. For example, three of the five nearest silicon atoms to Ti^{6g} (Ti^{6g} -Si II and Ti^{6g} -Si III) lie in the (001) plane; the others (Ti^{6g} -Si I) lie approximately 68° above/below this plane but are 5 to 7% farther away. In addition, the six silicon atoms surrounding Ti^{4d} lie only 29° above/below the (001) plane and thus have a significantly larger bonding component in the (001) plane. In the case of d(Ti)-d(Ti) interaction, all of the Ti nearest-neighbors to Ti^{4d} lie along the c-axis, and four of the six Ti nearest-neighbors to Ti^{6g} lie 54° above/below the (001) plane. Also note that the Ti^{6g} atomic separations are over 23% longer than the Ti^{4d} separations; therefore, the Ti^{6g} atomic interactions are expected to be much weaker. This picture of weak metallic bonding in the <001> direction and strong covalent bonding in the <100> direction is corroborated by other experimental evidence: both the electrical conductivity and thermal expansion are roughly twice as large along the <001> direction than along the <100> direction.[7]

The change in atomic separations as carbon or oxygen is added to Ti_5Si_3 is illustrated

in Figure 6. As seen in Figure 6, the changes due to carbon and oxygen are in general very similar. The most dramatic effects are the decrease of the Ti^{6g} -Ti^{6g} and Ti^{6g} -Z separations and increase of the Ti^{6g} -Si separations as interstitial content increases. These effects are a direct result of increased bonding between the Ti^{6g} and interstitial Z atoms and a possible reduction in bonding between the Ti^{6g} and Si atoms. Based on these bonding changes, one might expect a reduction of covalent bonding in the <100> direction and an increase of covalent/ionic bonding in the <001> direction. This is in full agreement with Thom *et al.*[5] who showed an increase in the thermal expansion along the <100> direction and a decrease along the <001> direction as carbon is added to Ti_5Si_3.

Further insight into the bonding may be inferred by comparing atomic separations in $Ti_5Si_3Z_X$ to other compounds. One comparison, as mentioned by Ekman and Ozolins[15], is that the Ti^{4d}-Ti^{4d} separation in $Ti_5Si_3Z_X$ is approximately 10% shorter than in titanium metal. This close separation is probably a result of significant electronic mixing with the six surrounding silicon atoms and a consequent reduction in orbital mixing between the two surrounding titanium atoms. In fact, the Ti^{4d}-Si separations in $Ti_5Si_3Z_X$ are only one to two percent longer than the shortest Ti-Si separation seen in $TiSi_2$ – a compound with very strong Ti-Si covalent mixing. However, direct d(Ti^{4d})-d(Ti^{4d}) interaction must also exist according to densities of state calculations. Based on electron deformation maps, Ekman and Ozolins[15,16] suggested that the electronic mixing between Ti and Si atoms is best described by complex multi-centered bonds and not by simple two-atom covalent bonds.

Another useful comparison is made between $Ti_5Si_3Z_X$ and TiZ for Z= carbon or oxygen. Both TiC and TiO form in the NaCl crystal structure; thus, the carbon and oxygen

atoms are surrounded by six titanium atoms similar to the octahedral coordination found in $Ti_5Si_3Z_X$. However, the Ti-O separation in $Ti_5Si_3O_X$ is six to eight percent longer than in TiO, and the Ti-C separation in $Ti_5Si_3C_X$ is two to four percent longer than in TiC. Additionally, whereas the coordinate octahedra in $Ti_5Si_3Z_X$ are face-shared, the octahedra in TiZ are edge shared. The face-shared octahedra in $Ti_5Si_3Z_X$ result in significantly closer Z-Z separations than those in TiZ. Whereas Ti-Z bonding leads to lattice contraction below 0.5 formula units of Z, the short Z-Z separations may be the cause of subsequent lattice expansion as more than 0.5 formula units of Z atoms are added.

IV. Conclusions

Much of the research on the properties of Ti_5Si_3 is marred by the presence of uncontrolled impurities of carbon, nitrogen and oxygen. This is readily seen by comparison of reported lattice parameters to the measured trends in lattice parameters as carbon, nitrogen or oxygen is intentionally added to Ti_5Si_3. The amount of interstitial contamination can be quickly estimated by measuring the integrated intensity ratio of the (100) and (110) diffraction peaks. Additionally, the highly anisotropic thermal expansion of Ti_5Si_3 is a direct result of strong covalent bonding in the (001) planes and metallic bonding along the <001> direction. However, additions of interstitial atoms change the bonding such as to reduce this anisotropy. These changes in bonding were seen in the effect interstitial atoms have on atomic separations. The most significant changes include the reduction of Ti^{6g} -Ti^{6g} and Ti^{6g} -Z distances and the expansion of Ti^{6g} -Si distances. This suggests a relative increase of covalent/ionic bonding along the <001> direction and a relative reduction of covalent

bonding in the (001) planes.

V. Acknowledgments

Ames Laboratory is operated for the U.S. Department of Energy by Iowa State University under contract number W-7405-ENG-82. The work at MURR was supported by the U.S. Department of Energy grant No. DE-FE02-90ER45427.

References

1. T. Kajitani, T. Kawase, K. Yamada and M. Hirabayashi Trans. Japan Inst. Metals **27**[9], 639 (1986).
2. D. G. Archer, D. Filor, E. Oakley and E. Cotts, J. Chem. Eng. Data **41,** 571 (1996).
3. R. Mitra, Metall. Mater. Trans. **A29,** 1629 (1998).
4. R. Rosenkranz, G. Frommeyer and W. Smarsly, Mater. Sci. Eng. **A152,** 288 (1992).
5. A.J.Thom, M. Akinc, O. B. Cavin and C.R. Hubbard, J. Mater. Sci. Lett. **13,** 1657 (1994).
6. L. Zhang and J. Wu, Scripta Mater. **38**[2], 307 (1998).
7. T. Nakashima and Y. Umakoshi, Philos. Mag. Lett. **66**[6], 317 (1992).
8. Y. Ikarashi, K. Ishizaki, T. Nagai, Y. Hashizuka and Y. Kondo, Intermet. **4**[1], 141 (1996).
9. Barin, *Thermochemical Data of Pure Substances, 2nd* (Weinhiem, New York: VCH, 1993).
10. H. J. Seifert, H. L. Lukas and G. Petzow, Z. Metallkd. **87**[1], 2 (1996).
11. R. Radhakrishnan, J.J. Williams, M. Kramer and M. Akinc, Ceram. Eng. Sci. Proc. **19**[3],

381 (1998).

12. A.J. Thom and M. Akinc, Ceram. Eng. Sci. Proc. **18**[4], 57 (1997).

13. J. Quakernaat and J. W. Visser, High Temp. - High Press. **6,** 515 (1974).

14. A.J. Thom, V.G. Young and M. Akinc, submitted to J. Alloys Compds. (1999).

15. M. Ekman and V. Ozolins, *Properties of Complex Inorganic Solids*, edited by Gonis, (Plenum Press, New York, 1997) 191.

16. M. Ekman and V. Ozolins, Phys. Rev. B. **57**[8], 4419 (1998)

Figure Captions

Fig. 1. (a) (001) orthographic projection of the Ti_5Si_3Z crystal structure. The Ti^{6g} octahedra and Si antiprisms are outlined at top left and bottom left, respectively. Both the Ti^{6g} and Si atoms occupy variable positions along the <100> direction, x_{Ti} and x_{Si}. (b) Portion of the $Ti_5Si_3Z_x$ crystal structure, illustrating how the antiprisms, which are higlighted in (a), are stacked along the c-axis. Also note the ABAC stacking sequence along the c-axis.

Fig. 2. XRD spectra of (a) $Ti_5Si_3O_{0.019}$ and (b) $Ti_5Si_3C_{0.47}$. From top to bottom of each plot is: diffraction spectrum, silicon peak markers, Ti_5Si_3 peak markers, and difference plot. The difference plot is the difference between the observed spectra and the calculated spectra using Rietveld refinement.

Fig. 3. Measured integrated intensity ratio of (100) peak divided by (110) peak. Solid curves represent theoretical integrated intensity ratios based on carbon or oxygen additions.

Fig. 4. Changes in the (a) a-lattice parameter or (b) c-lattice parameter as a function of formula units (f.u.) of interstitial atoms. The open symbols represent data taken from Thom *et al.*[14] The bars along the ordinate represent literature values for reportedly pure Ti_5Si_3. Values extrapolated back to zero were attributed to truly pure Ti_5Si_3.

Fig. 5. Atomic positions, x_{Ti} and x_{Si}, as a function of formula units (f.u.) of carbon or oxygen. Values extrapolated back to zero were attributed to pure Ti_5Si_3.

Fig. 6. Difference in atomic separations relative to atomic separations in Ti_5Si_3 for (a) $Ti_5Si_3C_X$ or (b) $Ti_5Si_3O_X$. The zero level (Ti_5Si_3) is based on extrapolated values listed in Table I. The values in parentheses are slopes of least-squares fitted lines in units of Angstroms/formula units.

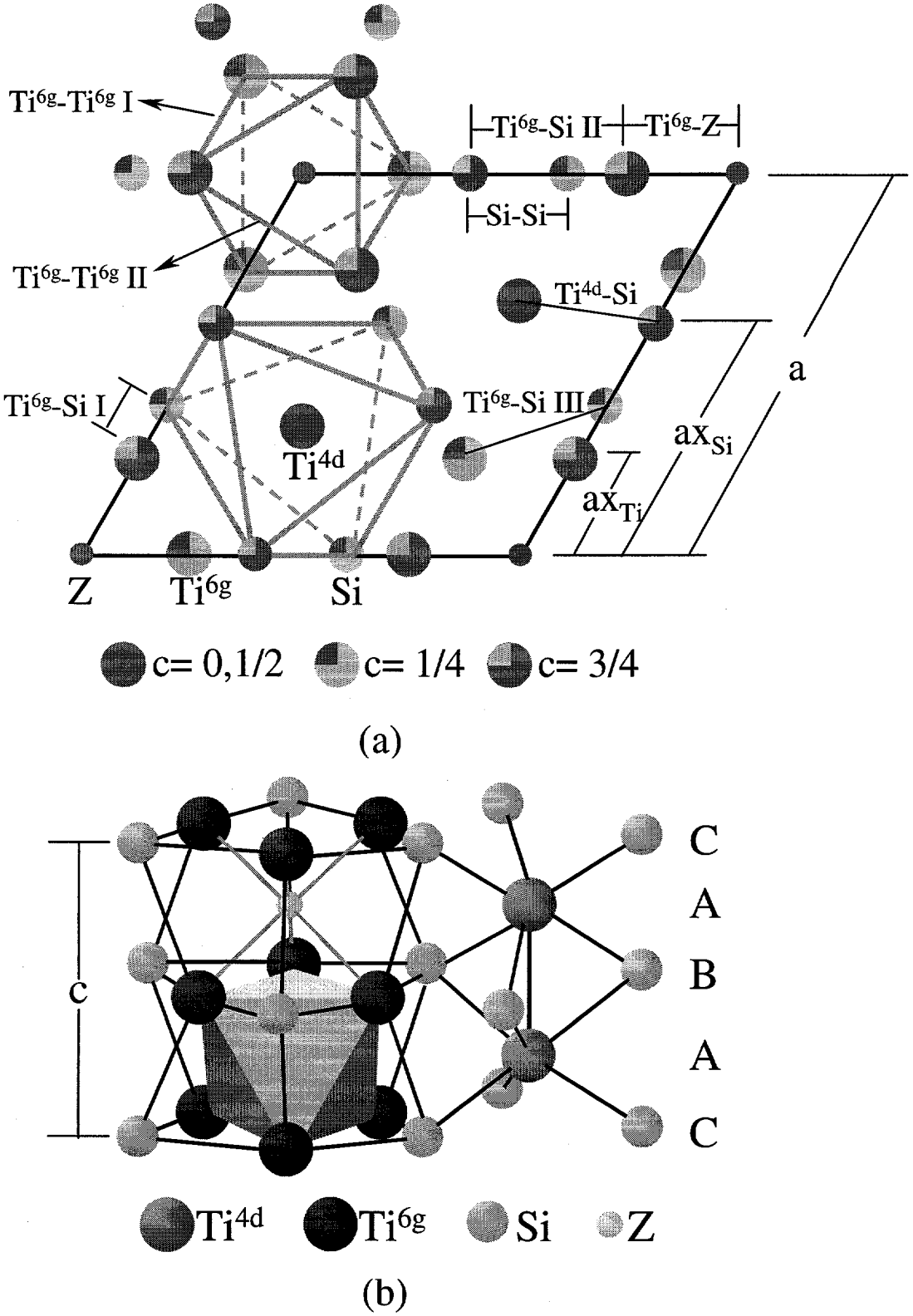
Ti6g-Ti6g I
Ti6g-Ti6g II
Ti6g-Si I
Ti6g-Si II
Ti6g-Z
Si-Si
Ti4d-Si
Ti6g-Si III
Ti4d
axSi
axTi
a
Z
Ti6g
Si
c= 0,1/2
c= 1/4
c= 3/4
(a)
c
C
A
B
A
C
Ti4d
Ti6g
Si
Z
(b)

Figure 1.

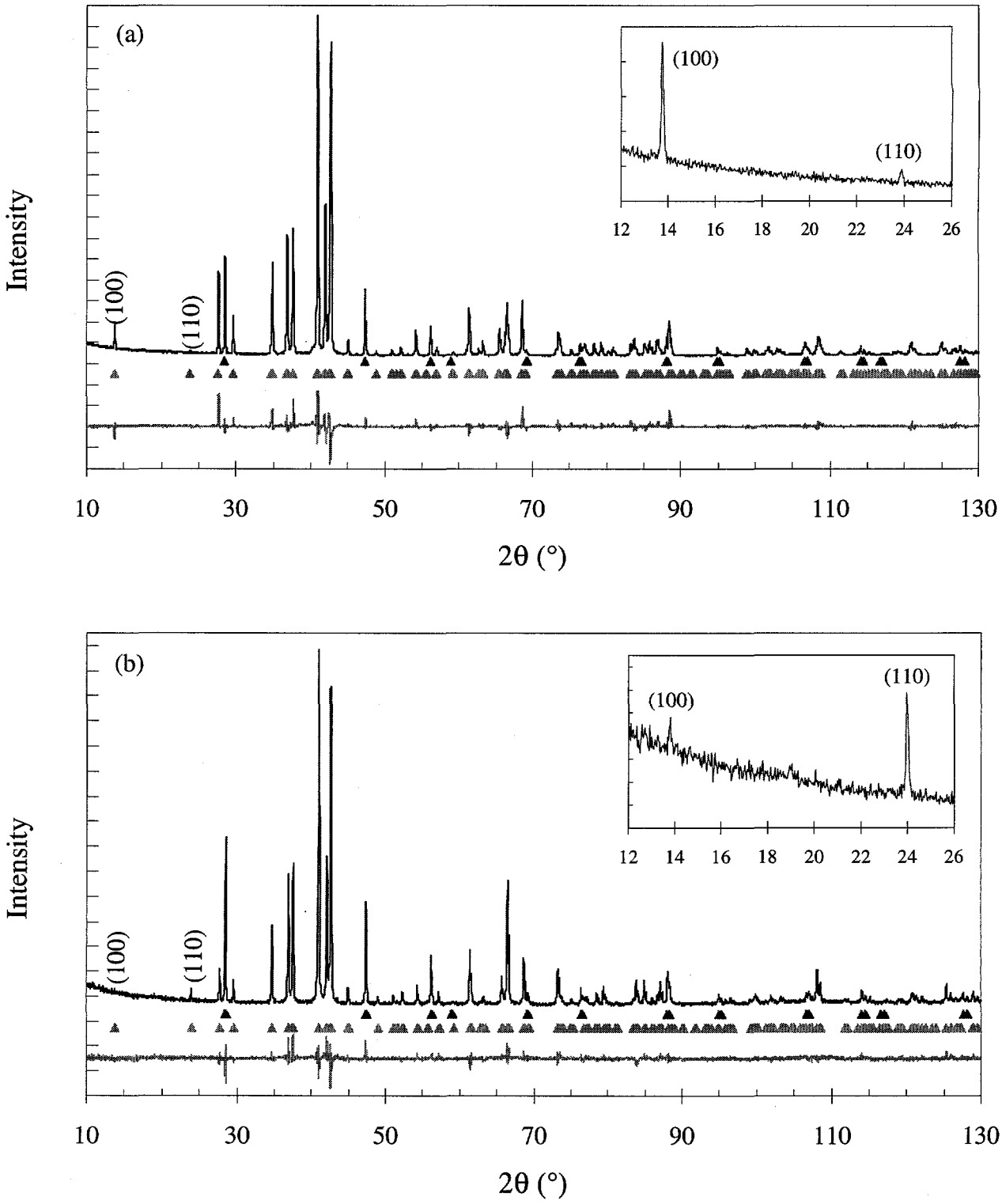
(a)
(100)
(110)
Intensity
10
30
50
70
90
110
130
2θ (°)
12
14
16
18
20
22
24
26
(b)
(100)
(110)
Intensity
10
30
50
70
90
110
130
2θ (°)
12
14
16
18
20
22
24
26

Figure 2.

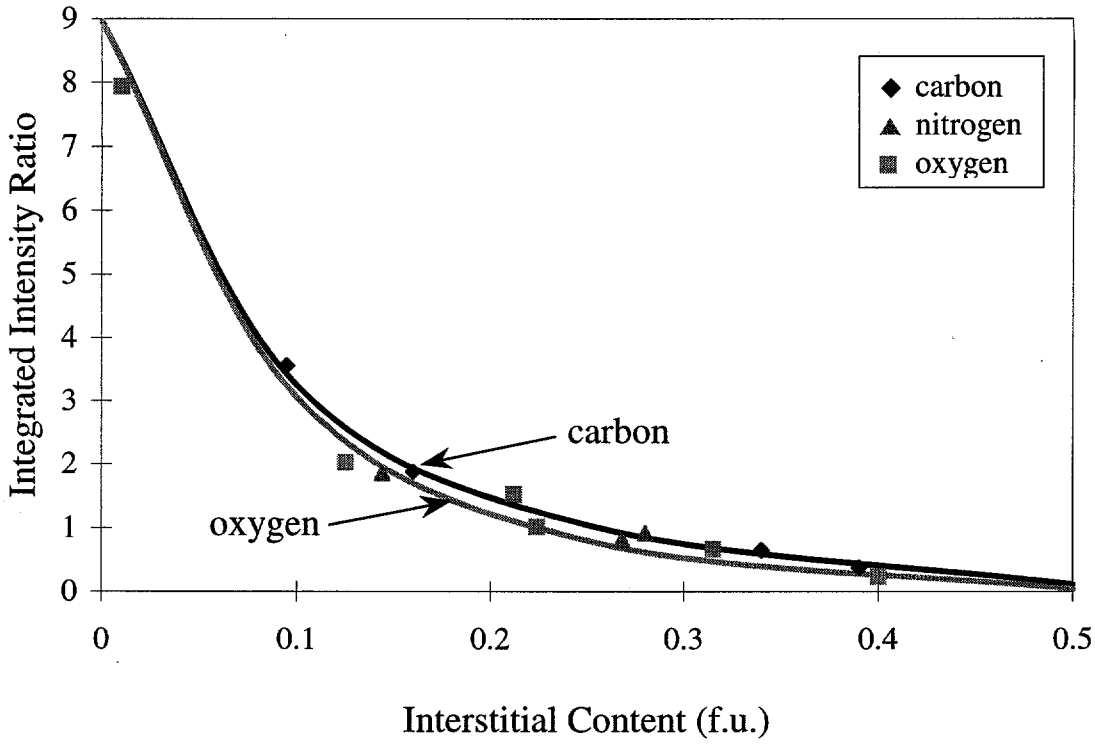
Integrated Intensity Ratio
9
8
7
6
5
4
3
2
1
0
0
0.1
0.2
0.3
0.4
0.5
Interstitial Content (f.u.)
carbon
nitrogen
oxygen
carbon
oxygen

Figure 3.

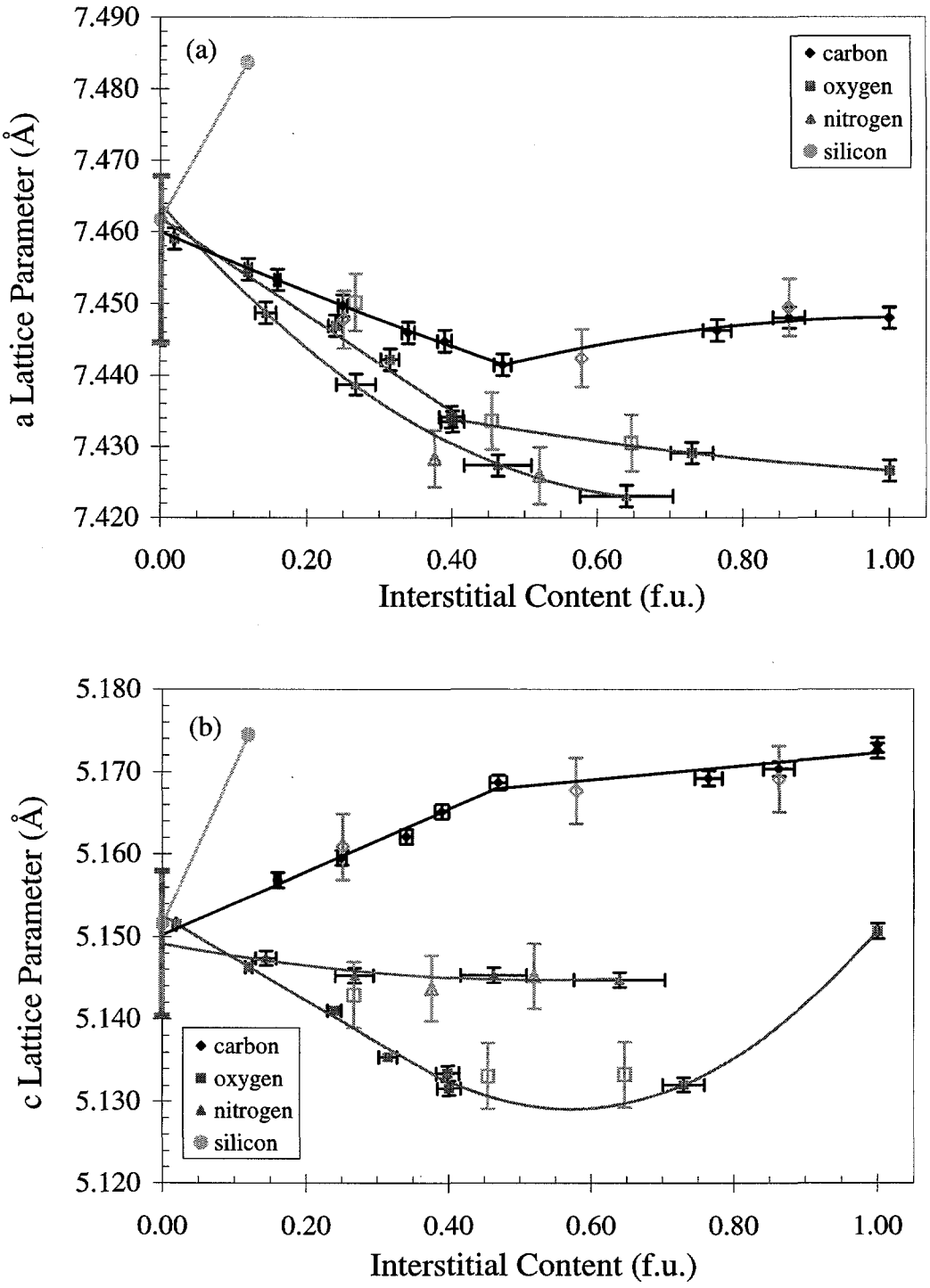
(a)
carbon
oxygen
nitrogen
silicon
a Lattice Parameter (Å)
7.490
7.480
7.470
7.460
7.450
7.440
7.430
7.420
0.00
0.20
0.40
0.60
0.80
1.00
Interstitial Content (f.u.)
(b)
carbon
oxygen
nitrogen
silicon
c Lattice Parameter (Å)
5.180
5.170
5.160
5.150
5.140
5.130
5.120
0.00
0.20
0.40
0.60
0.80
1.00
Interstitial Content (f.u.)

Figure 4.

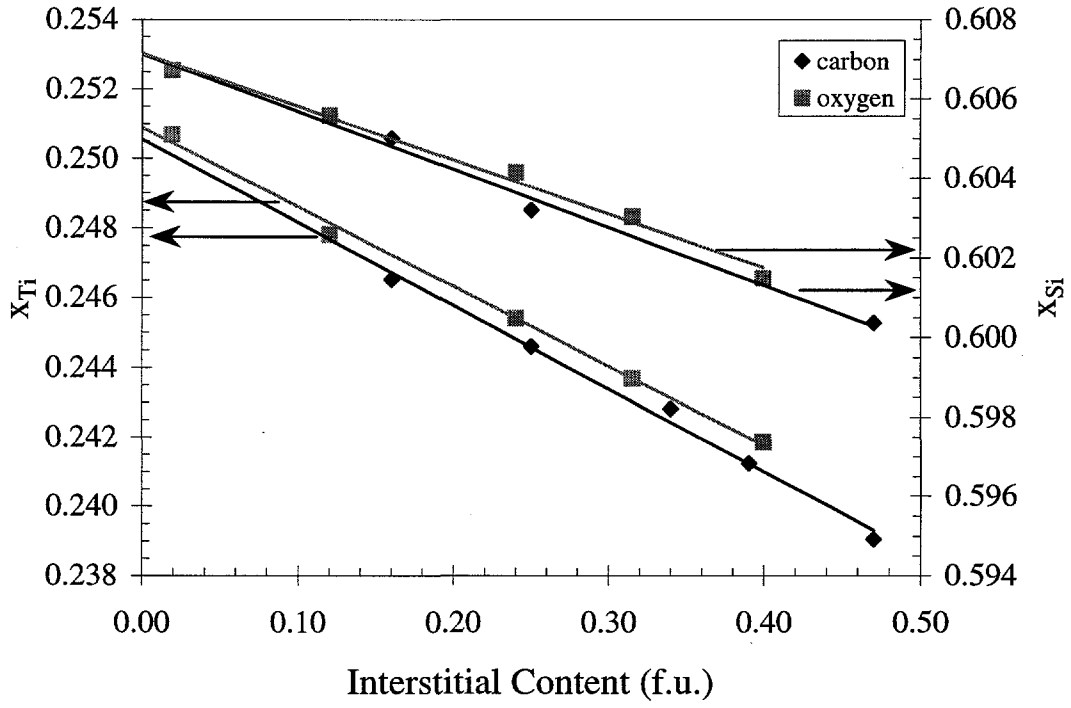
0.254
0.252
0.250
0.248
0.246
0.244
0.242
0.240
0.238
x_{Ti}
0.608
0.606
0.604
0.602
0.600
0.598
0.596
0.594
x_{Si}
carbon
oxygen
0.00
0.10
0.20
0.30
0.40
0.50
Interstitial Content (f.u.)

Figure 5.

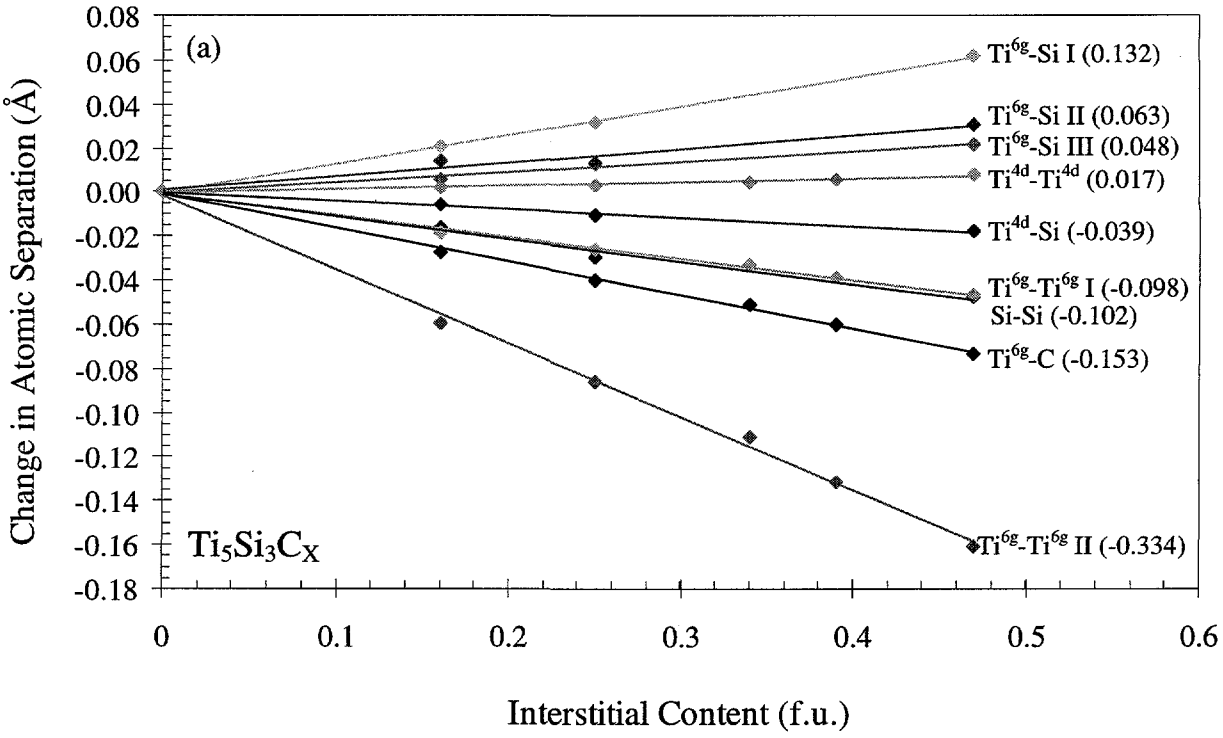
(a)
Change in Atomic Separation (Å)
Interstitial Content (f.u.)
$Ti_5Si_3C_X$
Ti^{6g}-Si I (0.132)
Ti^{6g}-Si II (0.063)
Ti^{6g}-Si III (0.048)
Ti^{4d}-Ti^{4d} (0.017)
Ti^{4d}-Si (-0.039)
Ti^{6g}-Ti^{6g} I (-0.098)
Si-Si (-0.102)
Ti^{6g}-C (-0.153)
Ti^{6g}-Ti^{6g} II (-0.334)

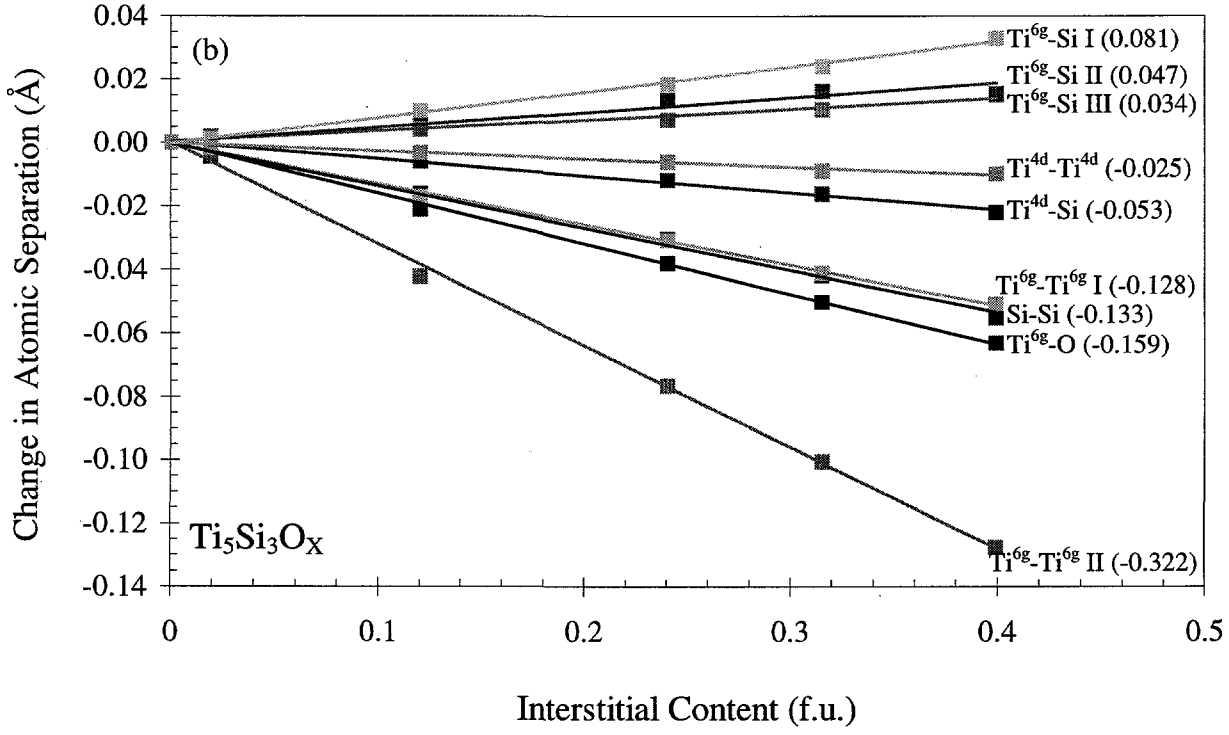
(b)
Change in Atomic Separation (Å)
Interstitial Content (f.u.)
$Ti_5Si_3O_X$
Ti^{6g}-Si I (0.081)
Ti^{6g}-Si II (0.047)
Ti^{6g}-Si III (0.034)
Ti^{4d}-Ti^{4d} (-0.025)
Ti^{4d}-Si (-0.053)
Ti^{6g}-Ti^{6g} I (-0.128)
Si-Si (-0.133)
Ti^{6g}-O (-0.159)
Ti^{6g}-Ti^{6g} II (-0.322)

Figure 6.

Table I. Extrapolated Lattice Data for Ti_5Si_3

	a, Å	**c, Å**	x_{Ti}	x_{Si}
This Study[a]	7.460±0.002	5.152±0.002	0.2509±0.0005	0.6072±0.0005
Kajitani *et al.*[1]	7.4610(3)	5.1508(1)	0.2473(9)	0.6063(9)

[a] Errors for this study represent 90% confidence intervals

Table II. Calculated Atomic Separations for Ti_5Si_3 in Angstroms

Ti^{6g}-Si I	Ti^{6g}-Si II	Ti^{6g}-Si III	Ti^{6g}-Ti^{6g} I	Ti^{6g}-Ti^{6g} II	Si-Si	Ti^{4d}-Si	Ti^{6g}-Z	Ti^{4d}-Ti^{4d}
2.785	2.658	2.570	3.184	3.242	3.032	2.634	2.272	2.576

CHAPTER 3: THERMAL EXPANSION OF Ti_5Si_3 WITH Ge, B, C, N OR O ADDITIONS

A paper submitted to the Journal of Materials Research

J.J. Williams, M.J. Kramer and M. Akinc

Abstract

The crystallographic thermal expansion coefficients of Ti_5Si_3 from 20° to 1000°C as a function of B, C, N, O or Ge content were measured by high temperature x-ray diffraction using synchrotron sources at Cornell University (CHESS) and Argonne National Laboratory (APS). Whereas the ratio of the thermal expansion coefficients along the c and a-axes was approximately three for pure Ti_5Si_3, this ratio decreased to about two when B, C, or N atoms were added. Additions of O and Ge were less efficient at reducing this thermal expansion anisotropy. The extent by which the thermal expansion is changed when B, C, N, or O atoms are added to Ti_5Si_3 correlates with their expected effect on bonding in Ti_5Si_3.

I. Introduction

Ti_5Si_3 displays a high melting point, low density and with certain interstitial additions[1], excellent oxidation resistance. However, the large thermal expansion anisotropy of Ti_5Si_3 severely limits its practical use. This large anisotropy unavoidably causes the development of strain and micro-cracks during high temperature synthesis and processing.

Four previous studies have quantified the thermal expansion anisotropy of Ti_5Si_3, three by high-temperature x-ray diffraction[2-5] and one by length-change measurements of a single crystal[7]. All studies measured a significantly larger expansion along the c-axis compared to the a-axis. The larger anharmonic vibration along the c-axis was attributed to weak metallic bonding along this axis compared to strong covalent bonding along the a-axis. This explanation is partly corroborated by electrical conductivity measurements that show the conductivity is twice as large along the c-axis than the a-axis.[7]

Although all studies reported similar relative thermal expansions, the absolute values varied considerably (see Table I). Specifically, the standard deviation of measurement between the four studies was 9.7% for the coefficient of thermal expansion along the c-axis (α_c) and 27% for the coefficient of thermal expansion along the a-axis (α_a). One reason for the differences may be due to the presence of oxygen and nitrogen impurities. Based on reported lattice parameters, the Ti_5Si_3 synthesized by Ikarashi *et al.*[8] must have had approximately 1.0wt% of oxygen, and the study by Thom *et al.*[5,6] suggests approximately 0.1 to 0.4wt% of oxygen. The study by Williams *et al.*[7], which systematically measured the change in lattice parameters of Ti_5Si_3 as a function of various interstitial additions, was used to estimate the impurity content. Due to similar effects on the lattice, nitrogen impurities may also be present. Regarding the remaining two studies, the lattice parameters reported by Zhang and Wu[2] were consistent with approximately 0.3wt% excess silicon, and Nakashima and Umakoshi[7] did not report any lattice parameters.

One purpose of this study is to compare the effects that oxygen, nitrogen, carbon and boron have on the thermal expansion anisotropy of Ti_5Si_3. This may aid in explaining the

scatter in the published values of supposedly pure Ti_5Si_3. A study by Thom *et al.*[5] did show that the addition of only 3.1wt% carbon to Ti_5Si_3 increased α_a by 8% and decreased α_c by 12%. One important ramification of this study is that incorporation of carbon can reduce the thermal expansion anisotropy of Ti_5Si_3, making it a more attractive engineering material. Furthermore, a similar result is expected for oxygen, nitrogen and boron additions. The reason is that all of these atoms occupy the same interstice as carbon and all have similar effects on atomic separations and bonding within Ti_5Si_3. Unfortunately, the 20% reduction in thermal expansion anisotropy as carbon is added to Ti_5Si_3 is not sufficient to avoid strain and micro-cracks during consolidation. A study by Kim *et al.*[8] modeled a maximum critical grain size needed to completely avoid micro-cracks for a given thermal expansion anisotropy. Based on this model and α values from Thom *et al.*[5], the carbon-containing Ti_5Si_3 had a critical grain size of 5 to 6μm, which is only a slight improvement over the critical grain size of 2 to 3μm for pure Ti_5Si_3.

A more substantial reduction in thermal expansion anisotropy has been reported in two studies, which replaced some of the titanium by zirconium, niobium or chromium.[2,8] Whereas carbon additions led to a 20% reduction in thermal expansion anisotropy, zirconium substitutions yielded a 30% reduction and chromium a 70% reduction. According to Zhang and Wu[2], very small quantities of niobium may actually reverse the thermal expansion anisotropy, although further studies are necessary to substantiate this result. Another purpose of this study is to partially substitute silicon with germanium, since the effect that this type of compositional modification has on the thermal expansion has yet to be studied. The hope is that germanium substitutions will also reduce the thermal expansion anisotropy, primarily by

weakening the strong silicon-titanium network located in the basal planes.

II. Experimental Procedure

Williams *et al.*[7] give a detailed description of sample synthesis and characterization. In summary, samples were synthesized via arc melting reagent grade pieces of titanium and silicon/germanium with boron, graphite, TiN or TiO_2 added to achieve the desired interstitial content. Weight losses were generally much less than 0.5wt%, and samples were single phase. In addition, total carbon, nitrogen and oxygen impurity content was less than 0.09wt% for all samples. Arc melted samples for x-ray analysis were ground to <20μm powder in an agate mortar.

Very detailed descriptions of the sample furnace and diffractometer geometry are given by Margulies *et al.*[9,10] Diffraction experiments were run using 45keV x-ray radiation. The high energy was necessary to achieve negligible absorption by the furnace tube, as well as to provide diffraction by transmission rather than by reflection, which is the conventional method of high-temperature x-ray diffraction. The transmission geometry reduces systematic and random errors associated with constantly shifting sample heights, a serious problem when using a conventional high-temperature diffractometer. However, the high x-ray energies that were used in this study significantly compress the measurable two-theta range of peak reflections. Thus, errors associated with calculations of lattice parameter are slightly larger. Specifically, the standard errors associated with lattice parameter refinements were approximately 0.001Å.

The tube furnace used in the experiments, as described by Margulies *et al.*[9,10], was

designed such that thermal gradients across the sample were less than 1°C. By comparison, vertical and horizontal thermal gradients of 50° to 100°C are not uncommon for typical hot stages of conventional diffractometers. In addition, the sample thermocouple was calibrated against a NIST traceable thermocouple ensuring a measurement accuracy of better than 1°C over the entire studied temperature range. Before heating, the furnace was purged with ultra-high-purity grade helium for at least one hour, and a slow helium flow was maintained throughout the experiment. Diffraction scans were acquired from approximately 2° to 20° two-theta. The positions of twelve to twenty peaks were measured by fitting Pearson VII profiles to each peak, and the lattice parameters were calculated by a least-squares refinement program.[11] The two-theta zero and x-ray energy were calculated by adding silicon as an internal standard to the room temperature scans.

III. Results and Discussion

Figure 1 illustrates typical peak profiles obtained during this study. For one sample of Ti_5Si_3 and one of $Ti_5Si_3B_{0.5}$, each diffraction line was actually composed of two peaks – a sharp, intense peak accompanied by a weak, diffuse peak at a lower angle. This indicates that these samples were heterogeneous such that a small portion of the arc melted ingot was not well crystallized. In these cases, two peaks were fit to each reflection when calculating thermal expansion. Other Ti_5Si_3 samples, which were not used in this study, showed additional peaks associated with each reflection, also indicating heterogeneity. Note that diffraction patterns taken by conventional diffractometers with Cu Kα radiation could not resolve this convoluted peak structure due to inherently larger instrumental broadening

compared to synchrotron sources and due to the added presence of the $K\alpha_2$ peak.[9] In contrast, samples with carbon, nitrogen and oxygen did not show a convoluted peak structure, which indicates well-crystallized and more homogeneous arc melted ingots. This suggests that interstitial atoms may enhance ordering during the solidification process. Although boron also primarily resides in the same interstitial site, the fact that it does not follow this pattern suggests that boron may also partially substitute for silicon during solidification. Several silicides are known to exist where silicon atoms can be substituted with boron -- $Mo_5(Si,B)_3$ is a common example. The reason that boron readily substitutes for silicon may be due to its larger size compared to carbon, nitrogen and oxygen.

A summary of lattice parameters as a function of temperature is illustrated in Figure 2. At least one data point was taken on cooling to compare with data taken on heating. In all cases but one, the lattice parameters obtained on cooling were within 0.002Å of the lattice parameter obtained on heating ($Ti_5Si_3O_{0.4}$ being the exception had a 0.004Å difference). This good agreement suggests the following: samples did not significantly react with their surroundings, the diffractometer remained in alignment, and the synchrotron energy did not change significantly throughout the experiment. Thus, no significant systematic errors are anticipated in most of these measurements. The largest error in this study is expected to be the random error associated with the determination of lattice parameters, about ±0.002Å. However, systematic errors associated with the measurement of germanium containing samples could not be entirely precluded. Unlike the other samples whose spectra were taken with a two-theta step scan and NaI detector, the spectra of germanium containing samples were collected with image plates. The difficulty in measuring the distance from the sample to

the image plate as a function of the position of the image plate can lead to systematic errors.

Table II lists the thermal expansion data of this study. The data assume linear thermal expansion along both crystallographic directions. The room temperature lattice parameters listed in Table II were measured by a conventional diffractometer with NIST silicon (SRM 640b) added as an internal standard (see Williams *et al.*[7] for additional details). The synchrotron energy and diffractometer zero were refined until the measured room temperature lattice parameters matched those listed in Table II. Only the data of Nakashima and Umakoshi[7] are consistent with the α's of Ti_5Si_3 as measured in this study. A comparison of the data is illustrated in Figure 3. The small difference in α's between studies could be attributed to a slightly different oxygen content (lower in this study) and/or a 5% systematic error in temperature measurement. The α_c/α_a ratio reported by Thom *et al.*[5] for Ti_5Si_3 is most consistent with a sample containing oxygen, and the ratio for the carbon-containing sample is in excellent agreement with the carbon-containing samples of this study. However, the α's for each axis reported by Thom *et al.*[5] are consistently larger by 23 to 27% than the α's reported in this study. This suggests a relatively large systematic error that is very reproducible from sample to sample between these two measurement techniques – most likely an error in measuring the temperature. The differences between other studies are more extreme and not easily explained. The results of Ikarishi *et al.*[8], whose samples are thought to have a high oxygen content, qualitatively agree with the α's of $Ti_5Si_3O_{0.4}$; however, α_a is significantly larger than this study suggests. One reason may be a significant error associated with their method of calculating lattice parameters – simultaneous solution of two equations based on the positions of only two peaks. This method of calculation is much less accurate

than the typical least-squares technique. Finally, the results of Zhang and Wu[2] are inconsistent with this and every other study.

The interstice that boron, carbon, nitrogen and oxygen occupy is formed by six titanium atoms in an octahedral configuration. These octahedra are face-shared along the c-axis. In pure Ti_5Si_3, most of the bonding along the c-axis is thought to be due to this chain of face-shared octahedra of titanium atoms as well as a linear chain of titanium atoms parallel to the octahedral chain. Furthermore, the bonding associated with the linear chain is expected to be stronger than the bonding associated with the octahedral chain. On addition of interstitial atoms, the weak bonding associated with the octahedral chain is replaced by stronger titanium – interstitial atom bonding. Whereas the weak titanium – titanium octahedral bonds are primarily directed along the c-axis, the titanium-interstitial atom bonds have nearly equal components along the a and c-axes. Thus, as carbon is added to Ti_5Si_3, for example, the α_c decreases due to replacement of weak metallic bonds with stronger covalent bonds. However, the anharmonic vibrations of these titanium – carbon bonds are large enough to increase the total α_a.

Comparison of α's in other compounds gives an indication of why α_a is increasing as interstitial atoms are added to Ti_5Si_3. The α of TiC, a compound composed solely of titanium – carbon bonds, is approximately $7.95\times10^{-6}{}^{\circ}C^{-1}$ and the α of TiN is approximately 8.2 to $9.1\times10^{-6}{}^{\circ}C^{-1}$.[12] Both values are significantly larger than the α_a of pure Ti_5Si_3. Thus, α_a increases as carbon and nitrogen are added to Ti_5Si_3 such as to approach the magnitude of anharmonic vibrations seen in TiC and TiN. Also, based on sublimation energies of TiZ compounds (Z = B, C, N or O), one would expect titanium – carbon bonds to be the strongest

and titanium – oxygen bonds the weakest. Furthermore, whereas the titanium – carbon separation in Ti_5Si_3 is similar to the separation in TiC, the titanium – oxygen separations are significantly longer. For these reasons, addition of carbon to Ti_5Si_3 has a significantly stronger influence on the α's than does addition of oxygen.

By comparing the properties of silicides to the properties of their germanide counterparts, one expects weaker, more anharmonic bonding in the germanides. Thus, partial substitution of silicon with germanium was expected to increase the overall thermal expansion coefficient. Additionally, since most of the titanium – silicon\germanium bonding is expected to fall in the (001) planes, a larger increase in α_a than α_c was expected. This study does show this assertion to be true. For example, $Ti_5Si_{1.5}Ge_{1.5}$ shows a 13.3% increase in α_a accompanied by only a 7.6% increase in α_c. Unfortunately, this leads to a relatively insignificant change in the thermal expansion anisotropy. Thus, substitution for silicon atoms is not a viable method of reducing the thermal expansion anisotropy.

Based on the crystallographic α's, bounds of the bulk thermal expansion, α_{bulk}, as derived by Hashin[13] can be determined by:

$$\alpha_{bulk} = (2\,\alpha_a + \alpha_c) / 3 \qquad (1)$$

$$\alpha_{bulk} = (2\,\alpha_a + \alpha_c) / 3 + 2\,\Psi\,(\alpha_a - \alpha_c) / 3 \qquad (2)$$

Equation (1) is based on the Reuss approximation of the bulk elastic modulus, Equation (2) is based on the Voight approximation, and Ψ is a function of the compliance tensor only. These bounds assume a random distribution of uniform grains such that the bulk material is statistically homogeneous. Because the compliance tensor for Ti_5Si_3 has not been measured, Figure 4 illustrates estimates for α_{bulk} based only on Equation (1). Nitrogen, oxygen and

germanium additions significantly increase the bulk thermal expansion coefficient of Ti_5Si_3. Thus, these elements would be most efficient at tailoring the bulk thermal expansion to a given application.

Reported values of the bulk thermal expansion of Ti_5Si_3, as measured by dilatometry, show very large deviations between studies.[5,14,15] One reason is due to the presence of impurities since typical powder processing routes can lead to significant amounts of interstitial carbon, nitrogen and oxygen. However, another major reason in the scatter may be due to the presence of micro-cracks and residual strain that will form because of the thermal expansion anisotropy. The magnitude of these effects will strongly depend on the processing method, e.g. hot pressing versus pressureless sintering.

IV. Conclusions

This study suggests that some of the scatter in published values of thermal expansion coefficients of Ti_5Si_3 can be explained by oxygen impurities. However, systematic errors must also exist in some or all of the studies, although this study did attempt to minimize these errors. The most probable reasons for discrepancies between studies are inaccurate temperature measurements, shifting sample heights and reactions on the surface of the samples.

In agreement with a previous study, this study has shown that carbon additions, as well as boron, nitrogen and oxygen additions do reduce the thermal expansion anisotropy of Ti_5Si_3 by as much as 34%. Reduction of this anisotropy is necessary to produce a strain-free and crack-free microstructure. Unfortunately, substitutions for silicon atoms or incorporation

of interstitial atoms alone are not sufficient to entirely eliminate the thermal expansion anisotropy. However, these compositional modifications may be an effective method of tailoring the bulk thermal expansion to a given application.

V. Acknowledgments

The authors would like to acknowledge the hard work of Dr. Stefan Kycia of CHESS and Dr. Dean Haeffner of APS in setting up and aligning the equipment associated with the synchrotron sources. The authors also acknowledge Larry Margulies for help in data acquisition.

Ames Laboratory is operated for the U.S. Department of Energy by Iowa State University under contract number W-7405-ENG-82. The Advanced Photon Source (APS) is supported by the U.S. Department of Energy, BES-Materials Sciences, under contract number W-31-109-ENG-38. The Cornell High Energy Synchrotron Source (CHESS) is supported by the National Science Foundation under award number DMR-9311772.

References

1. A.J. Thom and M. Akinc, *Advanced Ceramics for Structural and Tribological Applications*, edited by H.M. Hawthorne and T. Troczynski (Metall. Soc. of CIM Inter. Symp. Proc., Vancouver, British Columbia, 1995) 619.
2. L. Zhang and J. Wu, Scripta Mater. **38**[2], 307 (1998).
3. Y. Ikarashi, K. Ishizaki, T. Nagai, Y. Hashizuka and Y. Kondo, Intermet. **4**[1], 141 (1996).

4. A.J.Thom, M. Akinc, O. B. Cavin and C.R. Hubbard, J. Mater. Sci. Lett. **13,** 1657 (1994).

5. T. Nakashima and Y. Umakoshi, Phil. Mag. Lett. **66**[6], 317 (1992).

6. A.J. Thom, V.G. Young and M. Akinc, submitted to J. Alloys Compds. (1999).

7. J.J. Williams, M.J. Kramer, M. Akinc and S.K. Malik, submitted to J. Mater. Res. (1999).

8. Y. Kim, A.J. Thom, M. Akinc, *Processing and Fabrication of Advanced Materials for High Temperature Applications-II*, edited by T.S. Srivatsan and V.A. Ravi (TMS Symp. Proc., Warrendale, PA, 1992) 189.

9. L. Margulies, M.J. Kramer, J.J. Williams, E.M. Deters, R.W. McCallum, D.R. Haeffner, J.C. Lang, S. Kycia and A.I. Goldman, *Applications of Synchrotron Radiation Techniques to Materials Science IV* (MRS Symp. Proc. **524**, Pittsburgh, PA, 1998) 139.

10. L. Margulies, M.J. Kramer, R.W. McCallum, S. Kycia, D.R. Haeffner, J.C. Lang and A.I. Goldman, submitted to Rev. Sci. Instr. (1999).

11. D.E. Appleman and H.T. Evans, NTIS Document No. PB-216188 (1973).

12. *Carbide, Nitride and Boride Synthesis and Processing,* edited by A.W. Weimer (Chapman & Hall, London, 1997).

13. Z. Hashin, J. Mech. Phys. Solids **32**[2], 149 (1984).

14. R. Mitra, Metall. Mater. Trans. A **29**, 1629 (1998).

15. R Rosenkranz, G. Frommeyer and W. Smarsly, Mater. Sci. Eng. A **152**, 288 (1992).

Figure Captions

Fig. 1. Examples of peak profiles of $Ti_5Si_3Z_x$ obtained from synchrotron sources. Ti_5Si_3 and $Ti_5Si_3B_{0.5}$ were broader than samples with carbon, nitrogen and oxygen and showed a diffuse low-angle tail. This indicates that a small portion of the Ti_5Si_3 and $Ti_5Si_3B_{0.5}$ samples was not well crystallized. The BeO peak is from the furnace tube.

Fig. 2. (a) Expansion of the a-axis and (b) c-axis for all samples of this study. Lattice parameters as a function of temperature were calculated by least-squares refinement using the positions of twelve to twenty diffraction lines.

Fig. 3. Thermal expansion of Ti_5Si_3 as measured in this study compared to the thermal expansion measured by Nakashima and Umakoshi[5]. Note that both residual analysis and lack of fit tests suggest that the expansion of the c-axis is best fit by a quadratic equation. However, this study reports only linear expansion because the standard errors associated with the quadratic coefficient were large, 50 to 100%. Much finer temperature increments are needed to get an accurate estimate of this curvature. In contrast, the expansion of the a-axis over the studied temperature range of 25° to 1000°C is best fit by a linear equation.

Fig. 4. Estimated bulk thermal expansion coefficient based on the crystallographic thermal expansion coefficients α_a and α_c.

Table I. Published Values of Linear Coefficients of Thermal Expansion for Ti_5Si_3

α_a, $°C^{-1}\times10^{-6}$	α_c, $°C^{-1}\times10^{-6}$	α_c/α_a	Reference
5.9 ± 0.2[a]	16.9 ± 0.6[a]	2.9 ± 0.2[a]	This Study
6.3 ± 0.1[a,b]	17.8 ± 0.3[a,b]	2.8 ± 0.1[a]	Nakashima and Umakoshi[5]
8.7 ± 0.2[a]	22.1 ± 0.9[a,c]	2.5 ± 0.2[a]	Thom *et al.*[4]
10.4[d]	17.6[d]	1.7	Ikarashi *et al.*[3]
5.1	22.2	4.4	Zhang and Wu[2]

[a] Errors represent 90% confidence intervals.
[b] These thermal expansion coefficients were calculated by digitizing the plot given in Ref.[5].
[c] The α_c, as reported in Ref.[4] was incorrect. This is the correct value.
[d] These values were estimated from a bar chart.

Table II. Room Temperature Lattice Parameters and Linear Coefficients of Thermal Expansion

Sample	Source	Å, 25°C		$°C^{-1}\times10^{-6}$		α_c/α_a[b]
		a[a]	c[a]	α_a[b]	α_c[b]	
Ti_5Si_3	APS	7.4591(1)	5.1515(1)	5.8 ± 0.6	17.0 ± 2.2	2.9 ± 0.7
Ti_5Si_3	CHESS	7.4600(2)	5.1517(1)	6.0 ± 0.2	17.0 ± 0.4	2.8 ± 0.2
$Ti_5Si_3B_{0.5}$	CHESS	7.4782(1)	5.1788(1)	7.2 ± 0.3	14.5 ± 0.8	2.0 ± 0.2
$Ti_5Si_3C_{0.5}$	CHESS	7.4399(1)	5.1677(1)	7.6 ± 0.2	14.3 ± 0.5	1.9 ± 0.1
$Ti_5Si_3C_{0.5}$	APS	7.4415(1)	5.1687(1)	7.3 ± 0.3	14.1 ± 0.6	1.9 ± 0.2
$Ti_5Si_3C_{0.85}$	Thom *et al.*[4]	7.4438(4)	5.1643(4)	9.3 ± 0.4	17.9 ± 1.3	1.9 ± 0.2
$Ti_5Si_3N_{0.5}$	APS	7.4273(1)	5.1453(1)	7.9 ± 0.4	16.3 ± 0.4	2.1 ± 0.2
$Ti_5Si_3O_{0.4}$	APS	7.4342(1)	5.1334(1)	7.0 ± 0.7	17.4 ± 0.6	2.5 ± 0.3
$Ti_5Si_{2.25}Ge_{0.75}$	CHESS	7.4868(1)	5.1743(1)	6.4 ± 0.3	17.8 ± 0.5	2.8 ± 0.2
$Ti_5Si_{2.25}Ge_{0.75}C_{0.5}$	CHESS	7.4664(1)	5.1859(1)	7.9 ± 0.3	15.6 ± 0.5	2.0 ± 0.1
$Ti_5Si_{1.5}Ge_{1.5}$	CHESS	7.5140(2)	5.1964(1)	6.8 ± 0.2	18.3 ± 0.6	2.7 ± 0.2

[a] Values in parentheses represent the standard error of the lattice parameter calculation.
[b] Errors represent 90% confidence intervals.

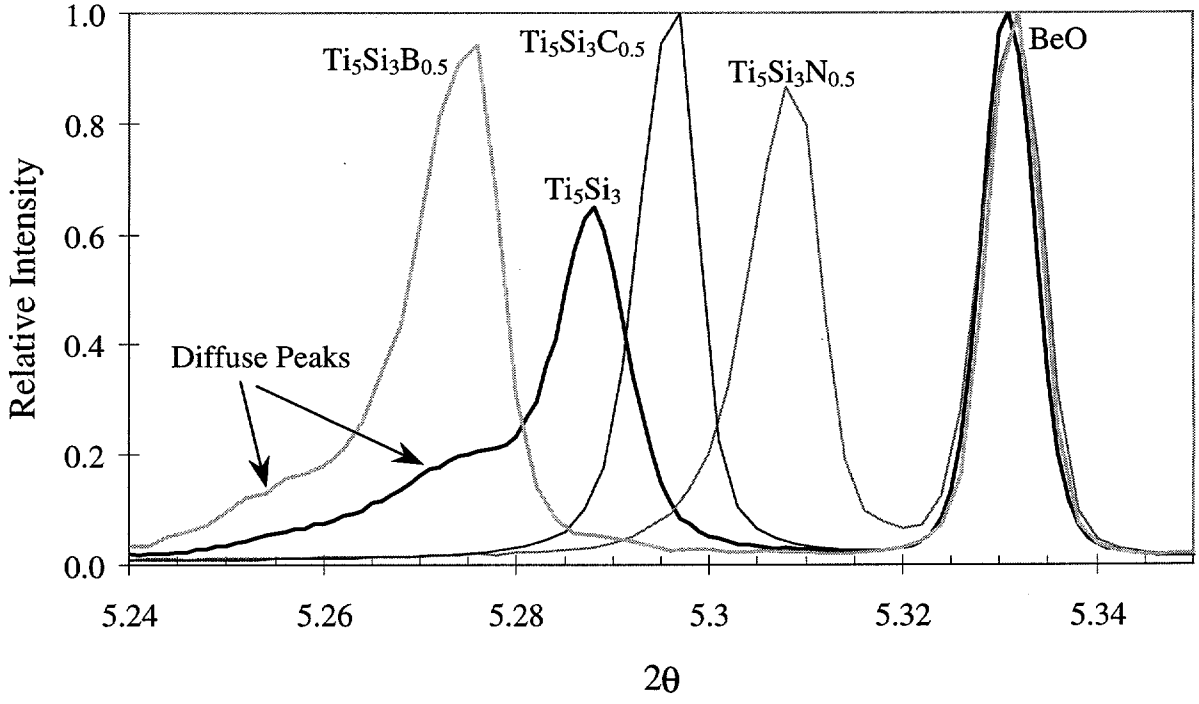
1.0
0.8
0.6
0.4
0.2
0.0
Relative Intensity
Ti5Si3B0.5
Ti5Si3C0.5
Ti5Si3N0.5
BeO
Ti5Si3
Diffuse Peaks
5.24
5.26
5.28
5.3
5.32
5.34
2θ

Figure 1.

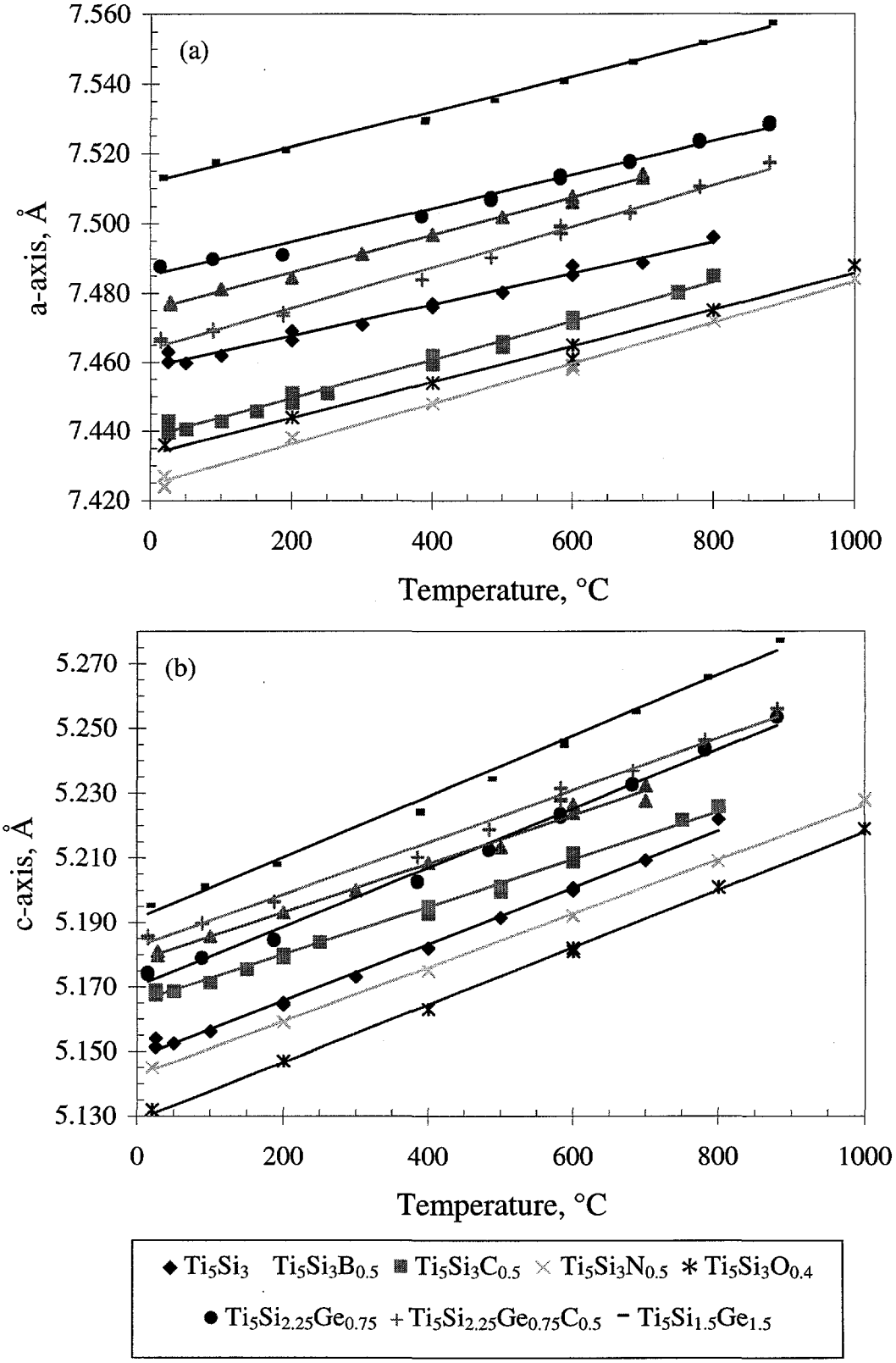
(a)
7.560
7.540
7.520
7.500
7.480
7.460
7.440
7.420
a-axis, Å
0
200
400
600
800
1000
Temperature, °C
(b)
5.270
5.250
5.230
5.210
5.190
5.170
5.150
5.130
c-axis, Å
0
200
400
600
800
1000
Temperature, °C
◆ Ti5Si3 Ti5Si3B0.5 ■ Ti5Si3C0.5 × Ti5Si3N0.5 * Ti5Si3O0.4
● Ti5Si2.25Ge0.75 + Ti5Si2.25Ge0.75C0.5 – Ti5Si1.5Ge1.5

Figure 2.

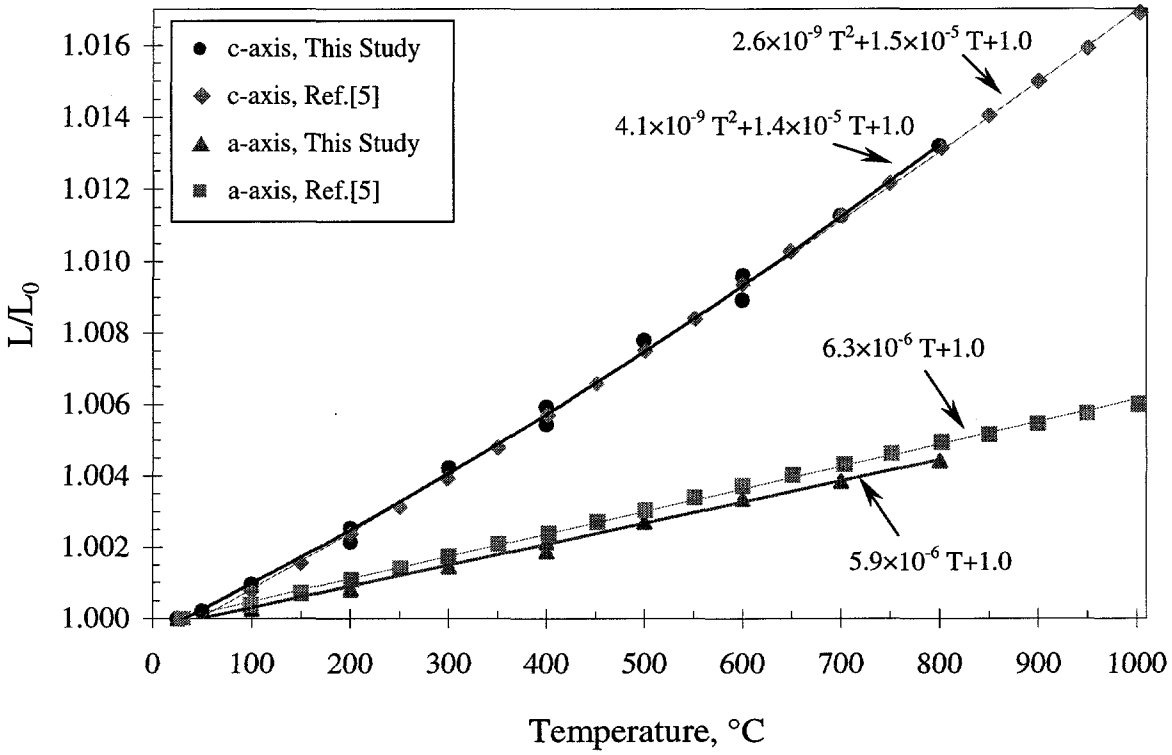
c-axis, This Study
c-axis, Ref.[5]
a-axis, This Study
a-axis, Ref.[5]
2.6×10-9 T2+1.5×10-5 T+1.0
4.1×10-9 T2+1.4×10-5 T+1.0
6.3×10-6 T+1.0
5.9×10-6 T+1.0
L/L0
1.016
1.014
1.012
1.010
1.008
1.006
1.004
1.002
1.000
0
100
200
300
400
500
600
700
800
900
1000
Temperature, °C

Figure 3.

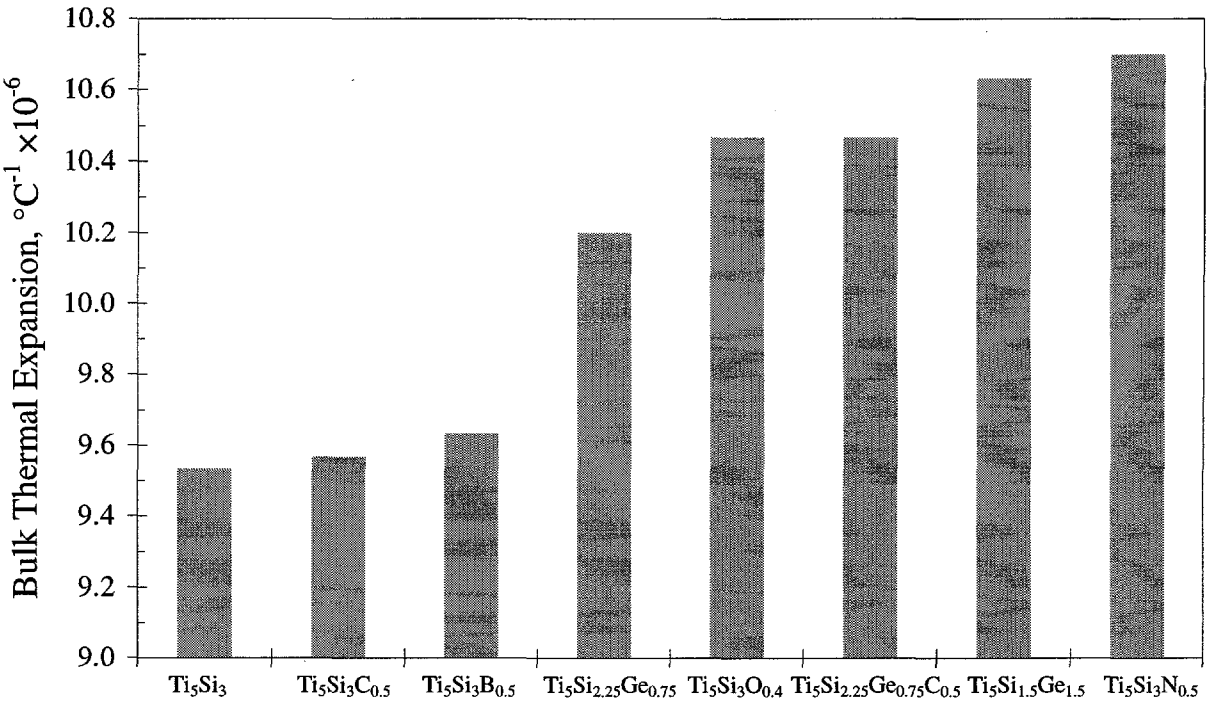
Bulk Thermal Expansion, °C^{-1} ×10^{-6}
10.8
10.6
10.4
10.2
10.0
9.8
9.6
9.4
9.2
9.0
Ti_5Si_3
$Ti_5Si_3C_{0.5}$
$Ti_5Si_3B_{0.5}$
$Ti_5Si_{2.25}Ge_{0.75}$
$Ti_5Si_3O_{0.4}$
$Ti_5Si_{2.25}Ge_{0.75}C_{0.5}$
$Ti_5Si_{1.5}Ge_{1.5}$
$Ti_5Si_3N_{0.5}$

Figure 4.

CHAPTER 4: THEORETICAL CALCULATIONS AND EXPERIMENTAL MEASUREMENTS OF THE STRUCTURE OF Ti_5Si_3 AND $Ti_5Si_3Z_{0.5}$ (Z = B, C, N OR O)

A paper to be submitted to Intermetallics

J.J Williams, Y.Y. Ye, M.J. Kramer, K.M. Ho, L. Hong, C.L. Fu and S.K. Malik

Abstract

The equilibrium structural parameters, enthalpies of formation and partial densities of state for Ti_5Si_3 and $Ti_5Si_3Z_{0.5}$ (Z= B, C, N or O) were calculated based on first-principle techniques. Enthalpy of formation calculations suggest that the $D8_8$ structure is the most stable form of Ti_5Si_3, and the stability of the structure increases as Z atoms are added. The theoretically determined structural trends as a function of interstitial element, Z, agreed well with experimentally determined values. Both indicate bonding between Ti and Z atoms based on contraction of Ti-Z separations. The calculated partial densities of state suggest that p(Si)-d(Ti) and d(Ti)-d(Ti) interactions are responsible for most of the bonding in pure Ti_5Si_3, which agrees with previous studies. As Z atoms are added, p(Z)-d(Ti) interactions become significant at the expense of weakening some of the d(Ti)-d(Ti) interactions.

1. Introduction

Interest in M_5Si_3 intermetallics (M= transition metal of group III through VI) which began

in the 1950's and continues today is primarily a result of their high melting points (>2000°C), wide homogeneity ranges and large alloying potentials. Nowotny and coworkers performed much of the early characterization of these materials.[1-3] The crystal structures were determined to be either a hexagonal Mn_5Si_3-type ($D8_8$, M= Sc, Ti, Mn, Y), tetragonal Cr_5B_3-type ($D8_l$, M= Cr, Nb, La, Ta) or tetragonal W_5Si_3-type ($D8_m$, M= V, Mo, W). Additionally, Nowotny discovered that all of these M_5Si_3 compounds, except La_5Si_3, reverted to the hexagonal form in the presence of boron, carbon, nitrogen, or oxygen.[1] M_5Si_3 compounds stabilized in the hexagonal structure by ternary additions have since become known as Nowotny phases.[2] Experimental observations also suggested that carbon was most efficient and oxygen least efficient in stabilizing the hexagonal structure. However no direct experimental or theoretical evidence currently exists which explains why this stabilization occurs.

Although experimental evidence suggests that Ti_5Si_3 does not require ternary additions to form the hexagonal structure, recent work has shown that small additions of carbon have a significant effect on the crystal structure, thermal expansion and high temperature oxidation resistance.[4,5] In fact, by adding carbon to the structure, Ti_5Si_3 becomes a considerably more promising material for engineering applications. However, little is known about why carbon additions have such a striking effect on these properties. The goal of this study is to combine experimentally determined structural data with first-principle electronic calculations to understand bonding changes that occur with the addition of boron, carbon, nitrogen or oxygen to Ti_5Si_3. Determining these bonding changes will aid in understanding and predicting the changes that occur in the thermal and electronic properties.

No previous first-principle calculations have been attempted on ternary $Ti_5Si_3Z_x$ (Z= B, C, N or O); however, two studies do exist on binary Ti_5Si_3. The first study, by Long and Chong[6], used a semi-empirical tight binding energy band method with the extended Hückel approximation to calculate band structure and densities of state (DOS). They concluded that bonding-antibonding in Ti_5Si_3 is primarily a result of d(Ti)-p(Si) interaction above and below the Fermi energy (E_f) as well as d(Ti)-d(Ti) interactions spanning energies around E_f. These orbital interactions are very typical of transition metal silicides in general and explain their good electrical conductivity.[7,8] The second study, by Ekman and Ozolins[9], made calculations based on the full potential version of the linear muffin tin orbital (LMTO) method. Their conclusions of d(Ti)-p(Si) and d(Ti)-d(Ti) hybridization were identical to those above. However, their electron density maps suggest that all Ti-Si interactions in Ti_5Si_3 are multi-centered bonds as opposed to simple two-atom covalent bonds. The study also calculated the equilibrium volume, bulk modulus and enthalpy of formation, all of which were only slightly lower than the experimental values.

This study used the LMTO method with the atomic sphere approximation (ASA) to calculate the angular-momentum decomposed electronic DOS, but unlike the previous studies, equilibrium lattice parameters and atomic positions were also calculated. These calculations were made for Ti_5Si_3, $Ti_5Si_3Z_{0.25}$ and $Ti_5Si_3Z_{0.5}$ (Z=B, C, N or O) and compared to experimentally determined values. Heats of formation were also calculated for most compositions including Ti_5Si_3 in the equilibrium Mn_5Si_3 structure ($D8_8$) as well as in the possible alternate structures of W_5Si_3 ($D8_m$) and Cr_5B_3 ($D8_l$).

2. Crystal Structure of Ti_5Si_3

Figure 1 gives the hexagonal structure of Ti_5Si_3. The unit cell contains two distinct titanium sites and one silicon site:

Ti at 4d sites at (1/3, 2/3, 0)

Ti at 6g sites at (x_{Ti}, 0, 1/4)

Si at 6g sites at (x_{Si}, 0, 1/4)

Theoretical calculations were based on this unit cell, which contains two formula units of atoms (i.e. $Ti_{10}Si_6$). The Ti^{4d} atoms form a linear chain parallel to the c-axis, and the Ti^{6g} atoms form a chain of face-shared trigonal antiprisms along the c-axis. The silicon atoms form a chain of distorted face-shared trigonal antiprisms parallel to the c-axis such that one Ti^{4d} site is at the center of each antiprism. This structure leads to an ABAC stacking sequence along the c-direction. The B and C planes consist of Ti^{6g} and Si atoms, which form the shared faces of the antiprsims, and the A planes consist solely of Ti^{4d} atoms. The Z atoms are thought to occupy the interstitial region at the center of the antiprism formed by the Ti^{6g} atoms, and hence, would also lie in the A plane with the Ti^{4d} atoms.

Strong experimental evidence exists to support the assertion that Z atoms occupy this interstitial site. Neutron diffraction studies of Mo_5Si_3C by Parthe *et al*[3] and of $Ti_5Si_3H_x$ by Kajitani *et al*[10], as well as single crystal x-ray diffraction studies of $La_5Ge_3O_x$ by Guloy and Corbett[11] and of $Er_5Si_3C_x$ by Al-Shahery *et al*[12] all agree that occupation of this antiprismatic interstice by Z atoms is most probable. Thus the solubility of Z in Ti_5Si_3 should vary from zero to the stoichiometric limit of $Ti_5Si_3Z_1$ (There are only two antiprismatic interstices in the

unit cell, which is equivalent to a maximum of one Z atom per formula unit.). This is in full agreement with the actual solubility limits of C, N or O in Ti_5Si_3 as measured by diffusion couple experiments.[13,14]

3. Theoretical Approach

Calculations were made within the local density approximation[15] by using the Hedin-Lundqvist[16] form for the local exchange and correlation potential. Electronic Bloch states[17] were expanded as a mixed basis set with norm conserving scalar-relativistic pseudopotentials[18] used for the constituent elements. Relaxation of atomic coordinates was facilitated by computing the Hellmann-Feynman forces[19] acting on the atoms. A Broyden algorithm for estimating and updating this force matrix was used to predict the new atomic coordinates during the relaxation process. The atomic positions and lattice parameters were fully relaxed to the true equilibrium structure. Using these calculated equilibrium lattice parameters, electronic densities of state (DOS) were calculated by the LMTO-ASA method. To improve efficiency and accuracy of the calculations, unoccupied octahedral interstices were filled with empty spheres. For Ti_5Si_3, the radius of these spheres was set to 0.7 times the radius of the Ti atom. For $Ti_5Si_3Z_x$, the radius was set to the radius of the Z atom, which ranged from 0.68 to 0.7 times the radius of the Ti atom. Heats of formation were also calculated (see Section 5.1).

4. Experimental Approach

All $Ti_5Si_3Z_x$ samples were synthesized by arc-melting. The starting materials included

sponge titanium (Timet, 99.7%), silicon pieces (Alfa Æsar, 99.9999%), spectrographic grade graphite electrodes for carbon, boron pieces (Alfa Æsars, 99.5%), titanium nitride for nitrogen (Johnson Matthey, 99.8%) and titanium dioxide for oxygen (Fischer Scientific, 99.8%). Arc melting was performed in a ultra-high-purity argon atmosphere on a water-chilled copper hearth. Samples were melted at least three times via a non-consumable tungsten electrode. Total weight losses after arc-melting were typically much less than 0.5wt%.

Arc-melted samples were then ground to < 20μm and mixed with a silicon line position standard (NIST SRM 640b). Room temperature x-ray diffraction spectra were obtained from a Scintag diffractometer with solid state detector. Room temperature neutron diffraction spectra were obtained from the Missouri University Research Reactor (MURR) using a curved Ge monochromator and position sensitive detector. Rietveld analysis software (GSAS, Los Alamos National Laboratory 1985) was used to refine the lattice parameters and the two variable atomic coordinates, x_{Ti} and x_{Si}. Oxygen and nitrogen content were measured by a Leco TC-436 analyzer; carbon content was measured by a Horiba EMIA-520 analyzer.

5. Results and Discussion

5.1 Enthalpy of Formation

The enthalpies of formation were calculated from total energies, E, according to:

$$H = E_{Ti_5Si_3Z_x} - \Sigma_i (X_i E_i),$$

where X_i is the concentration of the i^{th} elemental component. The total energies of the elements, E_i, were calculated using their most stable structures: titanium ($P6_3/mmc$), silicon

(Fd-3m), boron (R-3m) and graphite ($P6_3/mmc$), as well as O_2 and N_2 gas. Total energies, $E_{Ti_5Si_3Z_x}$, were calculated for $Ti_5Si_3Z_x$ using the relaxed atomic positions and lattice parameters that were determined by the pseudopotential method described in Section 3.

Table I lists the results of these calculations. Of the three possible crystal structures in which M_5Si_3 compounds form, the $D8_8$ structure has the most negative value. Thus, these calculations agree with experimental observations that suggest that the $D8_8$ structure is the most stable structure for Ti_5Si_3. In most other M_5Si_3 compounds, where M is heavier than Ti, the $D8_8$ structure becomes favorable only in the presence of interstitial atoms. As an example, Mo_5Si_3, which exists in the $D8_m$ structure, converts to the $D8_8$ structure when carbon is added. In a study by Fu *et al*[20], calculations of enthalpies of formations did suggest that in agreement with experimental evidence, Mo_5Si_3 should form in the $D8_m$ structure instead of the $D8_8$ and $D8_l$ structures. Thus, this study provides further support that theoretical calculations of the enthalpy of formation can be used to predict which crystal structure is most stable.

As seen in Table I, the enthalpy of formation becomes more negative, as more carbon or boron is added to the lattice. This suggests that these interstitial atoms, in accordance with experimental observations, do increase the stability of the $D8_8$ structure. A comparison of the enthalpy of formation of Ti_5Si_3 with that of $Ti_5Si_3Z_{0.5}$ indicate $Ti_5Si_3C_{0.5}$ is 3% more negative, $Ti_5Si_3N_{0.5}$ is 7% more negative and $Ti_5Si_3O_{0.5}$ is 38% more negative than Ti_5Si_3. This trend agrees well with experimental values of the Gibbs energy of formation at 1100°C for Ti_5Si_3Z. As reported in Goldstein *et al*[14], Ti_5Si_3C is 5% more negative, Ti_5Si_3N is 11% more negative and Ti_5Si_3O is 41% more negative than Ti_5Si_3.

5.2 Equilibrium Structural Parameters

Theoretical and experimental structural parameters are given in Tables II and III, respectively. The theoretical lattice parameters underestimate the experimental lattice parameters by 0.6 to 1.6% as is common for this method of calculation. However, the normalized trends between experimental and theoretical values are in good qualitative agreement, particularly for the change in c-axis as a function of interstitial content. Boron and carbon, being the larger atoms, expand the c-lattice parameter; whereas, the smaller oxygen and nitrogen contract it. The agreement between theoretical and experimental trends in the a-lattice parameter is not quite as good. Based on experimental measurements, all but boron contract the a-lattice parameter; although theoretical calculations show all but oxygen expand the a-lattice parameter. The reason for this discrepancy is due to the underestimation of the lattice by theoretical calculations, which leads to a significantly smaller interstitial volume.

Based on the experimental and theoretical structural parameters, nearest-neighbor atomic separations were calculated in order to infer bonding changes as interstitial atoms are added to Ti_5Si_3. Figure 2 shows the change in nearest-neighbor atomic separations as carbon is added to Ti_5Si_3. In general, all studied interstitial additions led to changes similar to those seen in Figure 2. As with the structural parameters, there is very good qualitative agreement between the experimental and theoretical changes as a function of interstitial content. The most striking effect of interstitial atoms is to contract the Ti^{6g}-Ti^{6g} and Ti^{6g} -Z separations and to expand the Ti^{6g} -Si separations. This suggests bonding between the Ti^{6g} and Z atoms and a

possible weakening of bonding between the Ti^{6g} and Si atoms. Furthermore, the theoretical calculations suggest that these changes are strongest for carbon. Thus, carbon atoms may be more strongly bonded than the other interstitial atoms.

5.3 Densities of State

Figure 3 gives the partial densities of state (PDOS's) for each of the atoms in Ti_5Si_3 and $Ti_5Si_3Z_{0.5}$. The calculated densities of state for Ti_5Si_3 qualitatively agree with the previously mentioned studies by Long and Chong[6] and Ekman and Ozolins[9]; that is, the region from -2 to -5.5 eV is dominated by d(Ti)- p(Si) mixing, and the region at the Fermi level (0 eV) to -2 eV is dominated by d(Ti) states. These d(Ti) states most likely consist of both bonding and non-bonding electrons. Also, little mixing occurs with the s(Si) states from -6.5 to -10.5 eV.

As boron, carbon, nitrogen or oxygen is added to the lattice, mixing occurs primarily between the interstitial atom's p-state and the surrounding Ti^{6g} atom's d-state. This is shown in Figure 4 for interstitial carbon and oxygen atoms, which is a plot of the cumulative area of the difference between the PDOS's of $Ti_5Si_3Z_{0.5}$ and Ti_5Si_3. A positive slope in Figure 4 indicates an increase in the PDOS of an atom in $Ti_5Si_3Z_{0.5}$ compared to that same atom in Ti_5Si_3. Similarly, a negative slope indicates a decrease and a zero slope indicates no change in the PDOS's in $Ti_5Si_3Z_{0.5}$ relative to Ti_5Si_3. Thus, as seen in Figure 4, addition of 0.5 formula units of oxygen leads to an increase of about 0.3 states for each Ti^{6g} atom at -6 to -7 eV which corresponds exactly to the position of the oxygen p-band. Also, addition of oxygen leads to a reduction of 0.1 states per Ti^{6g} atom at -4.5 to -5 eV and a reduction of 0.25 states per atom at -0.5 to -2 eV which corresponds to areas of d(Ti)-p(Si) and d(Ti)-d(Ti)

interaction, respectively. Furthermore, little change occurs between the PDOS's of Ti^{4d} and Si atoms in $Ti_5Si_3O_{0.5}$ relative to Ti_5Si_3. Based on these observations, addition of oxygen to Ti_5Si_3 leads to the formation of d(Ti^{6g})-p(O) bonds at the expense of d(Ti^{6g})-d(Ti^{6g}) interaction and to a lesser extent, d(Ti^{6g})-p(Si) interaction. However, d(Ti^{4d})-d(Ti^{4d}) and d(Ti^{4d})-p(Si) interactions remain relatively unaffected.

The effect of carbon additions is similar in that Ti^{6g} atoms show the most dramatic redistribution of electronic states. Also, the increase in states of the Ti^{6g} atoms coincides in energy with the carbon p-states (-2 to -5 eV) and the decrease in states of Ti^{6g} atoms coincides with states associated with d(Ti^{6g})-d(Ti^{6g}) interaction (-0.5 to -2 eV). However, unlike oxygen (and nitrogen), the carbon p-band is considerably broader and is located at similar energy levels as the Si p-band (-2 to -5 eV). This broader band may suggest that carbon is more strongly bonded to the Ti^{6g} atoms then oxygen (and nitrogen). Additionally, the d(Ti^{4d})-p(Si) interaction has shifted slightly to energies closer to the Fermi level.

Although not shown, the effect of nitrogen additions is very similar to that of oxygen additions. Boron additions, however, leads to a redistribution of Ti^{6g} states around boron's s-band, which is located at -6 to -7 eV. The majority of boron's p-states are located at -1 to -2 eV, where d(Ti)-d(Ti) interactions predominate.

Finally, although d(Ti^{6g})-p(Z) bonding apparently forms at the expense of d(Ti^{6g})-d(Ti^{6g}) interactions, no significant change in DOS occurs at the Fermi level for all studied compositions. Also, although not obvious in Figures 2 and 3, the overlap between Ti^{4d} and Si atoms increases slightly as interstitial atoms are added to Ti_5Si_3. This may suggest an increase in bonding between Ti^{4d} and Si atoms.

6. Conclusions

Based on enthalpy of formation calculations, the $D8_8$ structure appears to be the most stable structure for Ti_5Si_3 in accordance with experimental evidence. Also, interstitial additions appear to increase the stability of the $D8_8$ structure. This increase in stability is apparently a result of bonding between the interstitial atom's p-electrons and the Ti^{6g} atom's d-electrons, which results in a strong contraction in separation between the atoms. These bonds form at the expense of Ti^{6g} states located near the Fermi level. All other PDOS features remain relatively unaffected by the incorporation of interstitial atoms.

7. Acknowledgments

Ames Laboratory is operated for the U.S. Department of Energy by Iowa State University under contract number W-7405-ENG-82.

8. References

1. H. Nowotny, B. Lux and H. Kudielka, *Mh.Chem.* **87** (1956) 447.
2. H. Nowotny, Electronic Structure and Alloy Chemistry of the Transition Elements. ed. P.A. Beck, Plenum Press, New York, (1963) 179.
3. E. Parthe, W. Jeitschko and V. Sadagopan, *Acta Cryst.*, **19** (1965) 1031.
4. A.J. Thom and M. Akinc, *J. Mater. Sci. Letters*, **13** (1994) 1657.

5. A.J. Thom and M. Akinc, *Advanced Ceramics for Structural and Tribological Applications*, eds. H.M. Hawthorne and T. Troczynski, Vancouver, British Columbia, The Minerals, Metals & Materials Society, (1994) 413.

6. X. Long and Z. Chong, *Trans. Nonferrous Met. Soc. China*, **4**[3] (1994) 25.

7. W. Speier, L. Kumar, D.D. Sarma, R.A. de Groot and J.C. Fuggle, *J. Phys: Condens. Matter*, **1** (1989) 9117.

8. C.D. Gelatt, A.R. Williams and V.L. Moruzzi, *Phys. Rev. B*, **27** (1983) 2005.

9. M. Ekman adn V. Ozolins, *Phys. Rev .B*, **57** (1998) 4419.

10. T. Kaijitani, T. Kawase, K. Yamada and M. Hirabayashi, *Trans. Japan Institute of Metals*, **27**[9] (1986) 639.

11. A.M. Guloy and J.D. Corbett, *Inorg. Chem.*, **35** (1996) 4669.

12. G.M.Y. Al-Shahery, D.W. Jones, I.J. McColm and R. Steadman, *J. Less Comm. Metals*, **87** (1982) 99.

13. W. Wakelkamp, "Diffusion and Phase Relations in the Systems Ti-Si-C and Ti-Si-N". Technical University of Eindhoven Thesis. 1991.

14. J.I. Goldstein, S.K. Choi, F.J.J. Von Loo, G.F. Bastin and R. Metselaar, *J. Amer. Ceramic Soc.,* **78**[2] (1995) 313.

15. R.O. Jones, *Rev. Mod. Phys.*, **61** (1989) 689.

16. L.Hedin and B.I.Lundqvist, *J. Phys. C,* **4** (1971) 2064.

17. S.G. Louie, K.M. Ho and M.L. Cohen, *Phys. Rev. B*, **19** (1979) 1774.

18. D.R. Hamann, M. Schluter and C. Chiang, *Phys. Rev. B*, **25** (1982) 2103.

19. K.M. Ho, C. Elsasser, C.T. Chan and M. Fahnle, *J. Phys.: Condens. Matter,* **4** (1992) 5189.

20. C.L. Fu, X. Wang, Y.Y. Ye and K.M. Ho, *Intermet.*, **7** (1998) 1.

Figure Captions

Figure 1. $D8_8$ crystal structure of Ti_5Si_3. a) 001 orthographic projection of lattice with highlighted trigonal antiprisms. b) Depiction of the face-sharing of the trigonal antiprisms along the c-axis. Z atoms sit at the center of the trigonal antiprisms formed by six surrounding Ti^{6g} atoms.

Figure 2. Change in atomic separations as carbon is added to Ti_5Si_3. Dotted lines represent theoretical calculations, solid lines represent experimental data. The underestimation of lattice contraction by theoretical calculations is due to the underestimation of the calculated lattice volume for pure Ti_5Si_3.

Figure 3. PDOS's for Ti_5Si_3 and $Ti_5Si_3Z_{0.5}$. Thick, black lines represent Si states; thick, light lines are Z states; thin, black lines are Ti^{6g} states; thin, light lines are Ti^{4d} states.

Figure 4. a) Cumulative area of the difference between the DOS of an atom in $Ti_5Si_3O_{0.5}$ and the DOS of that same atom in Ti_5Si_3. b) Cumulative area of the difference between the DOS of an atom in $Ti_5Si_3C_{0.5}$ and the DOS of that same atom in Ti_5Si_3. Positive slopes in the Ti^{6g} curves correspond exactly in energy to the position of the interstitial atom's p-state. Smaller features in these figures are due to slight changes in the Fermi level as interstitial atoms are added to Ti_5Si_3.

Table I. Calculated Enthalpies of Formation

Composition	Structure	Enthalpy, eV/f.u.
Ti_5Si_3	$D8_l$	-6.060
Ti_5Si_3	$D8_m$	-6.170
Ti_5Si_3	$D8_8$	-6.410
$Ti_5Si_3B_{0.25}$	$D8_8$	-6.604
$Ti_5Si_3B_{0.5}$	$D8_8$	-7.104
$Ti_5Si_3C_{0.25}$	$D8_8$	-6.625
$Ti_5Si_3C_{0.5}$	$D8_8$	-7.251
$Ti_5Si_3N_{0.5}$	$D8_8$	-6.866
$Ti_5Si_3O_{0.5}$	$D8_8$	-8.870

Table II. Calculated Structural Parameters for $Ti_5Si_3Z_x$

Z_x	a, Å	c, Å	x_i, Å	x_{ii}, Å
--	7.3770	5.0840	0.2473	0.6063
$B_{0.25}$	7.4027	5.1079	--	--
$B_{0.5}$	7.4101	5.1130	0.2470	0.6023
$C_{0.25}$	7.3775	5.0892	--	--
$C_{0.5}$	7.3925	5.0956	0.2400	0.6023
$N_{0.5}$	7.3834	5.0746	0.2410	0.6025
$O_{0.5}$	7.3730	5.0829	0.2440	0.6025

Table III. Measured Structural Parameters for $Ti_5Si_3Z_x$

Z_x	a, Å	c, Å	x_i, Å	x_{ii}, Å
--	7.4601(1)	5.1510(1)	0.2507(3)	0.6067(2)
$B_{0.24}$	7.4670(2)	5.1722(2)	0.2495(3)	0.6076(5)
$B_{0.47}$	7.4781(1)	5.1788(1)	0.2478(3)	0.6053(5)
$C_{0.25}$	7.4497(1)	5.1596(1)	0.2446(3)	0.6032(2)
$C_{0.47}$	7.4415(1)	5.1687(1)	0.2391(3)	0.6004(2)
$N_{0.27}$	7.4387(1)	5.1453(1)	0.2439(2)	0.6049(3)
$N_{0.46}$	7.4273(1)	5.1543(1)	0.2379(3)	0.6025(5)
$O_{0.22}$	7.4469(2)	5.1410(1)	0.2454(2)	0.6041(2)
$O_{0.4}$	7.4342(1)	5.1334(1)	0.2419(2)	0.6015(2)

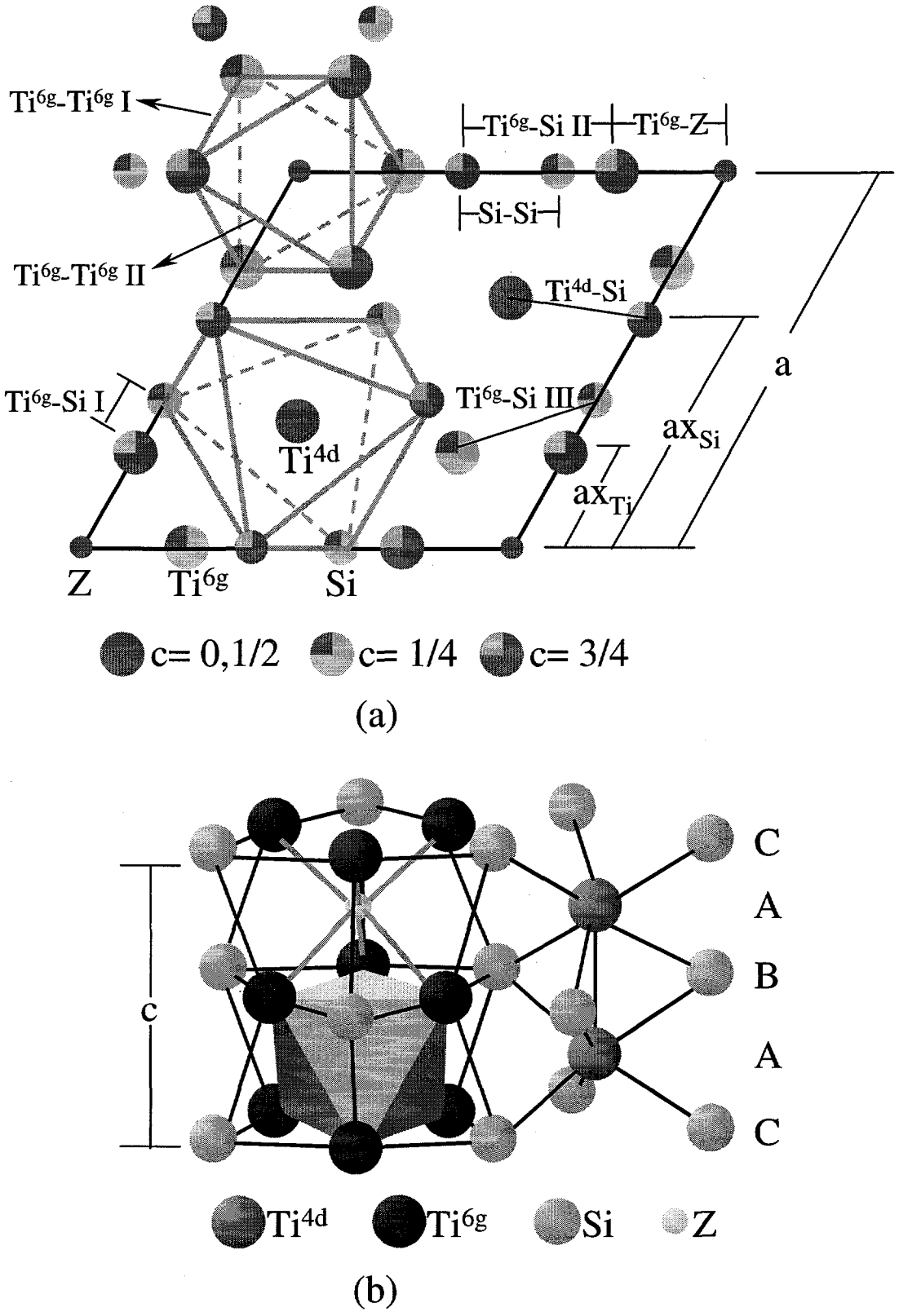
Ti6g-Ti6g I
Ti6g-Si II
Ti6g-Z
Si-Si
Ti6g-Ti6g II
Ti4d-Si
a
Ti6g-Si I
Ti6g-Si III
axSi
Ti4d
axTi
Z
Ti6g
Si
c= 0,1/2
c= 1/4
c= 3/4
(a)
C
A
B
A
C
c
Ti4d
Ti6g
Si
Z
(b)

Figure 1.

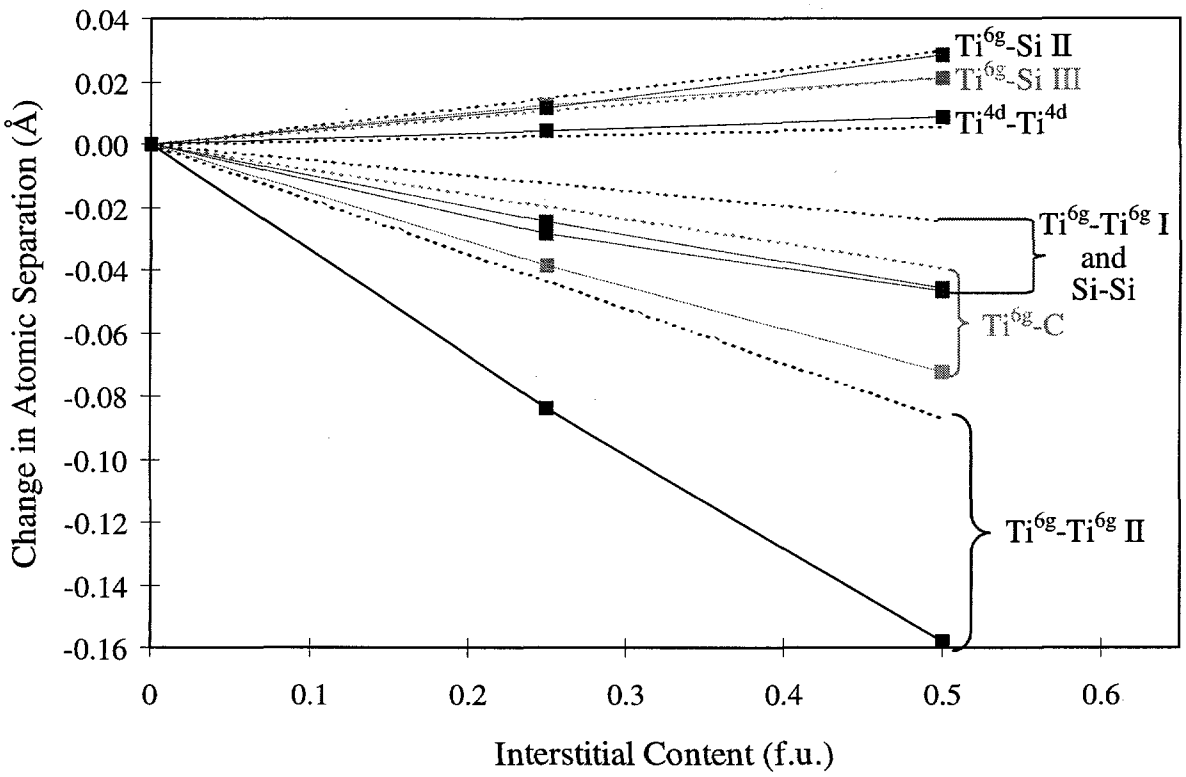
0.04
0.02
0.00
-0.02
-0.04
-0.06
-0.08
-0.10
-0.12
-0.14
-0.16
Change in Atomic Separation (Å)
0
0.1
0.2
0.3
0.4
0.5
0.6
Interstitial Content (f.u.)
Ti6g-Si II
Ti6g-Si III
Ti4d-Ti4d
Ti6g-Ti6g I
and
Si-Si
Ti6g-C
Ti6g-Ti6g II

Figure 2.

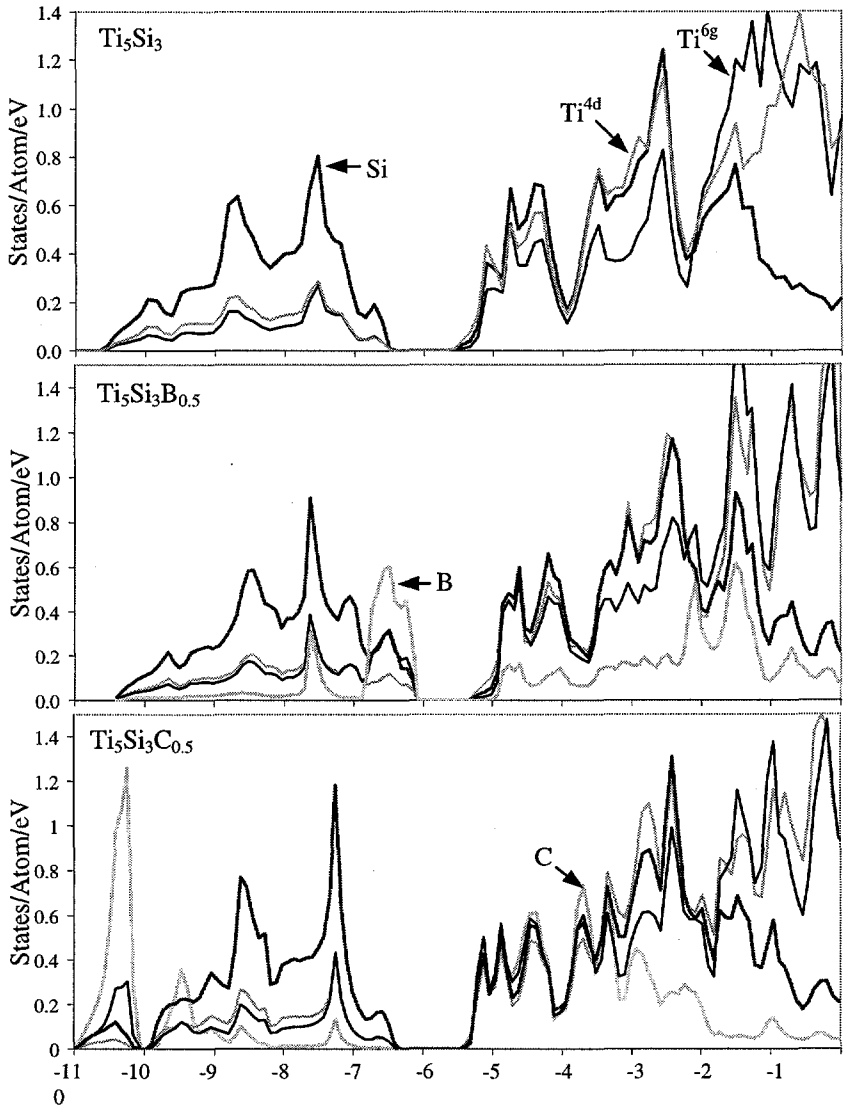
Ti5Si3
Ti6g
Ti4d
Si
Ti5Si3B0.5
B
Ti5Si3C0.5
C
States/Atom/eV
0.0
0.2
0.4
0.6
0.8
1.0
1.2
1.4
1
0
-11
-10
-9
-8
-7
-6
-5
-4
-3
-2
-1

Figure 3

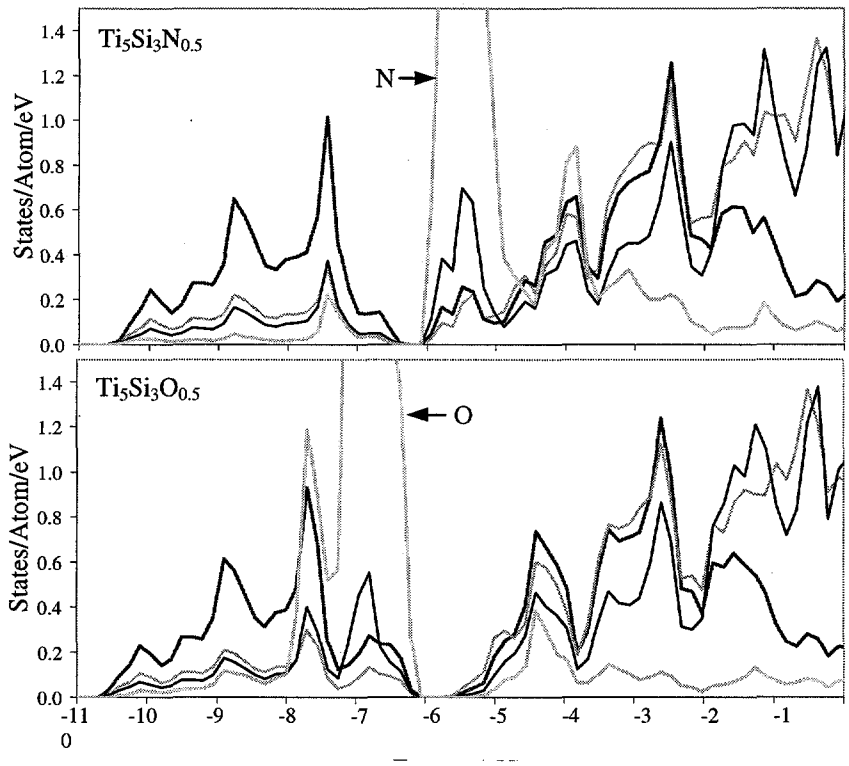

Figure 3. (continued)

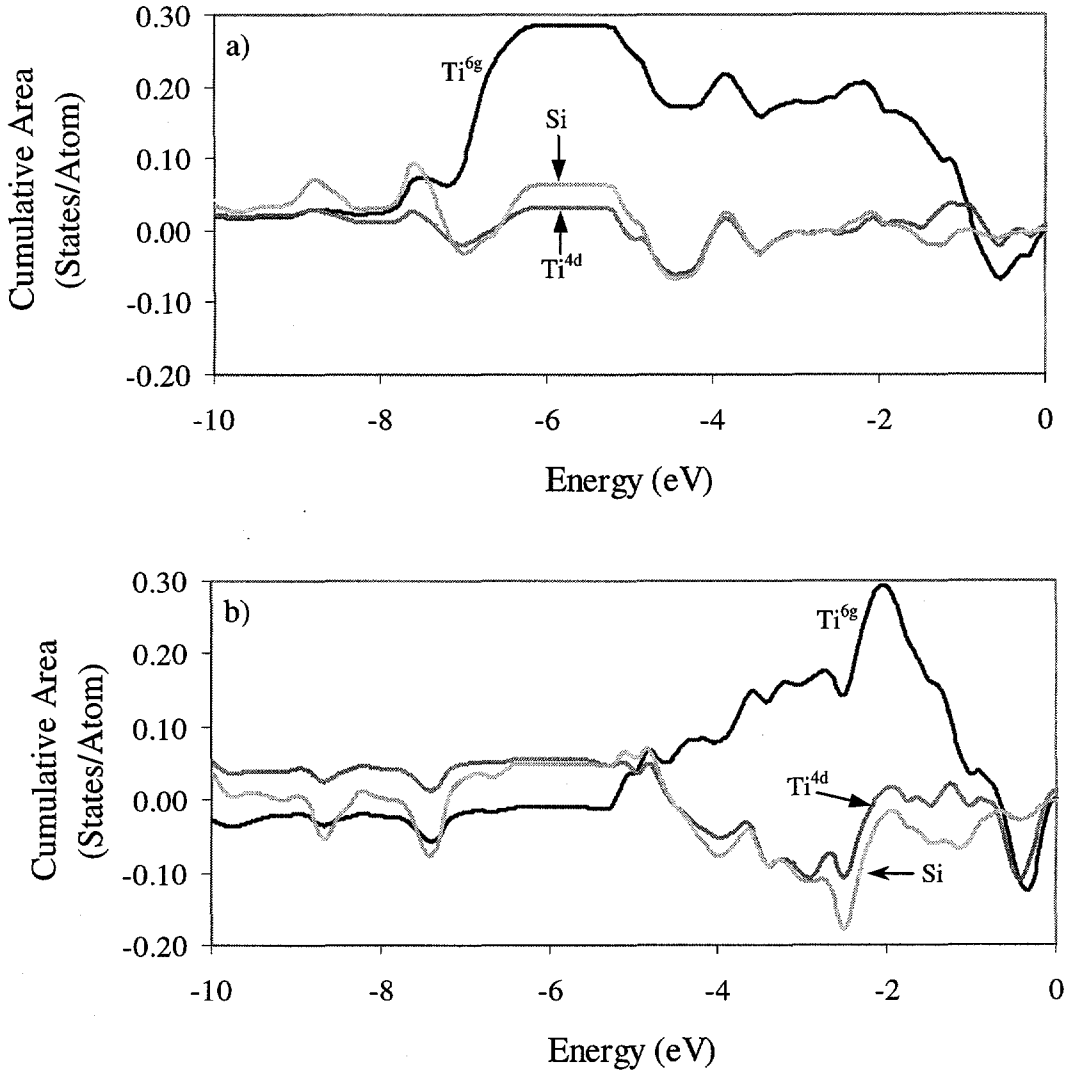
a)
Ti6g
Si
Ti4d
0.30
0.20
0.10
0.00
-0.10
-0.20
-10
-8
-6
-4
-2
0
Cumulative Area
(States/Atom)
Energy (eV)
b)
Ti6g
Ti4d
Si
0.30
0.20
0.10
0.00
-0.10
-0.20
-10
-8
-6
-4
-2
0
Cumulative Area
(States/Atom)
Energy (eV)

Figure 4.

CHAPTER 5: OXIDATION RESISTANCE OF Ti_5Si_3 AND $Ti_5Si_3Z_X$ AT 1000°C (Z = C, N OR O)

A paper to be submitted to *Oxidation of Metals*

J.J. Williams and M. Akinc

Abstract

The oxidation behavior of Ti_5Si_{3+y} (y = 0 or 0.2) and $Ti_5Si_3Z_x$ (Z = C, N or O, x= 0.25 or 0.5) was studied at 1000°C in air or argon-oxygen mixtures for up to 500 hours. Ti_5Si_3 has poor oxidation resistance in air due to an oxide scale rich in rutile and sub-scale formation of TiN, TiSi, $TiSi_2$ and Si. In contrast, $Ti_5Si_{3.2}$ forms a silica scale because the activity of silicon is orders-of-magnitude higher and thus, has excellent oxidation resistance. Samples with oxygen or nitrogen show only slight improvements in the early stages of oxidation compared to Ti_5Si_3. However, samples with carbon displayed excellent resistance over 500 hours at 1000°C.

Introduction

Ti_5Si_3 has been extensively studied over the past decade as a candidate material for demanding, high temperature applications. The reasons are due to its high melting point (2130°C), low density (~4.3 g/cm^3) and good creep and oxidation resistance (< 0.05 mg/cm^2/h) at and below 850°C. However, published research on the oxidation resistance of Ti_5Si_3 above 850°C has been notably inconsistent. Specifically, two previous studies by

Mitra and Rao[1] and Taniguchi *et al.*[2] have reported excellent oxidation resistance to 1250°C, whereas studies by Thom *et al.*[3-6], Kim *et al.*[7] and Abba *et al.*[8] reported poor oxidation resistance above 850°C. Based on thermodynamic data, these discrepancies may be explained by small differences in the chemical composition of Ti_5Si_3.

Current studies on thermodynamic phase equilibria indicate that Ti_5Si_3 exists over a significant solubility range of silicon (35.7 mol% to 39.0 mol% at 1000°C). Furthermore, the titanium-to-silicon activity ratio in Ti_5Si_3 changes by twelve orders of magnitude across this solubility range. According to Rahmel and Spencer[9], this extreme change in activity ratio from titanium rich to silicon rich compositions changes the stable oxide on Ti_5Si_3 from titanium oxide to silicon oxide. This would significantly change the measured oxidation resistance since diffusion through titanium oxide is several orders of magnitude faster than diffusion through silicon oxide. At 1000°C, for example, titanium metal, which forms a rutile (TiO_2) scale, gains weight at a rate greater than 1 mg/cm^2/h.[10] In contrast, silicon, which forms an amorphous silica scale, gains weight at a rate less than 1×10^{-4} mg/cm^2/h.[11] Thus, Ti_5Si_3 with excess silicon is expected to have excellent oxidation resistance because a continuous layer of SiO_2 is likely to form. Similarly, Ti_5Si_3 with excess titanium is expected to have poor oxidation resistance because a scale rich in titanium oxide should form.

This simple thermodynamic argument seems to accurately describe the actual oxidation behavior of Ti_5Si_3. For example, both studies that reported excellent oxidation resistance for Ti_5Si_3 below 1250°C also reported that their samples had small amounts (~5 vol%) of silicon-rich phases.[1-2] These silicon-rich samples had excellent oxidation resistance because a continuous layer of SiO_2 formed on Ti_5Si_3. In contrast, the samples used in the

study by Abba *et al.*[8] were 10 μm films of Ti_5Si_3 deposited on titanium metal, suggesting a higher titanium activity relative to silicon. This study found that a mixed scale of rutile (TiO_2) and amorphous silica forms on Ti_5Si_3. Furthermore, the rutile content was sufficiently high to provide little resistance to further oxidation above 850°C. The samples in the studies by Thom *et al.*[3-6] and Kim *et al.*[7] were reported to be single phase and assumed to be stoichiometric Ti_5Si_3. These oxidized samples had a mixed rutile-silica scale in contact with Ti_5Si_3 and similarly poor resistance to further oxidation at 1000°C like those found in the study by Abba *et al.*[8] Unlike other studies, however, the studies by Thom *et al.*[3-6] and Kim *et al.*[7] also reported additional unknown phases beneath the rutile-silica mixed scale.

Unfortunately, this argument, which is used to explain the discrepancies in the published oxidation resistance of Ti_5Si_3, is simplistic because several of the studies used samples that were contaminated with interstitial oxygen and/or carbon. Furthermore, studies on the oxidation behavior of Ti_5Si_3 with interstitial oxygen or carbon intentionally added have suggested that the oxidation resistance is vastly improved by these interstitial elements.[5,6] Unfortunately, those studies also suffered from interstitial impurities, and thus, the exact effects of interstitial elements and silicon-to titanium ratios on the oxidation resistance of Ti_5Si_3 remains unclear.

This study attempts to clarify these compositional effects on the oxidation behavior of Ti_5Si_3. Specifically, this study has measured the oxidation behavior of well-characterized and chemically pure samples of Ti_5Si_{3+y}, $Ti_5Si_{3-y}C_x$, $Ti_5Si_3O_x$ and $Ti_5Si_3N_x$ (y = 0 or 0.2, x = 0.25 or 0.5) at 1000°C. Oxidation kinetics were measured by thermogravimetric analysis (TGA), and oxidation products were quantified by scanning electron microscopy (SEM), x-

ray diffraction (XRD) and residual gas analysis (RGA).

Experimental Procedure

Starting materials included sponge titanium (Timet, 99.7 wt%), silicon pieces (Alfa Æsar, 99.9999 wt%), spectrographic grade graphite electrodes for carbon, titanium nitride for nitrogen (Johnson Matthey, 99.8 wt%) and titanium dioxide for oxygen (Fischer Scientific, 99.8 wt%) (all listed purities are metals basis). The sponge titanium was pre-melted two times to volatilize surface contamination before being used in synthesis. Sample compositions, which weighed approximately 10 g each, were synthesized via arc-melting in an ultra-high purity (UHP) argon atmosphere. Weight losses after arc-melting were generally much less than 0.5 wt%, and samples were single phase except those specifically synthesized in two-phase regions: the titanium-rich and silicon rich compositions. Based on high-resolution x-ray diffraction and lattice parameter measurements, samples were well crystallized and homogeneous. In addition, total carbon, nitrogen and oxygen impurity content was less than 0.09 wt% for all samples. Table I lists the lattice parameters and secondary phase content determined by XRD. With the exception of $Ti_5Si_3N_{0.25}$, the lattice parameters of all compositions are in excellent agreement with those reported by Williams *et al.*[12] The larger than expected lattice parameters for $Ti_5Si_3N_{0.25}$ might suggest that this sample has a slight excess of silicon.

All oxidation experiments were run on arc-melted material. However, TGA experiments could not be run with as-arc-melted ingots because the large number of micro-cracks made sample surface areas difficult to control and measure (to compare the rates at

which samples oxidize by TGA one must normalize rate of mass gain to the sample's surface area). Thus, ingots were ground and sieved to granular material such that each granule was a crack-free single crystal. From SEM analysis of approximately sixty granules from three different samples, the average particle size and particle surface area were estimated to be 465±64 μm and 0.010±0.003 cm^2, respectively. Each TGA sample, which weighed approximately 75 mg (roughly 500 granules), was placed in a quartz sample pan and hung from a Cahn 2000 microbalance. The TGA apparatus was then evacuated to –100 kPa and subsequently back-filled with an oxidizing atmosphere four to five times to purge the system. Oxidizing atmospheres included zero-grade air or 79% UHP argon - 21% UHP oxygen. The oxidizing gas was then allowed to flow for two hours at 50 cm^3/min with the sample heated to 250°C. This was done to insure a pure atmosphere, as well as to burn off possible surface contaminants from the sample. Finally, the sample was heated to 1000°C at 20 °C/min and held for one to 500 hours. Gas flow was maintained at 50 cm^3/min throughout the experiment. During select oxidation runs, the gas atmosphere was analyzed by an RGA. After the granular samples were oxidized in the TGA, they were ground to < 20 μm for phase analysis via XRD. A silicon standard (NIST SRM 640b) was added to most samples for accurate lattice parameter measurements. Rietveld analysis software (GSAS, Los Alamos National Laboratory 1985) was used to determine phase fractions and lattice parameters.

The use of granular arc-melted materials in the TGA experiments insured high-purity samples, good control over starting surface areas and high product-to-reactant ratios. However, quantitative measurements on the rate of oxidation can not be made for samples with poor oxidation resistance because the reaction surface area becomes significantly

reduced in a non-uniform manner over the course of the experiment. In addition, scale morphology cannot be easily observed. Thus, cut surfaces of the arc-melted ingots were also oxidized in conditions identical to those used in the TGA experiments. Cross-sections of these oxide scales were then analyzed under an SEM. The phases determined from XRD in the TGA experiments were then correlated to the scale morphologies observed in the SEM with EDS.

Results and Discussion

Oxidation of Ti_5Si_3 at 1000°C in Air

The measured oxidation resistance of stoichiometric Ti_5Si_3 granules agrees well with the studies of Abba *et al.*[8], Thom *et al.*[3-6] and Kim *et al.*[7] Like these other studies, the initial oxide products consist of an inner mixed scale of rutile and amorphous silica and an external scale of pure rutile (see Figure 1a). Observations made on the formation of the oxide scales clearly suggest that the external rutile scale grows by outward diffusion of titanium. The primary growth mechanism of the inner mixed scale is somewhat unclear, but research has shown that silica primarily grows by inward diffusion of oxygen. Figure 2 illustrates the weight gain as a function of time for a Ti_5Si_3 sample that was oxidized in flowing zero-grade air at 1000°C. Like previous studies, the curve displays an inflection point where an accelerated oxidation regime begins after approximately 11 hours. Superimposed on this weight-gain curve in Figure 2 is a plot of the measured lattice volume. Initially the lattice volume contracts sharply as oxygen and nitrogen diffuse into the vacant interstitial sites in Ti_5Si_3. This lattice volume, as measured by XRD, is only the average volume because a

compositional gradient of oxygen and nitrogen must exist in Ti_5Si_3 for further diffusion to occur. Nonetheless, the kinetics in the early stages of oxidation are certainly affected by the filling of interstitial sites with oxygen and nitrogen.

Also shown in Figure 2, the accelerated oxidation regime is apparently caused by the growth of sub-scale phases such as $TiSi_2$ and TiN. Figure 1b shows a portion of the surface shortly after this accelerated oxidation begins. Based on this figure, nucleation and growth of phases beneath the original oxide scale cause a large volume expansion. The stresses that develop due to this volume expansion apparently disrupt the external oxide scale allowing accelerated oxidation to occur. The study by Thom *et al.*[4] observed that oxide scales on monolithic Ti_5Si_3 do spall, giving support to the argument that stresses do develop during oxidation. Furthermore, the study by Abba et al[8] observed cracks in the external oxide scales of Ti_5Si_3.

The x-ray spectrum of oxidized granules, given in Figure 3, indicates that several phases form during the oxidation of Ti_5Si_3 by air at 1000°C. With the exception of one study that showed the presence of $TiSi_2$[4] and a different study that showed the presence of TiN[8], no other studies have reported the presence of anything other than rutile and amorphous silica during the oxidation of Ti_5Si_3. The use of granular material in this study yielded a significantly higher product to reactant ratio compared to previous studies. Thus, the products could be easily detected with XRD. Furthermore, these detected products agree with the Ti-Si-N-O phase diagram calculated by Bhansali and Sinclair.[13] Figure 4 depicts a Ti_5Si_3-N-O pseudo-ternary cut from this quaternary phase diagram. The only predicted phase not actually detected in the oxidation products was Si_2N_2O. Also, one minor peak, as shown

in Figure 3, could not be positively identified.

Oxidation of Ti_5Si_3 at 1000°C in 79% Ar - 21% O_2

Figures 5 and 6 illustrate the results of oxidizing Ti_5Si_3 in an argon-oxygen mixture. As was the case with samples oxidized in air, these samples form an external rutile scale and an inner mixed scale of rutile and amorphous silica. Based on the pseudo-ternary diagram (Fig. 4) other titanium oxide phases should have formed beneath these scales, although none were detected. Unlike the samples oxidized in air, the samples oxidized in the absence of nitrogen maintain good oxidation resistance over 100 hours. In fact, the rate of weight gain is fit well by a typical diffusion-controlled model with a parabolic rate constant of approximately 0.002 $mg^2/cm^4/h$. In contrast, published rate constants of Ti_5Si_3 in air at 1000°C suggests a linear rate constant of 0.1 $mg/cm^2/h$.[6] Thus, the presence of nitrogen and its effect on thermodynamic phase equilibria and reaction kinetics play a key role in the poor oxidation resistance of Ti_5Si_3. This also indicates that rutile is not an effective diffusion barrier for nitrogen, although no quantitative diffusion studies are know to exist.

Effect of Carbon, Nitrogen, or Oxygen on the Oxidation of Ti_5Si_3

Figure 7 illustrates the effects of interstitial carbon, nitrogen or oxygen on the oxidation resistance of Ti_5Si_3. In the early stages of oxidation, all samples with interstitial elements show measurably smaller weight gains over pure Ti_5Si_3. As noted earlier, some of the weight gain in pure Ti_5Si_3 is due to interstitial incorporation of oxygen and nitrogen. Thus, samples with a portion of the interstices already filled should gain less weight in the

initial stages of oxidation, as is observed in Figure 7. However, if this were the only reason for the difference in weight gain, all samples with the same level of interstitial elements, regardless of the type of interstitial element, should show the same amount of weight gain in the initial stages of oxidation.

Figure 7 clearly shows that the type of interstitial element does affect the initial amount of weight gain. In fact, based on quantitative XRD, the amount of rutile that forms on the interstitially modified samples is significantly less than that of pure Ti_5Si_3 in the early stages of oxidation. Additionally, as seen in Figure 8, the scales after one hour of oxidation are composed primarily of amorphous silica. Thus the rate of rutile formation has slowed in the early stages of oxidation on samples that initially contain interstitial atoms. This suggests that the presence of interstitial atoms increases the activation energy and/or lowers the driving force for rutile formation. In support of this hypothesis, studies have shown that interstitial elements, like carbon, nitrogen and oxygen, are bonded only to the titanium atoms in Ti_5Si_3.[12,14] Thus, this preferential bonding to titanium should increase the activation energy for rutile formation, and in the early stages of oxidation, would decrease the amount of rutile that forms relative to the amount of silica. Furthermore, carbon is suspected to be most strongly bonded and oxygen least strongly bonded to these titanium atoms. Thus, a correlation exists between interstitial bond strength and the initial amount of rutile formation – the higher the bond strength, the lower the initial rutile content.

With the exception of the carbon-containing samples, however, all samples eventually show a similar transition to accelerated oxidation kinetics as Ti_5Si_3 becomes saturated with oxygen and nitrogen, and additional phases begin to grow beneath the scale. Only the carbon

containing samples maintain a silica rich scale over long periods of time. Additionally, the lattice volume of carbon-containing samples remained unchanged over 500 hours at 1000°C, which indicates negligible diffusion of atmospheric nitrogen or oxygen into the interstices of Ti_5Si_3. Thus, a different mechanism for the improvement in oxidation behavior might exist. Figure 9 illustrates that CO_2 evolution during the early stages of oxidation of $Ti_5Si_3C_x$ compositions might also play a role in the initial scale development. Oxidation of carbon at the Ti_5Si_3 – oxide scale interface would reduce the amount of oxygen diffusing into the interstices and reduce the overall measured weight gain.

Effect of Titanium to Silicon Ratios on the Oxidation behavior of Ti_5Si_3

As noted in the introduction, previous data suggest that the titanium-to-silicon ratio might have a profound effect on the oxidation resistance of Ti_5Si_3. Thus two additional samples were oxidized in air: $Ti_5Si_{3.2}$ and $Ti_5Si_{2.8}C_{0.5}$. Figure 10 displays the TGA results of these experiments, and Table II gives the reaction rate constants. Although a large initial mass gain exists due to filling of empty interstices in $Ti_5Si_{3.2}$, the sample did yield a continuous layer of amorphous silica and excellent oxidation resistance at 1000°C. As previously mentioned, the carbon containing samples do not show this initial mass gain. This may be due to a reduction of the flux of oxygen atoms into the interstices because of the oxidation of carbon at the $Ti_5Si_3C_x$ -- oxide scale interface. The assertion that oxygen diffuses into $Ti_5Si_{3.2}$ and not $Ti_5Si_3C_x$ is substantiated by XRD lattice volume measurements. Whereas the lattice volume of $Ti_5Si_{3.2}$ contracts by 2%, the measured changes in lattice volume of $Ti_5Si_3C_x$ were less than 0.1%. More importantly, the silicon-deficient, carbon-

containing sample also had relatively good oxidation resistance at 1000°C. This provides conclusive proof that the presence of carbon in the interstices of Ti_5Si_3 does vastly improve the oxidation resistance.

Conclusions

Stoichiometric Ti_5Si_3 has poor oxidation resistance at 1000°C due to the formation of a scale rich in rutile. This scale does not provide an effect diffusion barrier for oxygen and nitrogen, and hence allows additional phases to grow beneath the external scale. The phases that form when Ti_5Si_3 is oxidized in air cause a large volume expansion and eventual disruption of the external scale. These phases, which include TiN, Si, $TiSi_2$ and TiSi, were predicted from thermodynamic data and published phase diagrams. When oxidized in nitrogen-free atmospheres, however, Ti_5Si_3 maintains relatively good oxidation resistance at 1000°C.

In agreement with previous research, both $Ti_5Si_{3.2}$ and $Ti_5Si_3C_x$ possess excellent oxidation resistance at 1000°C. Based on thermodynamic data of Ti_5Si_3, only a slight excess in silicon is needed to shift the oxide scale from rutile-rich to silica-rich, which explains the good oxidation resistance of $Ti_5Si_{3.2}$. The reason for the improvement in oxidation resistance due to carbon additions remains unclear. It may be due to an increase in the activation energy of rutile formation, as well as a reduction of oxygen flux into Ti_5Si_3 because of the oxidation of carbon beneath the oxide scale. In contrast to previous research, $Ti_5Si_3O_x$ does not maintain good long-term oxidation resistance. This discrepancy is most likely due to impure samples used in previous studies.

Acknowlegments

Ames Laboratory is operated for the U. S. Department of Energy by Iowa State University under contract number W-7405-ENG-82. The United States Government has assigned the DOE Report Number IS-T 1880 to this thesis.

References

1. R. Mitra and V.V. Rama Rao, *Metall. Mater. Trans. A* **29**, 1665 (1998).
2. S. Taniguchi, T. Minamida and T. Shibata, *Mater. Sci. Forum* **251-254**, 227 (1997).
3. A.J. Thom, Y. Kim and M. Akinc. *Mat. Res. Soc. Symp. Proc.* **288**, 1037 (1992).
4. A.J. Thom, M. K. Meyer, Y. Kim and M. Akinc. *Processing and Fabrication of Advanced Materials III*, Ed. V. A. Ravi, T. S. Srivatsan and J. J. Moore. (The Minerals, Metals & Materials Society, 1994). 438.
5. A.J. Thom and M. Akinc. *Advanced Ceramics for Structural and Tribological Applications*, Vancouver, British Columbia, Ed. H. M. Hawthorne and T. Troczynski. (The Metallurgical Society of CIM, 1995). 627.
6. A.J. Thom, M. K. Meyer, J.J Williams and M. Akinc. *International Symposium on Processing and Fabrication of Advanced Materials IV*, Cleveland, Ohio, Ed. T. S. Srivatsan and J. J. Moore. (The Minerals, Metals, and Materials Society, 1995). 139.
7. Y. Kim, A. J. Thom and M. Akinc. *Processing and Fabrication of Advanced Materials for High Temperature Applications-II*, Eds. V. A. Ravi and T. S. Srivatsan. (The Minerals, Metals and Materials Society, 1993) 189.
8. A. Abba., A. Galerie and M. Caillet. *Oxidation of Metals* **17**[1], 43 (1982).
9. A. Rahmel and P. J. Spencer. *Oxidation of Metals* **35**[1-2], 53 (1991).

10. P. Kofstad, P.B. Anderson and O.J. Krutaa. *J. Less Comm. Met.* **3**, 89 (1961).

11. B.E. Deal and A.S. Grove. *J. Appl. Phys.* **36**[12], 3770 (1965).

12. J.J. Williams, M.J. Kramer, M. Akinc and S. Malik, submitted to *J. Mater. Res.*

13. A.S. Bhansali and R. Sinclair, *Mat. Res. Soc. Symp. Proc.* **148**, 71 (1989).

14. J.J. Williams, Y.Y. Ye, M.J. Kramer, K.M. Ho, to be submitted to *Intermet.*

Figure Captions

Figure 1a. Oxide scale on Ti_5Si_3 after 10 h at 1000°C in air consist of an external rutile scale (top, lighter layer) and an inner mixed scale of rutile and silica. b. In the accelerated oxidation regime, secondary phases begin to develop within the Ti_5Si_3 matrix, causing a large volume expansion. These phases included a layer of TiSi in contact with Ti_5Si_3 followed by a thicker layer of $TiSi_2$, as well as mixed areas of Si, TiN, silica and rutile.

Figure 2. The rate of mass gain during the oxidation of Ti_5Si_3 begins to accelerate after roughly 11 h. Contraction of the Ti_5Si_3 lattice suggests that incorporation of oxygen and nitrogen into Ti_5Si_3 plays a role in reaction kinetics. Also, growth rates of rutile, TiN and $TiSi_2$ increase rapidly in the accelerated regime.

Figure 3. X-ray diffraction spectra of a Ti_5Si_3 sample oxidized in air at 1000°C for 50 h. One peak at 39.9° remains unidentified. All identified phases were expected based on published thermodynamic calculations.

Figure 4. Pseudo-ternary phase diagram taken from a quaternary diagram published by Bhansali and Sinclair.[13] Their study failed to recognize solubility ranges of Ti_5Si_3, TiN, Si_2N_2O, TiO and Ti, thus the phase boundaries are not rigorously correct. The dashed line represents 79% N_2-21% O_2 (air). The phase triangles at right, which are too closely spaced for labeling, are composed of titanium oxides (Ti_2O_3, Ti_3O_5, Ti_4O_7 and TiO_2), TiN and SiO_2.

Figure 5. The rate of mass gain of Ti_5Si_3 is significantly slowed when oxidized in the absence of atmospheric nitrogen.

Figure 6. The scale on Ti_5Si_3 consists of an external rutile scale and inner mixed scale of rutile and silica after oxidation at 1000°C in 79% Ar – 21% O_2. The scale is sufficiently rich in silica to provide marginally good oxidation resistance.

Figure 7. Mass gains of various compositions oxidized in air at 1000°C. All samples with interstitial atoms originally incorporated into Ti_5Si_3 show less mass gain than pure Ti_5Si_3 in the early stages. However, only $Ti_5Si_3C_x$ maintains resistance for extended time periods.

Figure 8a. Oxidation of Ti_5Si_3 after one hour at 1000°C under flowing zero-grade air. The scale of Ti_5Si_3 is a mixture of SiO_2 (dark areas) and TiO_2 (lighter areas). b. Oxidation of $Ti_5Si_3C_{0.25}$ after one hour at 1000°C under flowing zero-grade air. The scale of $Ti_5Si_3C_{0.25}$ (as well as, $Ti_5Si_3N_{0.25}$ and $Ti_5Si_3O_{0.25}$) is primarily SiO_2 after one hour.

Figure 9. RGA during the oxidation of various compositions in air. The oxidation of carbon to CO_2 may play an important role in early scale development of $Ti_5Si_3C_x$ compositions as well as the rate at which oxygen diffuses into the interstices of Ti_5Si_3. Note that the subsequent drop in measured CO_2 evolution above 750°C is a result of the growth of the oxide scale. Carbon should continue to oxidize, although the diffusion barrier provided by the oxide scale drops the rate of CO_2 formation below the detection limit of the RGA.

Figure 10. Long term mass gains of various compositions oxidized in air at 1000°C. $Ti_5Si_{3.2}$ and $Ti_5Si_3C_x$ compositions form a passivating layer of silica and maintain excellent oxidation resistance over extended periods of time.

Table I. X-Ray Diffraction Results of Starting Materials

Sample	a, Å	c, Å	Second Phases, vol%
Ti_5Si_3	7.4600(2)	5.1517(1)	---
$Ti_5Si_{3.2}$	7.4842(2)	5.1749(2)	8% Ti_5Si_4, 2% TiSi
$Ti_5Si_3O_{0.25}$	7.4470(3)	5.1392(3)	---
$Ti_5Si_3O_{0.5}$	7.4335(1)	5.1316(1)	---
$Ti_5Si_3N_{0.25}$	7.4494(3)	5.1495(3)	---
$Ti_5Si_3N_{0.5}$	7.4273(1)	5.1453(1)	---
$Ti_5Si_3C_{0.25}$	7.4506(1)	5.1565(1)	---
$Ti_5Si_3C_{0.5}$	7.4399(1)	5.1677(1)	---
$Ti_5Si_{2.8}C_{0.5}$	7.4446(2)	5.1620(1)	2% Ti

Table II. Oxidation Rate Constants at 1000°C

Sample	Rate Constant*	Model*	Atmosphere	Reference
Ti_5Si_3	0.1	Linear	Air	[6]
$Ti_5Si_3C_{0.5}$	2×10^{-5}	Parabolic	Air	This Study
$Ti_5Si_{3.2}$	5×10^{-5}	Parabolic	Air	This Study
$Ti_5Si_{2.8}C_{0.5}$	4×10^{-3}	Parabolic	Air	This Study
Si	2×10^{-4}	Parabolic	O_2	[11]
Ti	> 1	Linear	Air	[10]
Ti_5Si_3	2×10^{-3}	Parabolic	79% Ar – 21% O_2	This Study

* For a parabolic model, units of the rate constant are $mg^2/cm^4/h$, for a linear model, units are $mg/cm^2/h$.

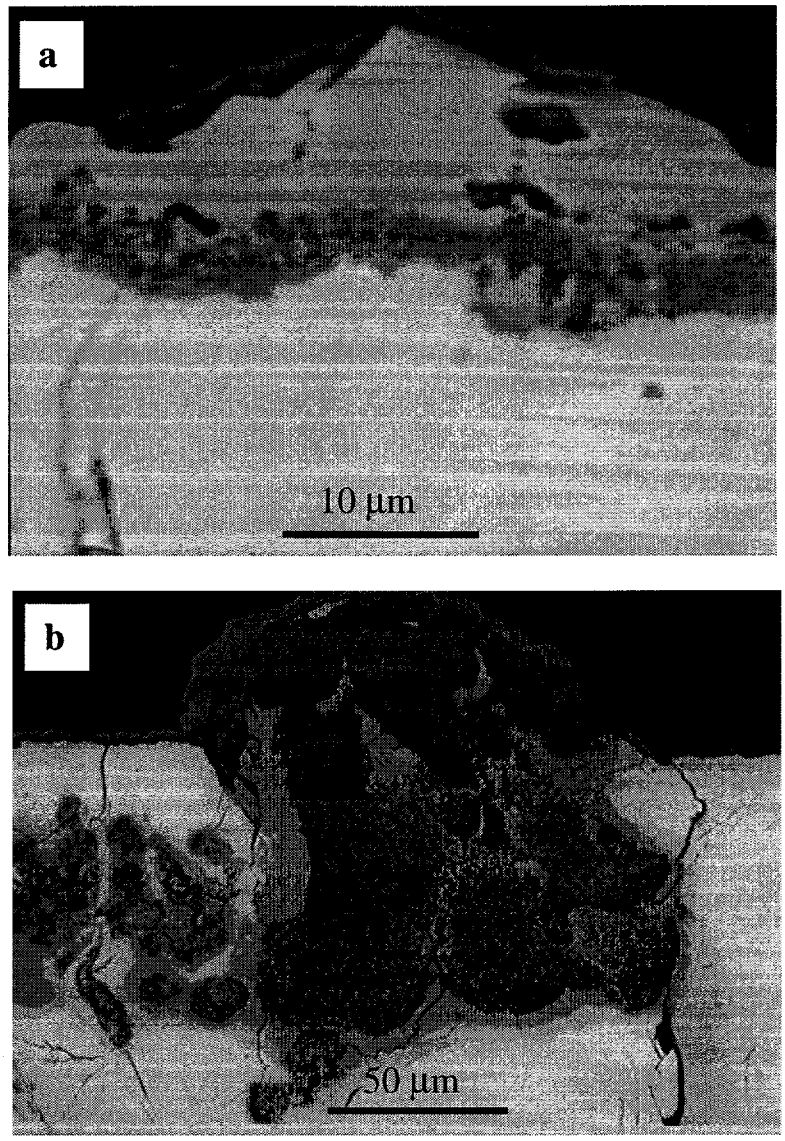

Figure 1

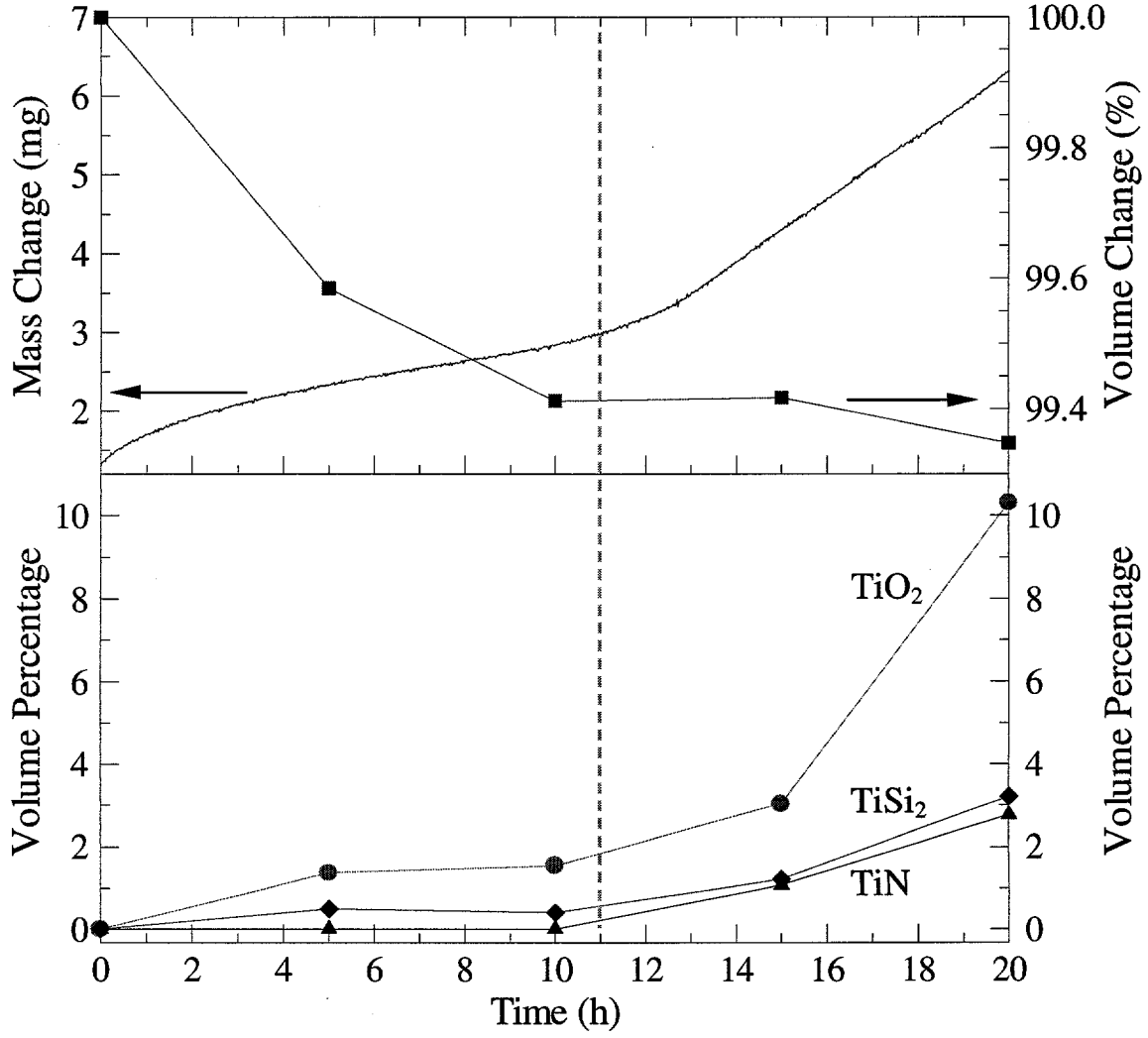
Mass Change (mg)
Volume Change (%)
Volume Percentage
Volume Percentage
Time (h)
TiO2
TiSi2
TiN
7
6
5
4
3
2
100.0
99.8
99.6
99.4
10
8
6
4
2
0
0
2
4
6
8
10
12
14
16
18
20

Figure 2

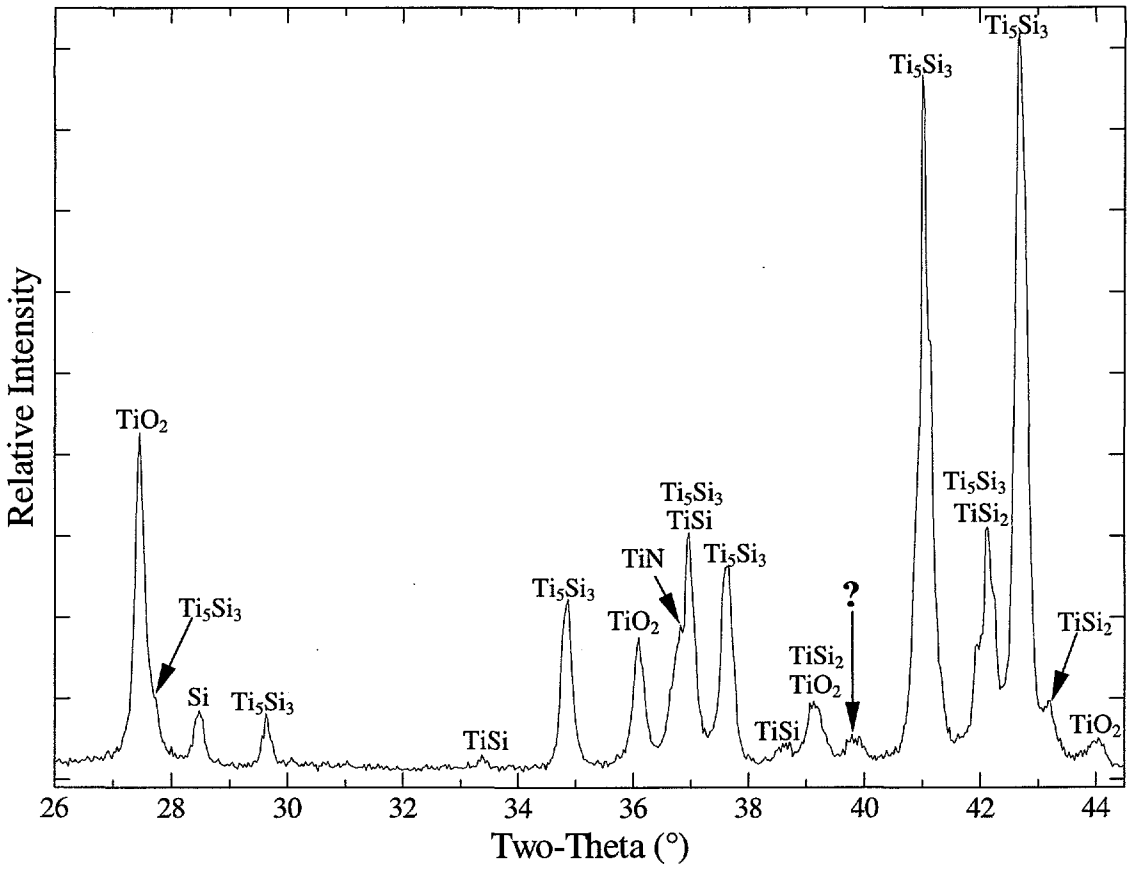
Relative Intensity
Two-Theta (°)
26
28
30
32
34
36
38
40
42
44
TiO2
Ti5Si3
Si
Ti5Si3
TiSi
Ti5Si3
TiO2
TiN
Ti5Si3
TiSi
Ti5Si3
TiSi2
TiO2
?
TiSi
Ti5Si3
Ti5Si3
TiSi2
Ti5Si3
TiSi2
TiO2

Figure 3

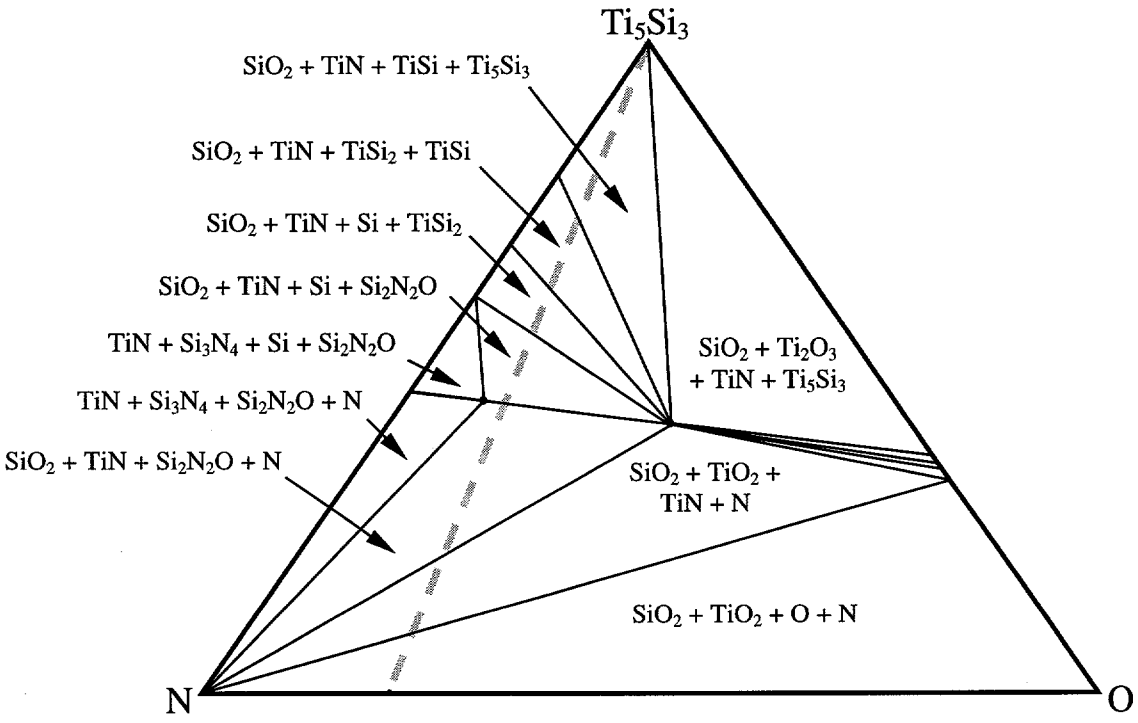
Ti_5Si_3
$SiO_2 + TiN + TiSi + Ti_5Si_3$
$SiO_2 + TiN + TiSi_2 + TiSi$
$SiO_2 + TiN + Si + TiSi_2$
$SiO_2 + TiN + Si + Si_2N_2O$
$TiN + Si_3N_4 + Si + Si_2N_2O$
$TiN + Si_3N_4 + Si_2N_2O + N$
$SiO_2 + TiN + Si_2N_2O + N$
$SiO_2 + Ti_2O_3$
$+ TiN + Ti_5Si_3$
$SiO_2 + TiO_2 +$
$TiN + N$
$SiO_2 + TiO_2 + O + N$
N
O

Figure 4

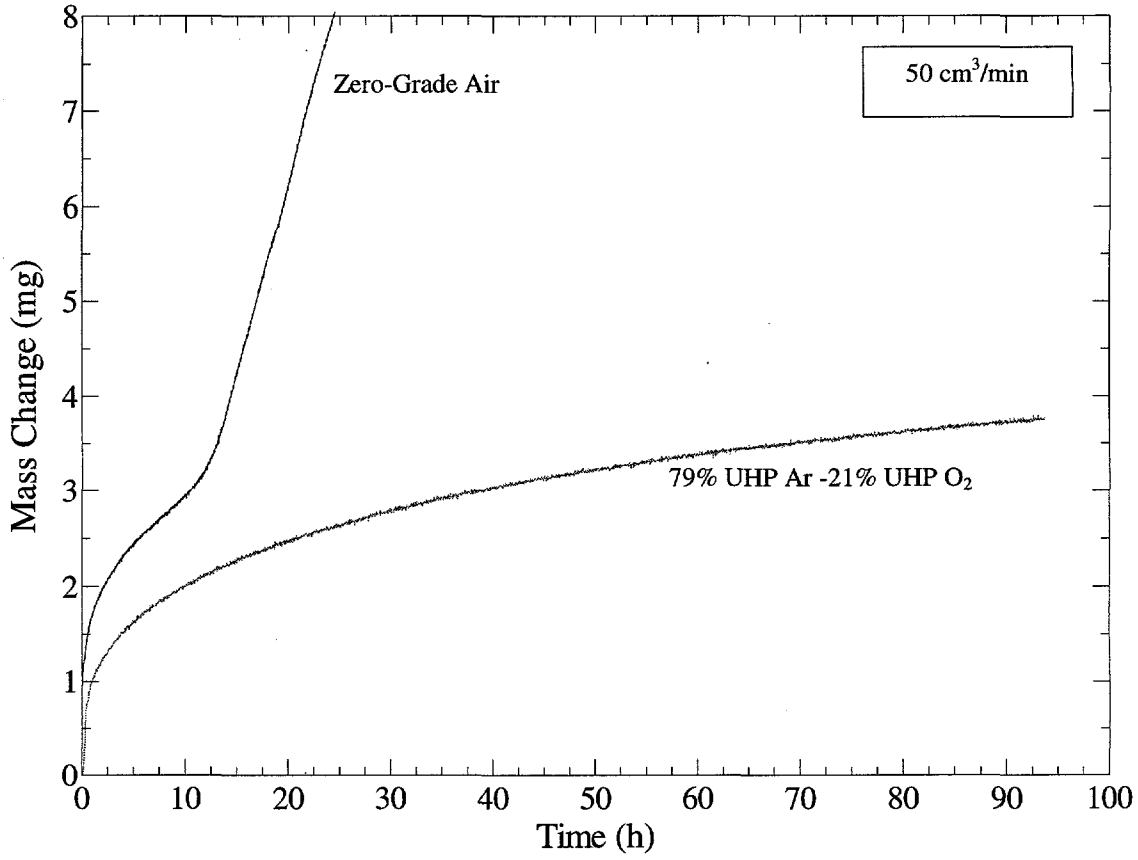
Zero-Grade Air
50 cm³/min
79% UHP Ar -21% UHP O₂
Mass Change (mg)
Time (h)
0
1
2
3
4
5
6
7
8
0
10
20
30
40
50
60
70
80
90
100

Figure 5

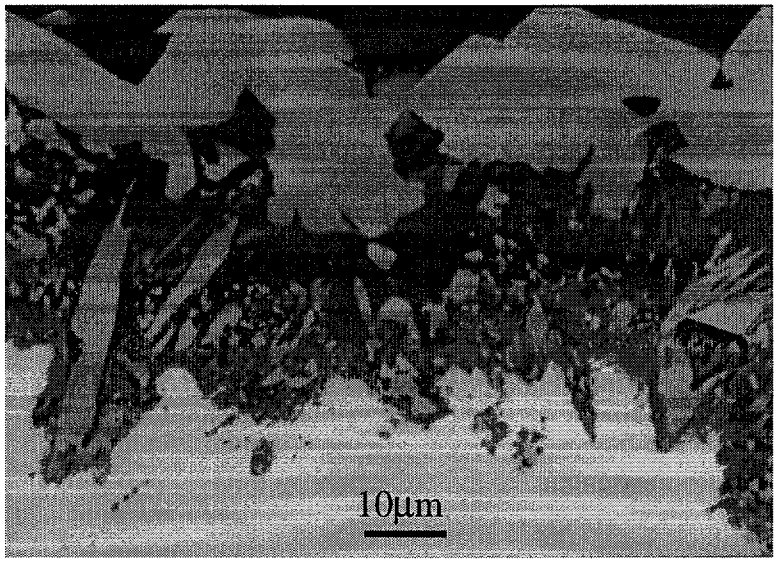

Figure 6.

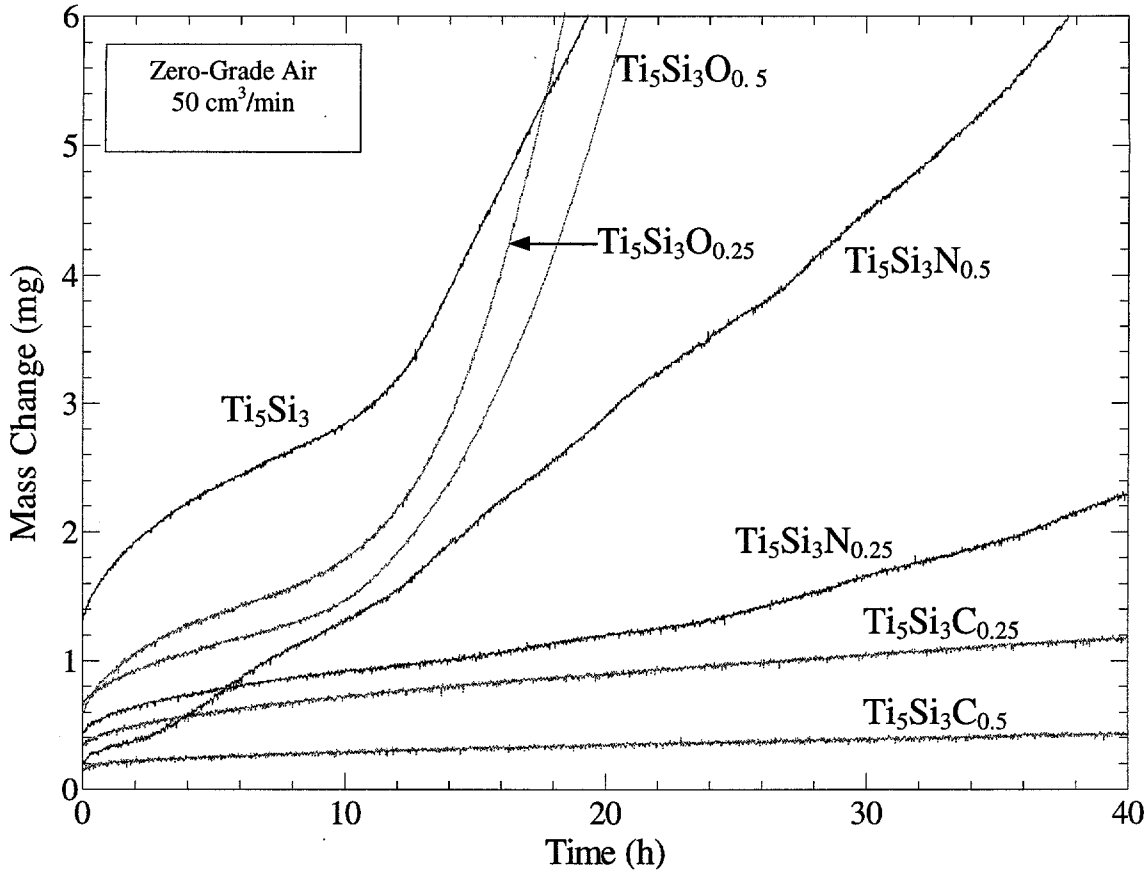
Zero-Grade Air
50 cm³/min
Ti5Si3O0. 5
Ti5Si3O0.25
Ti5Si3N0.5
Ti5Si3
Ti5Si3N0.25
Ti5Si3C0.25
Ti5Si3C0.5
Mass Change (mg)
Time (h)
0
1
2
3
4
5
6
0
10
20
30
40

Figure 7

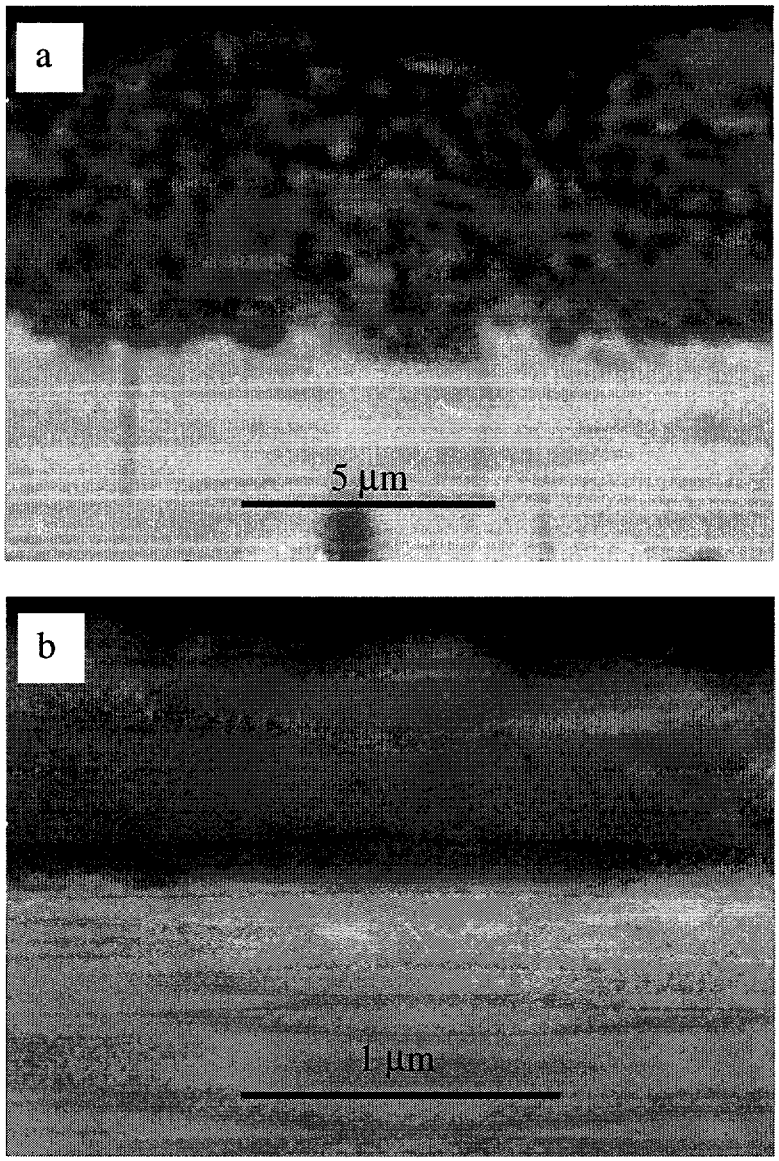

Figure 8

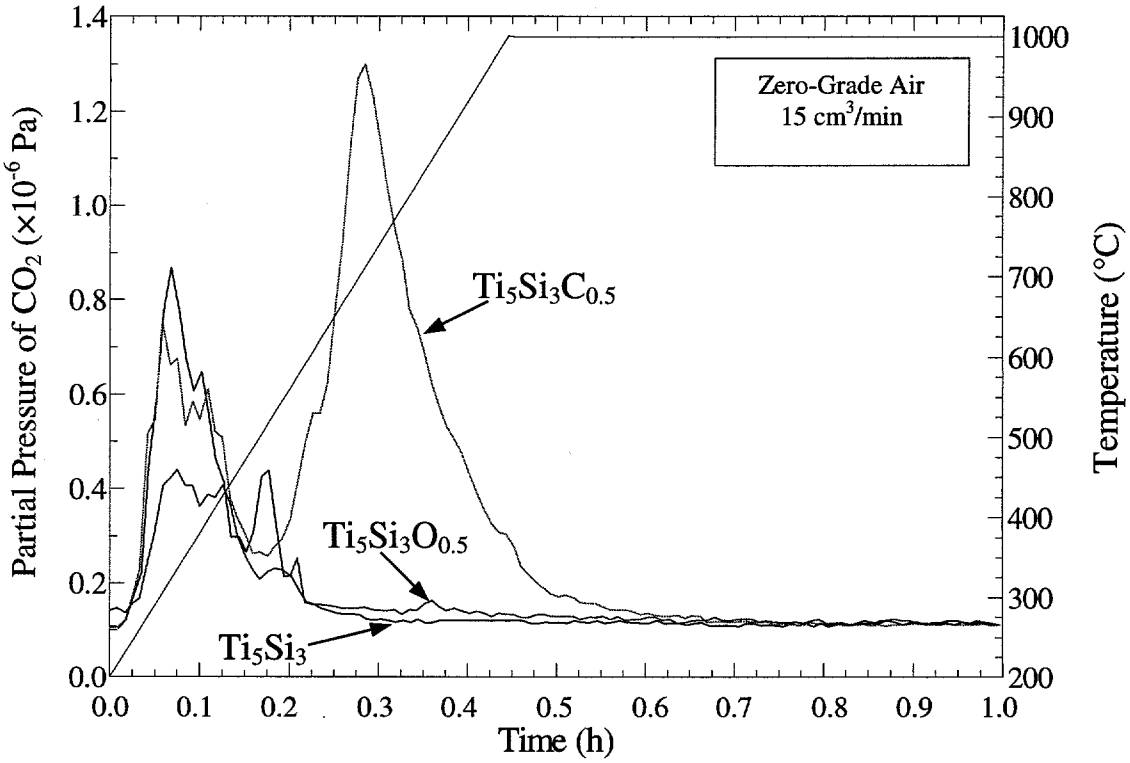
Zero-Grade Air
15 cm³/min
Ti5Si3C0.5
Ti5Si3O0.5
Ti5Si3
Partial Pressure of CO2 (×10⁻⁶ Pa)
Temperature (°C)
Time (h)
0.0
0.2
0.4
0.6
0.8
1.0
1.2
1.4
200
300
400
500
600
700
800
900
1000
0.1
0.3
0.5
0.7
0.9

Figure 9

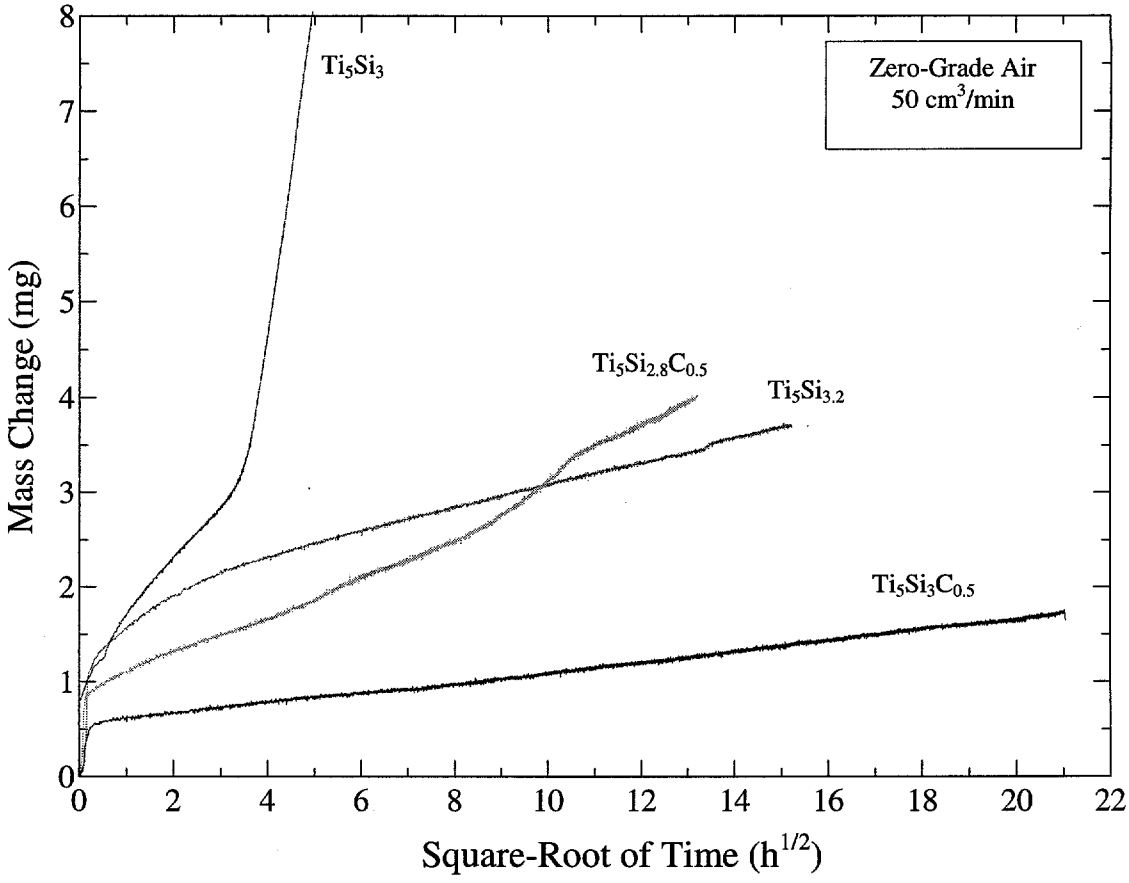
Ti5Si3
Zero-Grade Air
50 cm3/min
Ti5Si2.8C0.5
Ti5Si3.2
Ti5Si3C0.5
Mass Change (mg)
Square-Root of Time (h1/2)
0
1
2
3
4
5
6
7
8
0
2
4
6
8
10
12
14
16
18
20
22

Figure 10

CHAPTER 6: GENERAL CONCLUSIONS

This study was motivated by the fact that previous research on the structure and properties of Ti_5Si_3 showed unacceptably inconsistent results. The primary reason for these inconsistencies was interstitial contamination of Ti_5Si_3 by carbon, nitrogen and oxygen. Thus, this study measured the effects that these interstitial atoms have on some of the previously reported properties. These properties include crystalline structure, thermal expansion anisotropy, electronic structure and bonding, and high temperature oxidation resistance.

In Chapter 2 of this study, the lattice parameters and atomic positions of Ti_5Si_3 as a function of carbon, nitrogen or oxygen content were measured via x-ray and neutron diffraction. Comparing these lattice parameters to those reported in other studies on supposedly pure Ti_5Si_3 confirmed that the majority of the previous studies had samples with a considerable amount of interstitial impurities. In fact, the lattice parameter trends given in Chapter 2 can be used to estimate the types and level of impurities in these studies. Furthermore, Chapter 2 discusses how atomic positions change as interstitial atoms are incorporated into the lattice. These changes in atomic separations suggest that strong bonds form between the interstitial atoms and the surrounding titanium atoms. This is in full agreement with the electronic structure calculations given in Chapter 4. These calculations show that bonding does occur between titanium d-states and interstitial atom p-states at the expense of bonding between some of the titanium and silicon atoms. In addition, carbon seems to be the most strongly bonded interstitial atom.

Knowledge of the exact interstitial content and its effect on bonding is important

because Chapters 3 and 5 have shown that interstitial atoms have a marked effect on the thermal expansion and oxidation resistance. As discussed in Chapter 3, all interstitial atoms lower the thermal expansion anisotropy of Ti_5Si_3 due to the formation of bonds between the interstitial atom and the surrounding titanium atoms. Although interstitial atoms do have an effect on the thermal expansion of Ti_5Si_3, these effects were not strong enough to explain all the scatter of previous studies. These studies most likely suffered from systematic errors as a result of poor experimental design. The experimental procedure used in this study was designed to significantly reduce these systematic errors.

As illustrated in Chapter 3, samples with interstitial carbon had the greatest reduction in thermal expansion anisotropy compared to pure Ti_5Si_3. This makes $Ti_5Si_3C_x$-based compounds promising materials for engineering applications because, as shown in Chapter 5, $Ti_5Si_3C_x$ also has far superior oxidation resistance. The excellent oxidation resistance is due to the formation of a continuous layer of amorphous silica. This silica layer provides a much more effective diffusion barrier compared to the rutile-rich scale that forms on pure Ti_5Si_3. In fact samples with all types of interstitial atoms show better resistance than pure Ti_5Si_3 in the initial stages of oxidation because of scales richer in silica. However, contrary to previous research, only samples with interstitial carbon or excess silicon maintain a silica rich scale and long-term oxidation resistance. Samples that eventually form rutile-rich scales also form TiN, TiSi, $TiSi_2$ and Si beneath the oxide scale. The formation of these phases leads to a volume expansion which eventually causes disruption of the external oxide scale and hence, poor oxidation resistance.

Unfortunately, single phase Ti_5Si_3, even with interstitial carbon, is not an ideal

engineering material due to its ambient temperature brittleness and high creep rates above 1200°C. However, $Ti_5Si_3C_x$ could be an important component in a multi-phase system due to its low density, and excellent oxidation resistance. Future research should focus on partial substitution of Ti for other transition metals, such as niobium, zirconium and molybdenum. As mentioned in Chapter 3, partial substitution of the transition element may be the most effective method of reducing crystalline anisotropic properties. Also, this multi-component material will most likely require a metallic phase to impart better fracture toughness. Pure titanium metal would not be a good choice due to its high creep rate.

Much work is still required to realize the full potential of Ti_5Si_3-based materials. Additionally previous research on Ti_5Si_3, as well as all Mn_5Si_3-based materials must be viewed critically because processing these materials without interstitial impurities is exceedingly difficult. As discussed in this study, uncontrolled interstitial impurities will unpredictably affect the measured properties.